ISSN 1949-8470 (online)

World Journal of *Radiology*

World J Radiol 2017 May 28; 9(5): 217-252

Published by Baishideng Publishing Group Inc

WJR World Journal of Radiology

A peer-reviewed, online, open-access journal of Radiology

Editorial Board

2014-2017

The *World Journal of Radiology* Editorial Board consists of 365 members, representing a team of worldwide experts in radiology. They are from 36 countries, including Afghanistan (1), Argentina (2), Australia (5), Austria (7), Belgium (2), Brazil (8), Canada (6), Chile (1), China (43), Croatia (1), Denmark (4), Egypt (6), France (5), Germany (22), Greece (10), India (12), Iran (6), Ireland (2), Israel (3), Italy (47), Japan (13), Netherlands (1), New Zealand (1), Pakistan (1), Poland (2), Portugal (1), Serbia (1), Singapore (3), Slovakia (1), South Korea (18), Spain (4), Sweden (2), Switzerland (4), Thailand (1), Turkey (26), United Kingdom (11), and United States (82).

Yue-Qi Zhu, *Shanghai*

Croatia

Goran Kusec, Osijek

Denmark

Poul E Andersen, *Odense*
Lars J Petersen, *Aalborg*
Thomas Z Ramsoy, *Frederiksberg*
Morten Ziebell, *Copenhagen*

Egypt

Mohamed F Bazeed, *Mansoura*
Mohamed Abou El-Ghar, *Mansoura*
Reem HA Mohamed, *Cairo*
Mohamed R Nouh, *Alexandria*
Ahmed AKA Razek, *Mansoura*
Ashraf A Zytoon, *Shebin El-Koom*

France

Sabine F Bensamoun, *Compiègne*
Romaric Loffroy, *Dijon*
Stephanie Nougaret, *Montpellier*
Hassane Oudadesse, *Rennes*
Vincent Vinh-Hung, *Fort-de-France*

Germany

Henryk Barthel, *Leipzig*
Peter Bannas, *Hamburg*
Martin Beeres, *Frankfurt*
Ilja F Ciernik, *Dessau*
A Dimitrakopoulou-Strauss, *Heidelberg*
Peter A Fasching, *Erlanegn*
Andreas G Schreyer, *Regensburg*
Philipp Heusch, *Duesseldorf*
Sonja M Kirchhoff, *Munich*
Sebastian Ley, *Munich*
Adel Maataoui, *Frankfurt am Main*
Stephan M Meckel, *Freiburg*
Hans W Muller, *Duesseldorf*
Kay Raum, *Berlin*
Dirk Rades, *Luebeck*
Marc-Ulrich Regier, *Hamburg*
Alexey Surov, *Halle*
Martin Walter, *Magdeburg*
Axel Wetter, *Essen*
Christoph Zilkens, *Düsseldorf*

Greece

Panagiotis Antoniou, *Thessaloniki*
Nikos Efthimiou, *Athens*
Dimitris Karnabatidis, *Patras*
George Latsios, *Athens*
Stylianos Megremis, *Iraklion*
Alexander D Rapidis, *Athens*
Kiki Theodorou, *Larissa*
Ioannis A Tsalafoutas, *Athens*
Evanthia E Tripoliti, *Ioannina*
Athina C Tsili, *Ioannina*

India

Ritesh Agarwal, *Chandigarh*
Chandan J Das, *New Delhi*
Prathamesh V Joshi, *Mumbai*
Naveen Kalra, *Chandigarh*
Chandrasekharan Kesavadas, *Trivandrum*
Jyoti Kumar, *New Delhi*
Atin Kumar, *New Delhi*
Kaushala P Mishra, *Allahabad*
Daya N Sharma, *New Delhi*
Binit Sureka, *New Delhi*
Sanjay Sharma, *New Delhi*
Raja R Yadav, *Allahabad*

Iran

Majid Assadi, *Bushehr*
SeyedReza Najafizadeh, *Tehran*
Mohammad Ali Oghabian, *Tehran*
Amir Reza Radmard, *Tehran*
Ramin Sadeghi, *Mashhad*
Hadi Rokni Yazdi, *Tehran*

Ireland

Tadhg Gleeson, *Wexford*
Frederik JAI Vernimmen, *Cork*

Israel

Dafna Ben Bashat, *Tel Aviv*
Amit Gefen, *Tel Aviv*
Tamar Sella, *Jerusalem*

Italy

Adriano Alippi, *Rome*
Dante Amelio, *Trento*
Michele Anzidei, *Rome*
Filippo F Angileri, *Messinas*
Stefano Arcangeli, *Rome*
Roberto Azzoni, *San Donato milanese*
Tommaso V Bartolotta, *Palermo*
Tommaso Bartalena, *Imola*
Livia Bernardin, *San Bonifacio*
Federico Boschi, *Verona*
Sergio Casciaro, *Lecce*
Emanuele Casciani, *Rome*
Musa M Can, *Napoli*
Alberto Cuocolo, *Napoli*
Michele Ferrara, *Coppito*
Mauro Feola, *Fossano*
Giampiero Francica, *Castel Volturno*
Luigi De Gennaro, *Rome*
Giulio Giovannetti, *Pisa*
Francesca Iacobellis, *Napoli*
Formato Invernizzi, *Monza Brianza*
Francesco Lassandro, *Naples*
Lorenzo Livi, *Florence*
Pier P Mainenti, *Napoli*
Laura Marzetti, *Chieti*
Giuseppe Malinverni, *Crescentino*
Enrica Milanesi, *Turin*
Giovanni Morana, *Treviso*
Lorenzo Monti, *Milan*
Silvia D Morbelli, *Genoa*
Barbara Palumbo, *Perugia*
Cecilia Parazzini, *Milan*
Stefano Pergolizzi, *Messina*
Antonio Pinto, *Naples*
Camillo Porcaro, *Rome*
Carlo C Quattrocchi, *Rome*
Alberto Rebonato, *Perugia*
Giuseppe Rizzo, *Rome*
Roberto De Rosa, *Naples*
Domenico Rubello, *Rovigo*
Andrea Salvati, *Bari*
Sergio Sartori, *Ferrara*
Luca M Sconfienza, *Milano*
Giovanni Storto, *Rionero*
Nicola Sverzellati, *Parma*
Alberto S Tagliafico, *Genova*
Nicola Troisi, *Florence*

Japan

Yasuhiko Hori, *Chiba*
Hidetoshi Ikeda, *Koriyama*
Masahito Kawabori, *Sapporo*
Tamotsu Kamishima, *Sapporo*
Hiro Kiyosue, *Yufu*
Yasunori Minami, *Osaka-sayama*
Yasuhiro Morimoto, *Kitakyushu*
Satoru Murata, *Tokyo*
Shigeki Nagamachi, *Miyazaki*
Hiroshi Onishi, *Yamanashi*
Morio Sato, *Wakayama Shi*
Yoshito Tsushima, *Maebashi*
Masahiro Yanagawa, *Suita*

Netherlands

Willem Jan van Rooij, *Tilburg*

New Zealand

W Howell Round, *Hamilton*

Pakistan

Wazir Muhammad, *Abbottabad*

Poland

Maciej S Baglaj, *Wroclaw*

Piotr Czauderna, *Gdansk*

Portugal

Joao Manuel RS Tavares, *Porto*

Serbia

Olivera Ciraj-Bjelac, *Belgrade*

Singapore

Gopinathan Anil, *Singapore*
Terence KB Teo, *Singapore*
Cher Heng Tan, *Singapore*

Slovakia

Stefan Sivak, *Martin*

South Korea

Ki Seok Choo, *Busan*
Seung Hong Choi, *Seoul*
Dae-Seob Choi, *Jinju*
Hong-Seok Jang, *Seoul*
Yong Jeong, *Daejeon*
Chan Kyo Kim, *Seoul*
Se Hyung Kim, *Seoul*
Joong-Seok Kim, *Seoul*
Sang Eun Kim, *Seongnam*
Sung Joon Kwon, *Seoul*
Jeong Min Lee, *Seoul*
In Sook Lee, *Busan*
Noh Park, *Goyang*
Chang Min Park, *Seoul*
Sung Bin Park, *Seoul*
Deuk Jae Sung, *Seoul*
Choongsoo Shin, *Seoul*
Kwon-Ha Yoon, *Iksan*

Spain

Miguel A De Gregorio, *Zaragoza*
Antonio Luna, *Jaén*
Enrique Marco de Lucas, *Santander*
Fernando Ruiz Santiago, *Granada*

Sweden

Dmitry Grishenkov, *Stockholm*
Tie-Qiang Li, *Stockholm*

Switzerland

Nicolau Beckmann, *Basel*
Christian Boy, *Bern*
Giorgio Treglia, *Bellinzona*

Stephan Ulmer, *Kiel*

Thailand

Sirianong Namwongprom, *Chiang Mai*

Turkey

Kubilay Aydin, *Istanbul*
Ramazan Akdemir, *Sakarya*
Serhat Avcu, *Ankara*
Ayse Aralasmak, *Istanbul*
Oktay Algin, *Ankara*
Nevbahar Akcar, *Meselik*
Bilal Battal, *Ankara*
Zulkif Bozgeyik, *Elazig*
Nazan Ciledag, Aakara
Fuldem Y Donmez, *Ankara*
Gulgun Engin, *Istanbul*
Ahmet Y Goktay, *Izmir*
Oguzhan G Gumustas, *Bursa*
Kaan Gunduz, *Ankara*
Pelin Ozcan Kara, *Mersin*
Kivanc Kamburoglu, *Ankara*
Ozgur Kilickesmez, *Istanbul*
Furuzan Numan, *Istanbul*
Cem Onal, *Adana*
Ozgur Oztekin, *Izmir*
Seda Ozbek (Boruban), *Konya*
Selda Sarikaya, *Zonguldak*
Figen Taser, *Kutahya*
Baran Tokar, *Eskisehir*
Ender Uysal, *Istanbul*
Ensar Yekeler, *Istanbul*

United Kingdom

Indran Davagnanam, *London*
M DC Valdés Hernández, *Edinburgh*
Alan Jackson, *Manchester*
Suneil Jain, *Belfast*
Long R Jiao, *London*
Miltiadis Krokidis, *Cambridge*
Pradesh Kumar, *Liverpool*
Peter D Kuzmich, *Derby*
Georgios Plataniotis, *Brighton*
Vanessa Sluming, *Liverpool*

United States

Garima Agrawal, *Saint Louis*
James R Brasic, *Baltimore*
Rajendra D Badgaiyan, *Buffalo*
Ulas Bagci, *Bethesda*
Anat Biegon, *Stony Brook*
Ramon Casanova, *Winston Salem*
Wenli Cai, *Boston*
Zheng Chang, *Durham*
Corey J Chakarun, *Long Beach*
Kai Chen, *Los Angeles*
Hyun-Soon Chong, *Chicago*
Marco Cura, *Dallas*
Ravi R Desai, *Bensalem*
Delia DeBuc, *Miami*
Carlo N De Cecco, *Charleston*
Timm-Michael L Dickfeld, *Baltimore*
Subba R Digumarthy, *Boston*
Huy M Do, *Stanford*
Todd A Faasse, *Grand Rapids*
Salomao Faintuch, *Boston*
Girish M Fatterpekar, *New York*
Dhakshinamoorthy Ganeshan, *Houston*
Robert J Griffin, *Little Rock*
Andrew J Gunn, *Boston*
Sandeep S Hedgire, *Boston*
Timothy J Hoffman, *Columbia*
Mai-Lan Ho, *San Francisco*
Juebin Huang, *Jackson*
Abid Irshad, *Charleston*
Matilde Inglese, *New York*
El-Sayed H Ibrahim, *Jacksonville*
Paul R Julsrud, *Rochester*
Pamela T Johnson, *Baltimore*
Ming-Hung Kao, *Tempe*
Sunil Krishnan, *Houston*
Richard A Komoroski, *Cincinnati*
Sandi A Kwee, *Honolulu*
King Kim, *Ft. Lauderdale*
Guozheng Liu, *Worcester*
Yiyan Liu, *Newark*
Venkatesh Mani, *New York*
Lian-Sheng Ma, *Pleasanton*
Rachna Madan, *Boston*
Zeyad A Metwalli, *Houston*
Yilong Ma, *Manhasset*
Hui Mao, *Atlanta*
Feroze B Mohamed, *Philadelphia*
Gul Moonis, *Boston*
John L Nosher, *New Brunswick*
Rahmi Oklu, *Boston*
Aytekin Oto, *Chicago*
Bishnuhari Paudyal, *Philadelphia*
Rajul Pandya, *Youngstown*
Chong-Xian Pan, *Sacramento*
Jay J Pillai, *Baltimore*
Neal Prakash, *Duarte*
Reza Rahbar, *Boston*
Ali S Raja, *Boston*
Gustavo J Rodriguez, *El Paso*
David J Sahn, *Portlsand*
Steven Schild, *Scottsdale*
Ali R Sepahdari, *Los Angeles*
Li Shen, *Indianapolis*
JP Sheehan, *Charlottesville*
Atul B Shinagare, *Boston*
Sarabjeet Singh, *Boston*
Charles J Smith, *Columbia*
Kenji Suzuki, *Chicago*
Monvadi Srichai-Parsia, *Washington*
Sree H Tirumani, *Boston*
Hebert A Vargas, *New York*
Sachit Verma, *Philadelphia*
Yoichi Watanabe, *Minneapolis*
Li Wang, *Chapel Hill*
Carol C Wu, *Boston*
Shoujun Xu, *Houston*
Min Yao, *Cleveland*
Xiaofeng Yang, *Atlanta*
Qingbao Yu, *Albuquerque*
Aifeng Zhang, *Chicago*
Chao Zhou, *Bethlehem*
Hongming Zhuang, *Philadelphia*

WJR World Journal of Radiology

Contents

Monthly Volume 9 Number 5 May 28, 2017

NAME OF JOURNAL
World Journal of Radiology

ISSN
ISSN 1949-8470 (online)

LAUNCH DATE
January 31, 2009

FREQUENCY
Monthly

EDITORIAL OFFICE
Xiu-Xia Song, Director
World Journal of Radiology
Baishideng Publishing Group Inc
7901 Stoneridge Drive, Suite 501, Pleasanton, CA 94588, USA
Telephone: +1-925-2238242
Fax: +1-925-2238243
E-mail: editorialoffice@wjgnet.com
Help Desk: http://www.f6publishing.com/helpdesk
http://www.wjgnet.com

PUBLISHER
Baishideng Publishing Group Inc
7901 Stoneridge Drive, Suite 501,
Pleasanton, CA 94588, USA
Telephone: +1-925-2238242
Fax: +1-925-2238243
E-mail: bpgoffice@wjgnet.com
Help Desk: http://www.f6publishing.com/helpdesk
http://www.wjgnet.com

PUBLICATION DATE
May 28, 2017

INSTRUCTIONS TO AUTHORS
http://www.wjgnet.com/bpg/gerinfo/204

ONLINE SUBMISSION
http://www.f6publishing.com

World Journal of Radiology

Submit a Manuscript: http://www.f6publishing.com

World J Radiol 2017 May 28; 9(5): 217-222

DOI: 10.4329/wjr.v9.i5.217

ISSN 1949-8470 (online)

MINIREVIEWS

Diffusion weighted imaging for the detection and evaluation of cholesteatoma

Benjamin Henninger, Christian Kremser

Benjamin Henninger, Christian Kremser, Department of Radiology, Medical University of Innsbruck, 6020 Innsbruck, Austria

Author contributions: Henninger B wrote the paper; Kremser C performed proofreading and wrote the physical part.

Conflict-of-interest statement: Authors declare no conflict of interests for this article.

Manuscript source: Invited manuscript

Correspondence to: Dr. Benjamin Henninger, PD, Department of Radiology, Medical University of Innsbruck, Anichstraße 35, 6020 Innsbruck, Austria. benjamin.henninger@i-med.ac.at
Telephone: +43-512-50480914
Fax: +43-512-50422758

Received: October 28, 2016
Peer-review started: November 2, 2016
First decision: February 15, 2017
Revised: February 23, 2017
Accepted: March 12, 2017
Article in press: March 13, 2017
Published online: May 28, 2017

Abstract

Cholesteatoma is a collection of keratinous debris and stratified squamous epithelium. It is trapped in the middle ear and can lead to bony erosion. The disease is treated surgically often followed by a second-look procedure to check for residual tissue or recurrence. Cholesteatoma has specific signal-intensity characteristics on magnetic resonance imaging with very high signal intensity on diffusion weighted imaging (DWI). Various DWI techniques exist: Echo-planar imaging (EPI)-based and non-EPI-based techniques as well as new approaches like multi-shot EPI DWI. This article summarizes all techniques, discusses the significance in detecting cholesteatoma and mentions actual studies. Further recommendations for daily clinical practise are provided.

Key words: Cholesteatoma; Diffusion weighted imaging; Computed tomography; Magnetic resonance imaging; Echo-planar imaging; Non-echo-planar imaging

Core tip: Imaging cholesteatoma is either performed by computed tomography (CT) or by magnetic resonance imaging (MRI). CT is the method of choice for detection and for assessing exact location and extent. MRI with diffusion weighted imaging (DWI) is a powerful tool for the detection of local recurrence or residual cholesteatoma. Many DWI-techniques are available today; this review article gives an overview of the different sequences and the diagnostic procedure when using DWI with a clinical focus.

Henninger B, Kremser C. Diffusion weighted imaging for the detection and evaluation of cholesteatoma. *World J Radiol* 2017; 9(5): 217-222 Available from: URL: http://www.wjgnet.com/1949-8470/full/v9/i5/217.htm DOI: http://dx.doi.org/10.4329/wjr.v9.i5.217

INTRODUCTION

Cholesteatomas are defined as enlarging collections of keratinous debris within a sack of stratified squamous

epithelium trapped in the middle ear[1]. It is a common inflammatory disease that grows progressively as the debris increases. It is seen as a kind of chronic otitis media with cell proliferation due to repeated inflammation or for congenital reason. Clinically the complications of cholesteatoma are related to bony erosion and destruction which is thought to be related to mechanical pressure. Evan small cholesteatoma can cause ossicular chain erosions with the threat of a conductive hearing loss. The diagnosis is usually made on clinical features.

Cholesteatomas of the middle ear are managed by surgery, generally with complete excision of the lesion with tympanoplasty or radical or modified radical mastoidectomy. This is often followed by a second-look procedure performed to check for residual or recurrent disease. This second-look is conducted 6-18 mo after the initial operation because most recur within the first 2 postoperative years, with 60% occurring during the first year after surgery[2,3]. The second-look surgery is mainly to assess residual or recurrent disease because both cannot adequately be diagnosed solely by clinical examination[4].

COMPUTED TOMOGRAPHY

Computed tomography (CT) of the temporal bone is widely accepted to detect or confirm cholesteatoma and to assess the extension, the exact location and possible complications of the disease. Therefore it is mandatory for the initial preoperative description of the extent of cholesteatoma and for correct surgical planning. CT is further recommended for the evaluation of recurrent disease but it is not reliable when the postoperative, formed cavity is completely filled with a soft-tissue mass or partially filled with nonspecific imaging abnormalities[5,6]. This can be caused by recurrent cholesteatoma, granulation or fibrous tissue. This differential diagnosis is important since recurrent cholesteatoma needs middle ear surgery but there is no need for surgery if only granulation tissue is detected.

MAGNETIC RESONANCE IMAGING

Magnetic resonance imaging (MRI) has several advantages over CT in detecting recurrent or residual disease: Beside delayed contrast-enhanced T1-weighted spin-echo (SE) imaging[7], diffusion weighted imaging (DWI) shows promising results in the data published so far[8-12]. Contrast-enhanced MRI can discriminate between the non-enhancing cholesteatoma and other contrast-enhancing findings, *e.g.*, inflammation, scar or granulation tissue[7,13]. DWI is more practical with a shorter examination time than delayed contrast material-enhanced imaging; there is also no need for contrast injection. The technique relies on the principles of the Brownian motion of water molecules[14]. Cholesteatomas appear hyperintens on DWI obtained with b-factors of 800 or 1000 s/mm^2 where the b-factor is a measure of the strength of the respective diffusion weighting. This visual characteristic is similar to a histologically identical lesion, the epidermoid cyst[15] - granulation tissue, fibrous tissue, cholesterol granuloma or serous fluid, on the other hand, have low signal intensity on DWI (at a b-factor of 800 s/mm^2). Visual assessment of DWI images obtained with a b-factor of 800 s/mm^2 without calculation of the apparent diffusion coefficient (ADC) is sufficient for the respective diagnostic analysis[9,12]. The reason for the high signal intensity is assumed to be due to a T2 shine-through effect or due to the restricted molecular diffusion of cholesteatoma. The T2 shine-through effect is observed in lesions with a prolonged relaxation time. Nevertheless, the real reason for the increased signal intensity on DWI is still unknown and under discussion in literature. DWI is a valuable tool to prevent unnecessary second-look surgeries in patients suspected for cholesteatomas and is therefore a reliable alternative to CT[16]. However, numerous artefacts can be generated during the acquisition of DWI, as, *e.g.*, susceptibility artefacts, motion artefacts, ghosting artefacts and eddy current artefacts with the risk of false positive results[17].

So far a variety of different DWI-techniques has been used, which basically can be divided into echo-planar imaging (EPI)-based and non-EPI-based techniques. The choice of the actually used technique is thereby mainly influenced by the fact that imaging has to be performed near the scull base where problems due to different artefacts (*e.g.*, motion, field inhomogeneities) can occur.

In addition DWI MRI is extremely useful for the assessment of possible complications such as erosion of the semicircular canal or invasion of the membranous labyrinth or the middle cranial fossa and to assess abscess formations[17].

EPI-DWI

Single-shot (SS) EPI-DWI can be seen as a widely available standard DWI technique. It is relatively insensitive to motion but prone to susceptibility artefacts, chemical shift and geometric distortion[14]. These artefacts can mask areas of restricted diffusion in a cholesteatoma[18]. A further limitation of EPI-DWI is its low spatial resolution and relatively thick sections. The size limit to detect a cholesteatoma with EPI-DWI is approximately 5 mm[9,11].

Non-EPI-DWI

Turbo spin-echo (TSE)-based DWI is a spin-echo based SS or multi-shot (MS) technique with longer echo time and a higher signal-to-noise ratio than SS EPI-DWI. The sequence is known to lack significant image distortions and it does not show the susceptibility artefacts that are observed with standard EPI-DWI. Therefore a better spatial resolution in the middle ear is possible and it permits fast multiplanar imaging[19]. Furthermore thinner slices can be obtained than with EPI-sequences. This so called non-EPI sequence has therefore hardly any false-positive findings. False-negative findings are mostly a consequence of motion or empty retraction pockets[20].

The signal intensity of other postoperative findings has been reported much lower than that of residual and/or recurrent cholesteatoma[19,21].

In a study by Geoffray *et al*[22] non-EPI DWI was reliable to diagnose recurrent cholesteatoma also in children with a high sensitivity (87%) and specificity (71%). Nevertheless, they concluded that follow-up must be prolonged because small recurrence less than 5 mm may be missed.

The TSE-DWI can be combined with half-Fourier acquisition single-shot turbo spin-echo (HASTE), a single-shot technique with excellent motion insensitivity. HASTE is also less prone to susceptibility artefacts and geometric distortion than the EPI-Sequence[23,24]. The sensitivity and specificity of non-EPI DWI in depicting residual or recurrent cholesteatoma is very high, in literature it is between 90%-100% and also postulated higher than with EPI DWI[19-21,23-25]. The study by De Foer *et al*[25] prospectively evaluated a SS TSE-DWI sequence in detecting cholesteatoma with evaluation of the size of the middle ear cholesteatoma. They found 21 middle ear cholesteatomas at surgery with a size between 2 mm and 19 mm and 19/21 could be detected with DWI. Years later another study by De Foer *et al*[26] compared non-EPI DWI, delayed gadolinium-enhanced T1-weighted MRI and the combination of both techniques in the evaluation of patients with cholesteatoma. Sensitivity and specificity was 56.7%/67.6% with the delayed gadolinium-enhanced T1-weigthed images, 82.6%/87.2% with the non-EPI DWI images and 84.2%/88.2% for the combination of both kinds of images. They concluded that for the detection of cholesteatoma non-EPI DWI can be used alone.

Non-EPI sequences with periodically rotated overlapping parallel lines with enhanced reconstruction (PROPELLER, GE Medical Systems, Milwaukee, Wisconsin/ BLADE, Siemens Medical Solutions, Erlangen, Germany) have been reported as useful in avoiding geometric distortions. The k-space data are acquired in the form of rotating sections (blades). The resulting oversampling of the central k-space leads to an improved signal-to-noise ratio (SNR) and to the reduction of motion and susceptibility artefacts[23,27,28]. MS TSE-based DWI increases sensitivity, specificity and diagnostic accuracy compared to conventional single-shot EPI DWI[29].

In a systematic review of DWI in the assessment of postoperative cholesteatoma by Jindal *et al*[30] a combined sensitivity of 91.4% and positive predictive value of 97.3% was calculated for the non-EPI sequences. Non-EPI also showed a negative predictive value of 85% which means that it is very useful in avoiding second-look operations in healthy ears[30].

MS EPI DWI

Recently it has been shown that an improved, MS EPI approach can provide high-resolution DWI with reduced geometric distortions, however, with longer imaging time[31-33]. Readout-segmented echo-planar (RESOLVE) DWI is a new approach for obtaining DWI images with high quality delivering sharp images at high spatial resolution and reduced slice thickness. Therefore it is possible to detect even small cholesteatomas. It uses the same diffusion preparation as SS EPI. By dividing the k-space trajectory into multiple segments in the phase encoding direction TE can be reduced to increase the quality of the acquired images. Further RESOLVE DWI is largely free of distortions, susceptibility and T2* blurring artefacts. As we mentioned before non-EPI seems to be superior to the EPI techniques in diagnosing recurrent or residual cholesteatoma, however, at the time of the systematic review by Jindal *et al*[30] the RESOLVE technique was not yet available. To date there are only few studies that evaluated this new approach, however, with promising results[31]. In our daily clinical routine RESOLVE has been proven as a robust and reliable approach for the detection of recurrent cholesteatoma.

DWI FOR THE DAILY CLINICAL PRACTISE

DWI is a powerful tool that can replace CT and delayed gadolinium enhanced T1-weighted sequences. At our department and others contrast agent is not used anymore[26]. The best approach is to use non-EPI sequences or (if available) newer EPI-techniques as RESOLVE which provides high resolution and allows thinner slice-thickness. Single-shot EPI-DWI techniques are not recommended as they can provide false positive results due to artefacts. Further anatomical sequences (T1- and T2-weighted) should be added in coronal and/or axial orientation to better localize suspected lesions. Our department uses an axial T1 und T2 TSE sequence and a coronal T2 TSE sequence with fat-saturation. The fat saturation can help to detect fatty content of any detected lesion or structure. These sequences can also help to differentiate, *e.g.*, the characteristic T1 hyperintensity of cholesterol granuloma. Dremmen *et al*[20] suggested to use conventional sequences to decrease the risk of misdiagnosis because transplanted fat within a postoperative cavity may show increased signal on DWI. Slice-thickness for the DWI (and its corresponding anatomical T1- or T2-weighted sequence) should not exceed 3 mm. If available, coloured image-fusion of DWI and anatomic sequences helps to better demonstrate the findings to patients or clinicians. On the basis of the findings by Steens *et al*[34] repeated follow-up DWI after surgery of cholesteatoma is recommended. Their study showed an evidence of cholesteatoma in 31% of the patients on repeated follow-up DWI.

For the interpretation of DWI the reporting radiologist should look for hyperintense lesions on high b-values (800 or 1000 s/mm^2), ADC-values should not be taken into the diagnostic decision as cholesteatomas can be hyperintense in ADC because of the T2 shine-through effect. If a lesion is detected the next step should be an anatomical correlation and signal interpretation on T1- and T2-contrast. This minimizes false positive results.

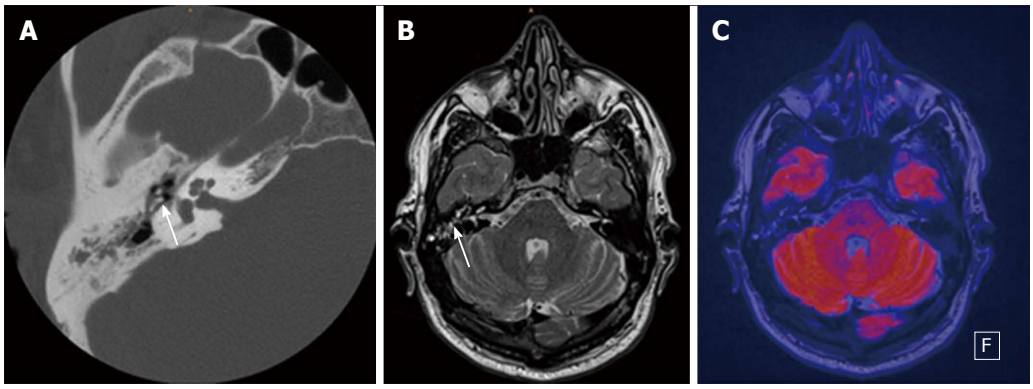

Figure 1 Thirty-nine-year-old male patient with clinically suspected cholesteatoma in the right middle ear. A: Axial CT of the temporal bone with soft-tissue mass in the tympanic space adjacent to malleolus and incus (white arrow); B: Axial T2-weighted MR depicts fluid-like signal in the tympanic space (white arrow); C: Fused axial T2-weighted image and axial EPI DWI RESOLVE without any sign of restriction. Therefore there is no evidence of cholesteatoma; the findings are consistent with chronic otitis media. CT: Computed tomography; DWI: Diffusion weighted imaging; EPI: Echo-planar imaging; RESOLVE: Readout-segmented echo-planar.

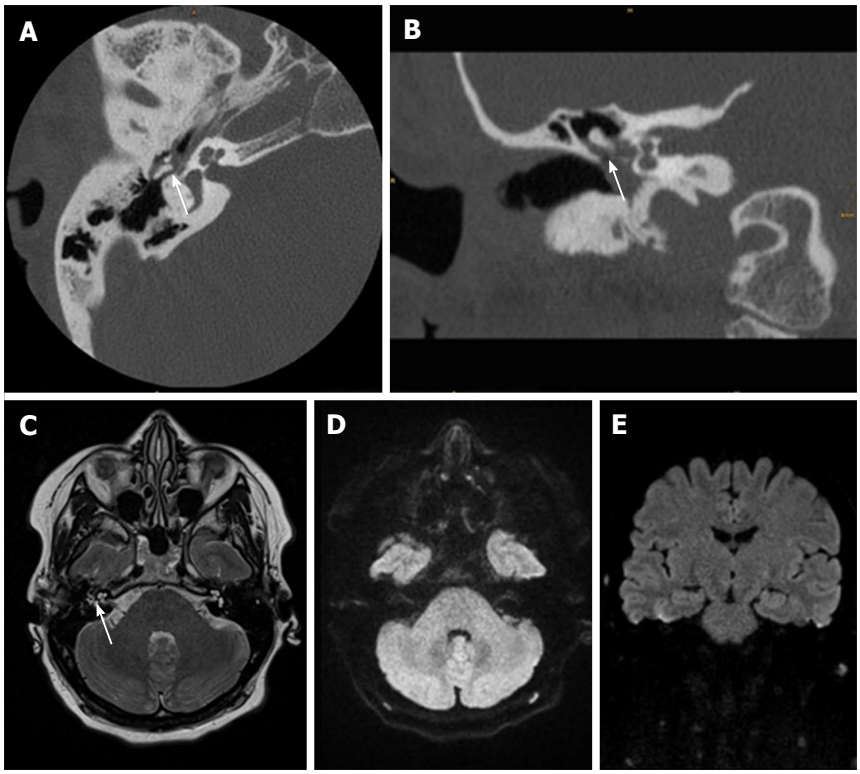

Figure 2 Thirty-one-year-old female after surgery for cholesteatoma. A, B: CT show a soft-tissue mass in the tympanic space adjacent to malleolus and scutum with suspected bony erosion (white arrow); C-E: Axial T2 weighted image shows fluid-like signal (white arrow) that has no restriction in EPI DWI RESOLVE (axial in D and coronal in E). There was no sign of recurrent cholesteatoma on follow-up surgery. CT: Computed tomography; DWI: Diffusion weighted imaging; EPI: Echo-planar imaging; RESOLVE: Readout-segmented echo-planar.

Clinical examples are provided in Figures 1-3.

CONCLUSION

In conclusion, MRI with DWI can prevent unnecessary revision surgery in patients who are suspected of having recurrent or residual disease. Many techniques exist but non-EPI DWI and new MS EPI approaches (RESOLVE) are recommended to avoid false positive results due to different artefacts. The interpretation is simple but additional anatomical sequences are needed for exact localisation and differential diagnosis.

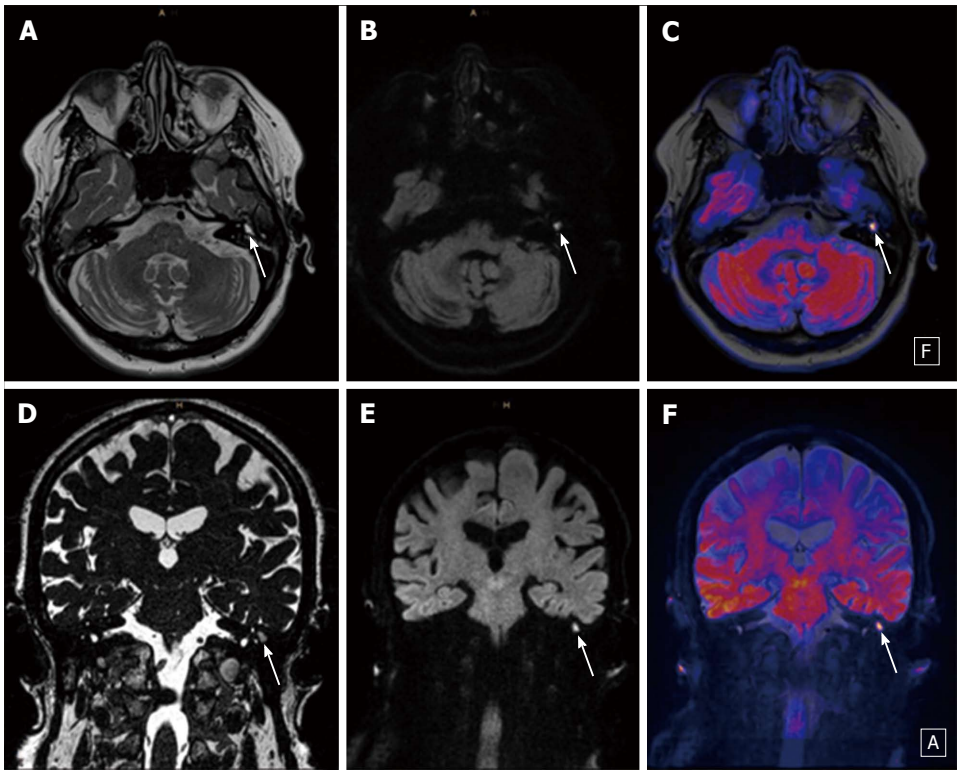

Figure 3 Twenty-three-year-old male patient with a typical cholesteatoma detected with diffusion weighted imaging. A, D: T2 weighted images (A and D) show a fluid-like mass in the left middle ear (white arrow); B, C, E, F: EPI DWI RESOLVE (B and E) depict a hyperintense signal (white arrow) consistent with restriction due to a small cholesteatoma that is better demonstrated on fused images (C and F). DWI: Diffusion weighted imaging; EPI: Echo-planar imaging; RESOLVE: Readout-segmented echo-planar.

REFERENCES

1 **Swartz JD**. Cholesteatomas of the middle ear. Diagnosis, etiology, and complications. *Radiol Clin North Am* 1984; **22**: 15-35 [PMID: 6709867]

2 **Shelton C**, Sheehy JL. Tympanoplasty: review of 400 staged cases. *Laryngoscope* 1990; **100**: 679-681 [PMID: 2362526 DOI: 10.1288/00005537-199007000-00001]

3 **Gyo K**, Sasaki Y, Hinohira Y, Yanagihara N. Residue of middle ear cholesteatoma after intact canal wall tympanoplasty: surgical findings at one year. *Ann Otol Rhinol Laryngol* 1996; **105**: 615-619 [PMID: 8712631]

4 **Yiğiter AC**, Pınar E, İmre A, Erdoğan N. Value of Echo-Planar Diffusion-Weighted Magnetic Resonance Imaging for Detecting Tympanomastoid Cholesteatoma. *J Int Adv Otol* 2015; **11**: 53-57 [PMID: 26223719 DOI: 10.5152/iao.2015.447]

5 **Williams MT**, Ayache D. Imaging of the postoperative middle ear. *Eur Radiol* 2004; **14**: 482-495 [PMID: 14749948 DOI: 10.1007/s00330-003-2198-8]

6 **Blaney SP**, Tierney P, Oyarazabal M, Bowdler DA. CT scanning in "second look" combined approach tympanoplasty. *Rev Laryngol Otol Rhinol* (Bord) 2000; **121**: 79-81 [PMID: 10997063]

7 **Williams MT**, Ayache D, Alberti C, Héran F, Lafitte F, Elmaleh-Bergès M, Piekarski JD. Detection of postoperative residual cholesteatoma with delayed contrast-enhanced MR imaging: initial findings. *Eur Radiol* 2003; **13**: 169-174 [PMID: 12541126 DOI: 10.1007/s00330-002-1423-1]

8 **Fitzek C**, Mewes T, Fitzek S, Mentzel HJ, Hunsche S, Stoeter P. Diffusion-weighted MRI of cholesteatomas of the petrous bone. *J Magn Reson Imaging* 2002; **15**: 636-641 [PMID: 12112513 DOI: 10.1002/jmri.10118]

9 **Aikele P**, Kittner T, Offergeld C, Kaftan H, Hüttenbrink KB, Laniado M. Diffusion-weighted MR imaging of cholesteatoma in pediatric and adult patients who have undergone middle ear surgery. *AJR Am J Roentgenol* 2003; **181**: 261-265 [PMID: 12818870 DOI: 10.2214/ajr.181.1.1810261]

10 **Maheshwari S**, Mukherji SK. Diffusion-weighted imaging for differentiating recurrent cholesteatoma from granulation tissue after mastoidectomy: case report. *AJNR Am J Neuroradiol* 2002; **23**: 847-849 [PMID: 12006291]

11 **Vercruysse JP**, De Foer B, Pouillon M, Somers T, Casselman J, Offeciers E. The value of diffusion-weighted MR imaging in the diagnosis of primary acquired and residual cholesteatoma: a surgical verified study of 100 patients. *Eur Radiol* 2006; **16**: 1461-1467 [PMID: 16514469 DOI: 10.1007/s00330-006-0160-2]

12 **Bergui M**, Zhong J, Bradac GB, Sales S. Diffusion-weighted images of intracranial cyst-like lesions. *Neuroradiology* 2001; **43**: 824-829 [PMID: 11688697]

13 **Lemmerling MM**, De Foer B, VandeVyver V, Vercruysse JP, Verstraete KL. Imaging of the opacified middle ear. *Eur J Radiol* 2008; **66**: 363-371 [PMID: 18339504 DOI: 10.1016/j.ejrad.2008.01.020]

14 **Bammer R**. Basic principles of diffusion-weighted imaging. *Eur J Radiol* 2003; **45**: 169-184 [PMID: 12595101]

15 **Chen S**, Ikawa F, Kurisu K, Arita K, Takaba J, Kanou Y. Quantitative MR evaluation of intracranial epidermoid tumors by fast fluid-attenuated inversion recovery imaging and echo-planar diffusion-weighted imaging. *AJNR Am J Neuroradiol* 2001; **22**: 1089-1096 [PMID: 11415903]

16 **Cimsit NC**, Cimsit C, Baysal B, Ruhi IC, Ozbilgen S, Aksoy EA. Diffusion-weighted MR imaging in postoperative follow-up: reliability for detection of recurrent cholesteatoma. *Eur J Radiol* 2010; **74**: 121-123 [PMID: 19231123 DOI: 10.1016/j.ejrad.2009.01.025]

17 **De Foer B**, Vercruysse JP, Pilet B, Michiels J, Vertriest R, Pouillon M, Somers T, Casselman JW, Offeciers E. Single-shot, turbo spin-echo, diffusion-weighted imaging versus spin-echo-planar, diffusion-weighted imaging in the detection of acquired middle ear cholesteatoma. *AJNR Am J Neuroradiol* 2006; **27**: 1480-1482

[PMID: 16908562]
18 **Attenberger UI**, Runge VM, Stemmer A, Williams KD, Naul LG, Michaely HJ, Schoenberg SO, Reiser MF, Wintersperger BJ. Diffusion weighted imaging: a comprehensive evaluation of a fast spin echo DWI sequence with BLADE (PROPELLER) k-space sampling at 3 T, using a 32-channel head coil in acute brain ischemia. *Invest Radiol* 2009; **44**: 656-661 [PMID: 19724235 DOI: 10.1097/RLI.0b013e3181af3f0e]
19 **Dubrulle F**, Souillard R, Chechin D, Vaneecloo FM, Desaulty A, Vincent C. Diffusion-weighted MR imaging sequence in the detection of postoperative recurrent cholesteatoma. *Radiology* 2006; **238**: 604-610 [PMID: 16304085 DOI: 10.1148/radiol.2381041649]
20 **Dremmen MH**, Hofman PA, Hof JR, Stokroos RJ, Postma AA. The diagnostic accuracy of non-echo-planar diffusion-weighted imaging in the detection of residual and/or recurrent cholesteatoma of the temporal bone. *AJNR Am J Neuroradiol* 2012; **33**: 439-444 [PMID: 22194383 DOI: 10.3174/ajnr.A2824]
21 **Dhepnorrarat RC**, Wood B, Rajan GP. Postoperative non-echo-planar diffusion-weighted magnetic resonance imaging changes after cholesteatoma surgery: implications for cholesteatoma screening. *Otol Neurotol* 2009; **30**: 54-58 [PMID: 19092558 DOI: 10.1097/MAO.0b013e31818edf4a]
22 **Geoffray A**, Guesmi M, Nebbia JF, Leloutre B, Bailleux S, Maschi C. MRI for the diagnosis of recurrent middle ear cholesteatoma in children--can we optimize the technique? Preliminary study. *Pediatr Radiol* 2013; **43**: 464-473 [PMID: 23160645 DOI: 10.1007/s00247-012-2502-3]
23 **Schwartz KM**, Lane JI, Bolster BD, Neff BA. The utility of diffusion-weighted imaging for cholesteatoma evaluation. *AJNR Am J Neuroradiol* 2011; **32**: 430-436 [PMID: 20488909 DOI: 10.3174/ajnr.A2129]
24 **De Foer B**, Vercruysse JP, Bernaerts A, Deckers F, Pouillon M, Somers T, Casselman J, Offeciers E. Detection of postoperative residual cholesteatoma with non-echo-planar diffusion-weighted magnetic resonance imaging. *Otol Neurotol* 2008; **29**: 513-517 [PMID: 18520587 DOI: 10.1097/MAO.0b013e31816c7c3b]
25 **De Foer B**, Vercruysse JP, Bernaerts A, Maes J, Deckers F, Michiels J, Somers T, Pouillon M, Offeciers E, Casselman JW. The value of single-shot turbo spin-echo diffusion-weighted MR imaging in the detection of middle ear cholesteatoma. *Neuroradiology* 2007; **49**: 841-848 [PMID: 17768611 DOI: 10.1007/s00234-007-0268-3]
26 **De Foer B**, Vercruysse JP, Bernaerts A, Meersschaert J, Kenis C, Pouillon M, De Beuckeleer L, Michiels J, Bogaerts K, Deckers F, Somers T, Hermans R, Offeciers E, Casselman JW. Middle ear cholesteatoma: non-echo-planar diffusion-weighted MR imaging versus delayed gadolinium-enhanced T1-weighted MR imaging--value in detection. *Radiology* 2010; **255**: 866-872 [PMID: 20501723 DOI: 10.1148/radiol.10091140]
27 **Forbes KP**, Pipe JG, Karis JP, Heiserman JE. Improved image quality and detection of acute cerebral infarction with PROPELLER diffusion-weighted MR imaging. *Radiology* 2002; **225**: 551-555 [PMID: 12409594 DOI: 10.1148/radiol.2252011479]
28 **Más-Estellés F**, Mateos-Fernández M, Carrascosa-Bisquert B, Facal de Castro F, Puchades-Román I, Morera-Pérez C. Contemporary non-echo-planar diffusion-weighted imaging of middle ear cholesteatomas. *Radiographics* 2012; **32**: 1197-1213 [PMID: 22787002 DOI: 10.1148/rg.324115109]
29 **Elefante A**, Cavaliere M, Russo C, Caliendo G, Marseglia M, Cicala D, Piccolo D, Di Lullo A, Brunetti L, Palma A, Iengo M, Brunetti A. Diffusion weighted MR imaging of primary and recurrent middle ear cholesteatoma: an assessment by readers with different expertise. *Biomed Res Int* 2015; **2015**: 597896 [PMID: 25722983 DOI: 10.1155/2015/597896]
30 **Jindal M**, Riskalla A, Jiang D, Connor S, O'Connor AF. A systematic review of diffusion-weighted magnetic resonance imaging in the assessment of postoperative cholesteatoma. *Otol Neurotol* 2011; **32**: 1243-1249 [PMID: 21921855 DOI: 10.1097/MAO.0b013e31822e938d]
31 **Yamashita K**, Yoshiura T, Hiwatashi A, Kamano H, Dashjamts T, Shibata S, Tamae A, Honda H. Detection of middle ear cholesteatoma by diffusion-weighted MR imaging: multishot echo-planar imaging compared with single-shot echo-planar imaging. *AJNR Am J Neuroradiol* 2011; **32**: 1915-1918 [PMID: 21778245 DOI: 10.3174/ajnr.A2651]
32 **Skare S**, Newbould RD, Clayton DB, Albers GW, Nagle S, Bammer R. Clinical multishot DW-EPI through parallel imaging with considerations of susceptibility, motion, and noise. *Magn Reson Med* 2007; **57**: 881-890 [PMID: 17457876 DOI: 10.1002/mrm.21176]
33 **Flook E**, Izzat S, Ismail A. Cholesteatoma imaging using modified echo-planar diffusion-weighted magnetic resonance imaging. *J Laryngol Otol* 2011; **125**: 10-12 [PMID: 20831846 DOI: 10.1017/S0022215110001805]
34 **Steens S**, Venderink W, Kunst D, Meijer A, Mylanus E. Repeated Postoperative Follow-up Diffusion-weighted Magnetic Resonance Imaging to Detect Residual or Recurrent Cholesteatoma. *Otol Neurotol* 2016; **37**: 356-361 [PMID: 26905824 DOI: 10.1097/MAO.0000000000000985]

P- Reviewer: Lim SM **S- Editor**: Song XX **L- Editor**: A
E- Editor: Li D

World Journal of Radiology

Submit a Manuscript: http://www.f6publishing.com

World J Radiol 2017 May 28; 9(5): 223-229

DOI: 10.4329/wjr.v9.i5.223

ISSN 1949-8470 (online)

ORIGINAL ARTICLE

Basic Study

Correlation of lumbar lateral recess stenosis in magnetic resonance imaging and clinical symptoms

Annina Splettstößer, M Fawad Khan, Bernd Zimmermann, Thomas J Vogl, Hanns Ackermann, Marcus Middendorp, Adel Maataoui

Annina Splettstößer, Radprax MVZ, 40721 Hilden, Germany

M Fawad Khan, Bernd Zimmermann, Thomas J Vogl, Adel Maataoui, Institute for Diagnostic and Interventional Radiology, Goethe University, 60590 Frankfurt/Main, Germany

Hanns Ackermann, Institute of Biostatistics and Mathematical Modeling, Goethe University, 60590 Frankfurt/Main, Germany

Marcus Middendorp, Department of Nuclear Medicine, Goethe University, 60590 Frankfurt/Main, Germany

Author contributions: Middendorp M and Maataoui A contributed equally to this work; Maataoui A and Vogl TJ supervised the project; Splettstößer A, Middendorp M, and Maataoui A wrote the main paper; all authors were involved in the study design, data analysis, and discussion of the results at all stages.

Institutional review board statement: The study inclusive of patient information and consent form was reviewed and approved by the ethics committee of the State Authorisation Association for Medical Issues of Hessen, Germany (FF 48/2014). Patients were not required to give informed consent to the study because the analysis used anonymous clinical data that were obtained after each patient agreed to examination by written consent.

Conflict-of-interest statement: All authors ensure that there are no conflicts of interest.

Data sharing statement: Consent was not obtained but the presented data are anonymized and risk of identification is very low. No additional data are available.

Manuscript source: Invited manuscript

Correspondence to: Adel Maataoui, MD, Institute for Diagnostic and Interventional Radiology, Goethe University, Theodor-Stern-Kai 7, 60590 Frankfurt/Main, Germany. adel.maataoui@gmx.de
Telephone: +49-69-63015534
Fax: +49-69-63014222

Received: October 7, 2016
Peer-review started: October 14, 2016
First decision: November 11, 2016
Revised: February 22, 2017
Accepted: March 16, 2017
Article in press: March 17, 2017
Published online: May 28, 2017

Abstract

AIM

To assess the correlation of lateral recess stenosis (LRS) of lumbar segments L4/5 and L5/S1 and the Oswestry Disability Index (ODI).

METHODS

Nine hundred and twenty-seven patients with history of low back pain were included in this uncontrolled study. On magnetic resonance images (MRI) the lateral recesses (LR) at lumbar levels L4/5 and L5/S1 were evaluated and each nerve root was classified into a 4-point grading scale (Grade 0-3) as normal, not deviated, deviated or compressed. Patient symptoms and disability were assessed using ODI. The Spearman's rank correlation coefficient was used for statistical analysis ($P < 0.05$).

RESULTS

Approximately half of the LR revealed stenosis (grade 1-3; 52% at level L4/5 and 42% at level L5/S1) with 2.2% and 1.9% respectively reveal a nerve root compression.

The ODI score ranged from 0%-91.11% with an arithmetic mean of 34.06% ± 16.89%. We observed a very weak statistically significant positive correlation between ODI and LRS at lumbar levels L4/5 and L5/S1, each bilaterally (L4/5 left: rho < 0.105, P < 0.01; L4/5 right: rho < 0.111, P < 0.01; L5/S1 left: rho 0.128, P < 0.01; L5/S1 right: rho < 0.157, P < 0.001).

CONCLUSION

Although MRI is the standard imaging tool for diagnosing lumbar spinal stenosis, this study showed only a weak correlation of LRS on MRI and clinical findings. This can be attributed to a number of reasons outlined in this study, underlining that imaging findings alone are not sufficient to establish a reliable diagnosis for patients with LRS.

Key words: Low back pain; Lumbar spine; Magnetic resonance imaging; Lateral recess stenosis; Oswestry Disability Score; Lumbar spinal canal stenosis

Core tip: In the presented study lateral recesses of nearly 1000 patients with low back pain were evaluated on magnetic resonance imaging (MRI) and correlated with patient symptoms. Though MRI is the method of choice for diagnosing lumbar spinal stenosis, we revealed only a very weak correlation of lateral recess stenosis (LRS) and patient symptoms. This can be attributed to numerous reasons outlined in this study, underlining that imaging findings alone are not sufficient for an adequate diagnostic approach of patients with LRS.

Splettstößer A, Khan MF, Zimmermann B, Vogl TJ, Ackermann H, Middendorp M, Maataoui A. Correlation of lumbar lateral recess stenosis in magnetic resonance imaging and clinical symptoms. *World J Radiol* 2017; 9(5): 223-229 Available from: URL: http://www.wjgnet.com/1949-8470/full/v9/i5/223.htm DOI: http://dx.doi.org/10.4329/wjr.v9.i5.223

INTRODUCTION

After arthritis and rheumatism[1] low back pain (LBP) is the second most cause of disability in United States adults, and thus is a major social and economic issue[2]. With the aging population the prevalence is even drastically rising[3]. Lumbar spinal stenosis (LSS) is one main cause of LBP. As a distinct syndrome LSS was already described by Verbiest *et al*[4] in 1954. Most studies about LSS focus on the central LSS. Failure to recognize or adequately treat lateral recess stenosis (LRS) is considered to be the main reason for failed back surgery on the lumbar spine[5]. On account of this we focused on the LRS in the presented study. Regarding imaging analyses LSS is defined by the reduced size of the spinal canal. Based on the anatomical regions, LSS is generally subdivided in central spinal stenosis, LRS and foraminal stenosis. The LRS affects the lateral region of the lumbar spinal canal that is bordered laterally by the pedicle, posteriorly by the superior articular facet, and anteriorly by the vertebral body, endplate margin, and disc margin[6] (Figure 1). LRS is most commonly caused by degenerative changes of the spine such as facet joint osteoarthritis, ligamentum flavum hypertrophy, intervertebral disc degeneration and endplate spur. Congenital abnormalities, bone diseases, tumors or trauma are rare causes of LRS[7]. According to Bartynski *et al*[8] two pathways for the development of degenerative LRS exist. On the one hand the congenital or acquired trefoil canal in which the nerve root remains in its position in the LR and the narrowing of the LR developes in an anteroposterior fashion. Regarding the acquired trefoil canal first of all facet joint osteoarthritis causes the trefoil-shape, subsequent following endplate and disc degeneration result in LRS. The second pathway is called acute angular pinch. The narrowing occurs simultaneously from all directions due to endplate, disc and facet joint degeneration. The nerve root is either deviated medially or compressed in the LR. Magnetic resonance imaging (MRI) is considered the standard imaging technique for evaluation of LSS[9-11] due to the best soft tissue contrast[7]. Although LSS as a distinct syndrome has already been described more than 60 years ago, the radiological classification systems remain inconsistent[12,13]. In 2014 the "Consensus conference of core radiological parameters to describe lumbar stenosis" with 15 internationally renowned experts focused on this problem[12]. Concerning the LRS they recommend the classification system of Bartynski *et al*[8] which focuses on the compression and the localization of the nerve root in the LR. In short Bartynski *et al*[8] divided the LRS in 4 grades: Normal (grade 0), small without root compression (grade 1), small with root compression (grade 2) and severe root compression (grade 3). LSS is usually diagnosed by clinical findings in correlation with imaging results. However in the daily routine we frequently experience a mismatch between LBP and MRI results. The aim of our study was to verify this mismatch regarding LBP and LRS. To the best of our knowledge there are no previous studies investigating the correlation of LBP and MRI findings of LRS in such a large group of patients.

MATERIALS AND METHODS

Study participants

The study was approved by the ethical committee. In total the study involved lumbar MR images of 927 patients (410 men and 517 women). The mean age of the patients included was 47.7 years (ranging from 13 to 92 years). All patients included in the study had suffered from LBP without any history of spinal surgery. Criteria for exclusion of patients were confirmed disc herniation, spinal stenosis, scoliosis and vertebral fractures. The MR images were gathered over a time of one year with

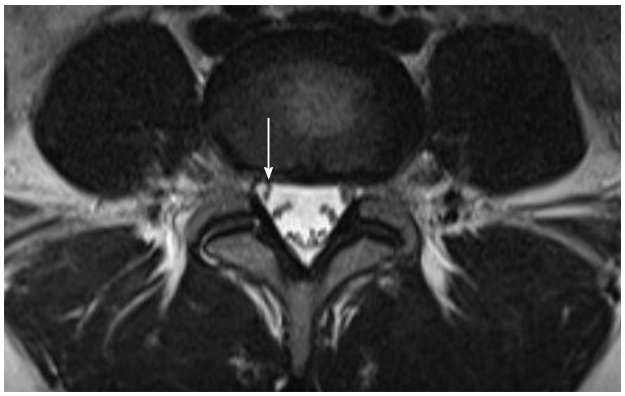

Figure 1 Axial T2-weighted magnetic resonance image of lumbar level L4/5 shows the lateral recess that is bordered laterally by the pedicle, posteriorly by the superior articular facet, and anteriorly by the vertebral body, endplate margin, and disc margin.

suspected disc herniation and facet joint degeneration being the main reasons for MRI.

Imaging technique

MRI of the lumbar spine was conducted with a 1.5 Tesla MRI system (Magnetom® Avanto, Siemens AG, Erlangen, Germany) and a dedicated receive only spine coil. For imaging analysis axial T2-weighted images were obtained using fast spin-echo sequences. The sequence parameters were: TR 3550; TE 90; matrix 448; field of view 210 mm; slice thickness 4 mm; interslice gap 10%, number of excitations.

Image analysis

All MR images were assessed in consensus by two blinded authors (Adel Maataoui, M Fawad Khan). Both authors are board certified radiologists with longstanding experience in imaging of the musculoskeletal system. Degeneration of lumbar spine concerns mostly segments L4/5 and L5/S1, for which reason the LR of these segments were graded on axial T2-weighted fast spin-echo images. All in all, an overall number of 3708 lateral recesses were rated.

Our grading system of LRS was based on Bartynski's classification. We defined grade 0 as a normal LR in which the nerve root is bathed in cerebrospinal fluid. There is no contact to the adjacent structures. Grade 1 represents a narrowing of the LR without root deviation. Grade 2 additionally reveals a root deviation. Grade 3 describes a compression of the nerve root (Table 1, Figure 2).

Oswestry Disability Index

By means of the Oswestry Disability Index (ODI) functional status was assessed. The ODI is one of the principle outcome measure questionnaires for LBP - it measures pain and disability, which are core items in patients with LBP[14]. We used the german version of the ODI developed by Mannion *et al*[15]. This standardized, self-administered questionnaire contains ten sections: One section about pain intensity and nine sections about limitations of various activities of daily life, namely personal care (washing, dressing, *etc.*), lifting, walking, sitting, standing, sleeping, sex life, social life and travelling[16]. The question about sex life was excluded on grounds of ethical aspects. Each section is scored on a scale of 0-5 points with 0 representing no disability and 5 the greatest disability. Section 2 "personal care" for example contains the following statements and scores: I can look after myself normally without causing extra pain (0); I can look after myself normally but it is very painful (1); It is painful to look after myself and I am slow and careful (2); I need some help but manage most of my personal care (3); I need help every day in most aspects of self care (4); and I do not get dressed, wash with difficulty and stay in bed (5)[16].

Finally the index is calculated by dividing the summed score by the total possible score (which has to be reduced by 5 for every question not answered). The result is then multiplied by 100 and expressed as a percentage. The result is interpreted as follows: Score of 0%-20%, minimal disability; 20%-40%, moderate disability; 40%-60%, severe disability; 60%-80%, crippled; 80%-100%, patients are bedbound.

Statistical analysis

Data were analysed with the use of the BIAS software package (Epsilon publisher, Frankfurt a.M., Germany). In order to evaluate the correlation of LRS and ODI Spearman's coefficient of rank correlation was determined. P value < 0.05 were considered statistically significant.

RESULTS

Grades of LRS in the patient cohort

Three thousand seven hundred and eight LR of 927 patients were assessed at lumbar level L4/5 and L5/S1. Table 2 presents the number of LR according to the relative grade of stenosis. The image evaluation revealed 430/461 grade 0 stenosis (48.1%), 357/349 grade 1 stenosis (38.1%), 113/103 grade 2 stenosis (11.7%) and 27/14 grade 3 stenosis (2.2%) for the left/right side of lumbar level L4/5 and 528/548 grade 0 stenosis (58%), 303/316 grade 1 stenosis (33.4%), 75/49 grade 2 stenosis (6.7%) and 21/14 grade 3 stenosis (1.9%) for the left/right side of lumbar level L5/S1, respectively.

Symptoms and disability

According to ODI scores patient symptoms and disability ranged from a minimal score of 0% to a maximal score of 91.11%. The mean value amounted to 34.06% ± 16.89%. Most patients (48.39%) showed a moderate functional disability (21%-40%). Regarding sex no statistical difference between the ODI scores could be revealed: Men 32.47% ± 16.55% and women 35.58% ± 16.55%.

The mean ODI scores for LRS grade 0, 1, 2, 3 of lumbar level L4/5 on the right side were 31.53% ± 15.46%, 31.53% ± 17.60%, 33.01% ± 17.17% and

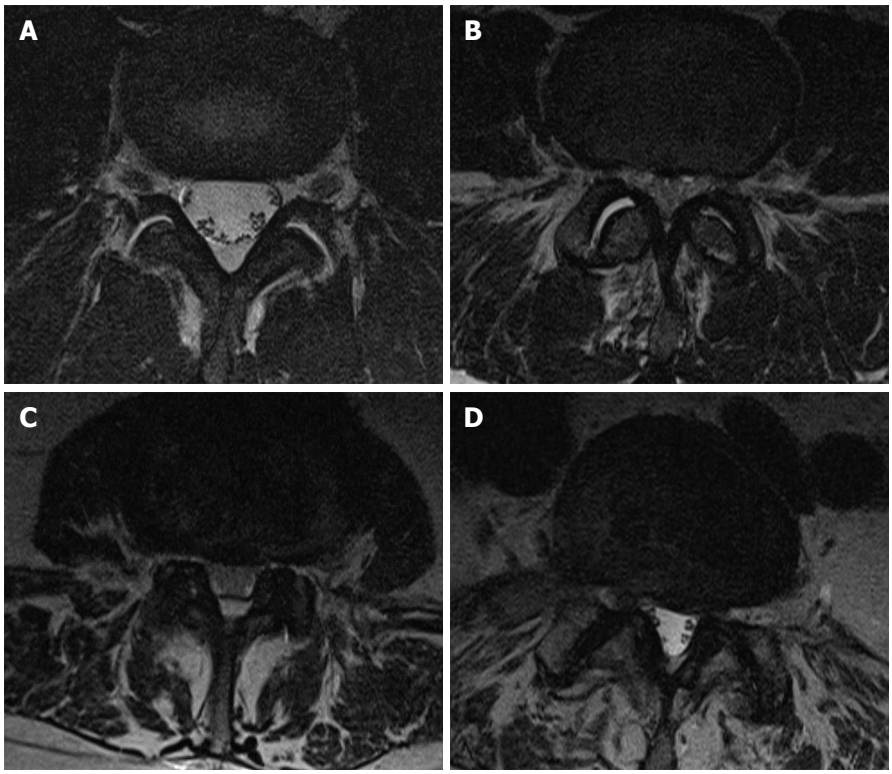

Figure 2 Axial T2-weighted magnetic resonance images illustrate the grading system of lateral recess stenosis. A: Grade 0 bilaterally; B: Grade 1 bilaterally; C: Grade 2 bilaterally; D: Grade 3 on the left, Grade 1 on the right.

Table 1 Grading system of lateral recess stenosis

Grade	Nerve root in the lateral recess
0	Normal
1	No deviation
2	Deviation
3	Compression

33.03% ± 16.89%. There was no statistical difference between the ODI score and the grade of LRS on lumbar level L4/5 on the right.

The mean ODI scores for LRS grade 0, 1, 2, 3 of lumbar level L4/5 on the left side were 30.75% ± 17.85%, 30.74% ± 17.03%, 32.39% ± 16.97% and 33.25% ± 16.90%. There was no statistical difference between the ODI score and the grade of LRS on lumbar level L4/5 on the left.

The mean ODI scores for LRS grade 0, 1, 2, 3 of lumbar level L5/S1 on the right side were 32.03% ± 16.58%, 32.03% ± 16.60%, 33.24% ± 16.41% and 33.88% ± 16.76%. There was no statistical difference between the ODI score and the grade of LRS on lumbar level L5/S1 on the right.

The mean ODI scores for LRS grade 0, 1, 2, 3 of lumbar level L5/S1 on the left side were 32.14% ± 16.90%, 33.15% ± 16.62%, 33.13% ± 16.60% and 33.46% ± 16.78%. There was no statistical difference between the ODI score and the grade of LRS on lumbar level L5/S1 on the left.

Table 2 Number of grades of lateral recess stenosis for lumbar levels L4/5 and L5/S1

Lumbar level	Grades			
	0	1	2	3
L4/5 left	430	357	113	27
L4/5 right	461	349	103	14
L5/S1 left	528	303	75	21
L5/S1 right	548	316	49	14

Correlation of ODI and LRS

We observed a very weak statistically significant positive correlation between ODI and LRS at lumbar levels L4/5 and L5/S1, each bilaterally.

L4/5 left and ODI: rho < 0.105, $P < 0.01$; L4/5 right and ODI: rho < 0.111, $P < 0.01$; L5/S1 left and ODI: rho 0.128, $P < 0.01$; L5/S1 right and ODI: rho < 0.157, $P < 0.001$.

DISCUSSION

Despite the high prevalence of LSS and that the combination of clinical and imaging findings are the standard diagnostic tools[17] clinical and imaging findings often do not correlate. Haig *et al*[9] and Geisser *et al*[18] could not find any difference between symptomatic and asymptomatic patients based on the size of the lumbar spinal canal measured on MR images. Lohmann *et al*[19] did also not detect a correlation between clinical findings and LSS on computed tomography (CT) images.

The aim of our study was to verify if the results of these studies which focused on central LSS, do also apply to LRS. In the presented study with a cohort of more than 900 patients we found only a very weak positive correlation between the severity of LBP and the severity of LRS. Our findings are supported by the results of Kuittinen *et al*[20]: By MR imaging and electromyography they evaluated 140 nerve roots of 14 patients, who were selected for surgical treatment of LRS. The findings were correlated with each other as well as with the clinical symptoms, measured by different tests including the ODI. In this little cohort they revealed a positive correlation between MR-findings and EMG and between EMG and patient symptoms. But they revealed no correlation between MR findings and patient symptoms. The study is limited by the very small cohort of patients and the fact that also neuroforaminal stenosis was included.

It is unclear why clinical and imaging findings do often not correlate. The compression of the nerve root is considered to be one of the main causes of symptoms in patients with LRS[21-23]. In an experimental study Lacroix-Fralish *et al*[24] observed that a nerve root ligation in a rat model produced mechanical allodynia. Mechanical root compression in a dog model revealed intraradicular edema and Wallerian degeneration[25]. Using a silicon tube Saal[26] and Xue *et al*[27] produced lumbar nerve root compression in a rat model, which resulted in disappearing of the myelin sheath and activation of microglia, which is assumed to participate in the genesis and maintenance of pain[24].

Thus, it must be considered that a possible reason for the discrepancy between MRI findings and patient symptoms could be that MRI does not sufficiently identify nerve compression. Bartynski *et al*[8] assessed the accuracy of MRI in 26 patients with symptomatic nerve root compression in the LR at lumbar levels L2/3 - L5/S1. Each patient underwent MRI, conventional myelograpy and CT myelography; the root compression was confirmed surgically and a post-operative pain improvement could be observed. In MRI the root compression was underestimated in nearly 30%.

LSS, in addition, has an important dynamic component. MRI was performed, as usual, with the patient lying in the supine position. Yet it is known and even a key feature for LSS that patient symptoms increase under axial loading and lumbar extension while they decrease under axial distraction and flexion[17,28]. This can be explained by anatomic alterations: Flexion and extension can change the size of the central lumbar canal, the LR and the neural foramen and can consecutively result in changes of the cauda equina as well as in isolated nerve root compression in the LR[29]. In experimental studies axial loading has caused alterations of the size of the lumbar canal and the neural foramen[30]. In the upright position axial loading can cause displacement of peridiscal structures that lead to a nerve root compression which is not observable in the supine position[31]. In addition the pressure in the lumbar canal can be altered by postural changes[32,33].

Two other aspects should be considered as possible explanations for the weak correlation. On the one hand the nerve root can be compressed without clinical symptoms. On the other hand clinical symptoms can be evident without imaging findings of root compression. Although there are single studies which reveal nerve root compression in approximately 20% of asymptomatic individuals[34], there is in total only a small number of asymptomatic individuals who reveal nerve root compression in MRI. In a study presented by Weishaupt *et al*[35] with 60 asymptomatic volunteers only one single root compression was observed in MRI by one of the readers. A study of nearly 100 asymptomatic elite junior tennis players revealed a nerve root compression in only 2%[36]. Boos *et al*[37] reported a "major nerve deformation" in 4% of asymptomatic adults.

A possible explanation for clinical symptoms without evident nerve root compression in imaging is the inflammation of the nerve root caused by inflammatory mediators[38,39], for example, Interleukin β1[40]. It is hypothesized, that these substances can diffuse in the spinal canal from the facet joints, the ligamentum flavum[40] and from the intervertebral disc[26,41].

Beside the nerve root nearly all lumbar structures are potential sources of LBP, such as the facet joints, the intervertebral discs, bones, fascial structures and muscles[42]. Especially facet joint osteoarthritis is known for radiating pain without evidence of nerve root compression[43,44]. Because of the fact that LRS is based on facet joint osteoarthritis, intervertebral disc degeneration, ligamentum flavum hypertrophy and endplate spur we have to consider that in our study each of these structures could be the crucial factor for patient symptoms.

LBP rarely causes objective endpoints so outcomes are best measured with patient-reported metrics[45]. We assessed patient symptoms by means of the ODI. It is one of the most commonly used measures of disability in back pain[46]. It has established psychometric properties, is easy to use and has a low administrative burden[46]. Yet, based on self-reported symptoms, the ODI remains subjective. Furthermore it does not measure nerve root level specific symptoms. A limitation of the presented study is that results of clinical, more objective, examinations were not included and that we assessed no nerve root level specific symptoms. In addition the LRS were not proved surgically.

In conclusion, in our broad study population we only found a very weak statistically significant positive correlation between LBP and LRS on MR-images, thus confirming the well-known problem that in the context of diagnosing LBP clinical and imaging findings often do not correlate. Our results underline the necessity not to evaluate LRS isolated on imaging but in relation to clinical findings.

COMMENTS

Background

Low back pain (LBP) is an important issue for healthcare systems all over the

world. One reason of LBP is lumbar spinal stenosis (LSS), with lateral recess stenosis (LRS) not gaining as much attention as central spinal stenosis, a fact that is assumed to be the main reason for failed back surgery. Concerning imaging techniques magnetic resonance imaging (MRI) is the standard imaging tool for evaluating LSS. However in the daily routine people frequently experience a mismatch between LBP and MRI results. The aim of this study was to verify this mismatch regarding LBP and LRS.

Research frontiers

The problem that in the context of LBP clinical and imaging findings often do not correlate has been the objective of numerous studies in the past. Yet the LRS as one reason of LBP is underrepresented and most studies have a small study population.

Innovations and breakthroughs

The authors assessed the correlation between LBP and LRS in a very broad study population including nearly 1000 patients. Functional status was assessed by means of the Oswestry Disability Index (ODI), and LRS was assessed on axial magnetic resonance images of lumbar level L4/5 and L5/S1 by evaluating the nerve root in the lateral recess on a 4 point grading scale. The authors revealed a very weak statistically significant positive correlation between ODI and LRS at the L4/5 segment as well as the L5/S1 segment.

Applications

The presented findings underline the necessity not to evaluate LRS isolated on imaging but in relation with the clinical findings.

Terminology

Lateral recess stenosis: It describes the stenosis of the lateral part of the lumbar spinal canal that is bordered laterally by the pedicle, posteriorly by the superior articular facet, and anteriorly by the vertebral body, endplate margin, and disc margin. It is most commonly caused by degenerative changes; Oswestry Disability Index: The Oswestry Disability Index is one of the principle outcome measure questionnaires for low back pain focussing on disability and pain.

Peer-review

The authors studied the correlation of lumbar recess stenosis in MRI with clinical symptoms.

REFERENCES

1 From the Centers for Disease Control and Prevention. Prevalence of disabilities and associated health conditions among adults--United States, 1999. *JAMA* 2001; **285**: 1571-1572 [PMID: 11302137]

2 **Balagué F**, Mannion AF, Pellisé F, Cedraschi C. Non-specific low back pain. *Lancet* 2012; **379**: 482-491 [PMID: 21982256 DOI: 10.1016/s0140-6736(11)60610-7]

3 **Freburger JK**, Holmes GM, Agans RP, Jackman AM, Darter JD, Wallace AS, Castel LD, Kalsbeek WD, Carey TS. The rising prevalence of chronic low back pain. *Arch Intern Med* 2009; **169**: 251-258 [PMID: 19204216 DOI: 10.1001/archinternmed.2008.543]

4 **Verbiest H**. A radicular syndrome from developmental narrowing of the lumbar vertebral canal. *J Bone Joint Surg Br* 1954; **36-B**: 230-237 [PMID: 13163105]

5 **Burton CV**, Kirkaldy-Willis WH, Yong-Hing K, Heithoff KB. Causes of failure of surgery on the lumbar spine. *Clin Orthop Relat Res* 1981; (**157**): 191-199 [PMID: 7249453]

6 **Lee CK**, Rauschning W, Glenn W. Lateral lumbar spinal canal stenosis: classification, pathologic anatomy and surgical decompression. *Spine* (Phila Pa 1976) 1988; **13**: 313-320 [PMID: 3388117]

7 **Andreisek G**, Hodler J, Steurer J. Uncertainties in the diagnosis of lumbar spinal stenosis. *Radiology* 2011; **261**: 681-684 [PMID: 22095990 DOI: 10.1148/radiol.11111086]

8 **Bartynski WS**, Lin L. Lumbar root compression in the lateral recess: MR imaging, conventional myelography, and CT myelography comparison with surgical confirmation. *AJNR Am J Neuroradiol* 2003; **24**: 348-360 [PMID: 12637281]

9 **Haig AJ**, Geisser ME, Tong HC, Yamakawa KS, Quint DJ, Hoff JT, Chiodo A, Miner JA, Phalke VV. Electromyographic and magnetic resonance imaging to predict lumbar stenosis, low-back pain, and no back symptoms. *J Bone Joint Surg Am* 2007; **89**: 358-366 [PMID: 17272451 DOI: 10.2106/jbjs.e.00704]

10 **Sasiadek MJ**, Bladowska J. Imaging of degenerative spine disease--the state of the art. *Adv Clin Exp Med* 2012; **21**: 133-142 [PMID: 23214277]

11 **Malfair D**, Beall DP. Imaging the degenerative diseases of the lumbar spine. *Magn Reson Imaging Clin N Am* 2007; **15**: 221-238, vi [PMID: 17599641 DOI: 10.1016/j.mric.2007.04.001]

12 **Andreisek G**, Deyo RA, Jarvik JG, Porchet F, Winklhofer SF, Steurer J. Consensus conference on core radiological parameters to describe lumbar stenosis - an initiative for structured reporting. *Eur Radiol* 2014; **24**: 3224-3232 [PMID: 25079488 DOI: 10.1007/s00330-014-3346-z]

13 **Andreisek G**, Imhof M, Wertli M, Winklhofer S, Pfirrmann CW, Hodler J, Steurer J. A systematic review of semiquantitative and qualitative radiologic criteria for the diagnosis of lumbar spinal stenosis. *AJR Am J Roentgenol* 2013; **201**: W735-W746 [PMID: 24147503 DOI: 10.2214/ajr.12.10163]

14 **Deyo RA**, Battie M, Beurskens AJ, Bombardier C, Croft P, Koes B, Malmivaara A, Roland M, Von Korff M, Waddell G. Outcome measures for low back pain research. A proposal for standardized use. *Spine* (Phila Pa 1976) 1998; **23**: 2003-2013 [PMID: 9779535]

15 **Mannion AF**, Junge A, Fairbank JC, Dvorak J, Grob D. Development of a German version of the Oswestry Disability Index. Part 1: cross-cultural adaptation, reliability, and validity. *Eur Spine J* 2006; **15**: 55-65 [PMID: 15856341]

16 **Fairbank JC**, Pynsent PB. The Oswestry Disability Index. *Spine* (Phila Pa 1976) 2000; **25**: 2940-2952; discussion 2952 [PMID: 11074683]

17 **Genevay S**, Atlas SJ. Lumbar spinal stenosis. *Best Pract Res Clin Rheumatol* 2010; **24**: 253-265 [PMID: 20227646 DOI: 10.1016/j.berh.2009.11.001]

18 **Geisser ME**, Haig AJ, Tong HC, Yamakawa KS, Quint DJ, Hoff JT, Miner JA, Phalke VV. Spinal canal size and clinical symptoms among persons diagnosed with lumbar spinal stenosis. *Clin J Pain* 2007; **23**: 780-785 [PMID: 18075405 DOI: 10.1097/AJP.0b013e31815349bf]

19 **Lohman CM**, Tallroth K, Kettunen JA, Lindgren KA. Comparison of radiologic signs and clinical symptoms of spinal stenosis. *Spine* (Phila Pa 1976) 2006; **31**: 1834-1840 [PMID: 16845360 DOI: 10.1097/01.brs.0000227370.65573.ac]

20 **Kuittinen P**, Sipola P, Aalto TJ, Määttä S, Parviainen A, Saari T, Sinikallio S, Savolainen S, Turunen V, Kröger H, Airaksinen O, Leinonen V. Correlation of lateral stenosis in MRI with symptoms, walking capacity and EMG findings in patients with surgically confirmed lateral lumbar spinal canal stenosis. *BMC Musculoskelet Disord* 2014; **15**: 247 [PMID: 25051886 DOI: 10.1186/1471-2474-15-247]

21 **Shobeiri E**, Khalatbari MR, Taheri MS, Tofighirad N, Moharamzad Y. Magnetic resonance imaging characteristics of patients with low back pain and those with sciatica. *Singapore Med J* 2009; **50**: 87-93 [PMID: 19224091]

22 **Ciric I**, Mikhael MA, Tarkington JA, Vick NA. The lateral recess syndrome. A variant of spinal stenosis. *J Neurosurg* 1980; **53**: 433-443 [PMID: 7420163 DOI: 10.3171/jns.1980.53.4.0433]

23 **Epstein JA EN**. Lumbar spondylosis and spinal stenosis. In: Willkins RH RS, eds., editor Neurosurgery. New York: McGraw Hill, 1996: 3831-3840

24 **Lacroix-Fralish ML**, Tawfik VL, Tanga FY, Spratt KF, DeLeo JA. Differential spinal cord gene expression in rodent models of radicular and neuropathic pain. *Anesthesiology* 2006; **104**: 1283-1292 [PMID: 16732101]

25 **Kobayashi S**, Yoshizawa H, Yamada S. Pathology of lumbar nerve root compression. Part 1: Intraradicular inflammatory changes induced by mechanical compression. *J Orthop Res* 2004; **22**: 170-179 [PMID: 14656677 DOI: 10.1016/s0736-0266(03)00131-1]

26 **Saal JS**. The role of inflammation in lumbar pain. *Spine* (Phila Pa 1976) 1995; **20**: 1821-1827 [PMID: 7502140]

27 **Xue F**, Wei Y, Chen Y, Wang Y, Gao L. A rat model for chronic spinal nerve root compression. *Eur Spine J* 2014; **23**: 435-446 [PMID: 24141952 DOI: 10.1007/s00586-013-2990-3]

28 **Schönström N**, Lindahl S, Willén J, Hansson T. Dynamic changes in the dimensions of the lumbar spinal canal: an experimental study in vitro. *J Orthop Res* 1989; **7**: 115-121 [PMID: 2908901 DOI: 10.1002/jor.1100070116]

29 **Penning L**, Wilmink JT. Posture-dependent bilateral compression of L4 or L5 nerve roots in facet hypertrophy. A dynamic CT-myelographic study. *Spine* (Phila Pa 1976) 1987; **12**: 488-500 [PMID: 3629399]

30 **Nowicki BH**, Yu S, Reinartz J, Pintar F, Yoganandan N, Haughton VM. Effect of axial loading on neural foramina and nerve roots in the lumbar spine. *Radiology* 1990; **176**: 433-437 [PMID: 2367657 DOI: 10.1148/radiology.176.2.2367657]

31 **Beattie PF**, Meyers SP, Stratford P, Millard RW, Hollenberg GM. Associations between patient report of symptoms and anatomic impairment visible on lumbar magnetic resonance imaging. *Spine* (Phila Pa 1976) 2000; **25**: 819-828 [PMID: 10751293]

32 **Olmarker K**, Rydevik B, Hansson T, Holm S. Compression-induced changes of the nutritional supply to the porcine cauda equina. *J Spinal Disord* 1990; **3**: 25-29 [PMID: 2134408]

33 **Takahashi K**, Kagechika K, Takino T, Matsui T, Miyazaki T, Shima I. Changes in epidural pressure during walking in patients with lumbar spinal stenosis. *Spine* (Phila Pa 1976) 1995; **20**: 2746-2749 [PMID: 8747254]

34 **van Rijn JC**, Klemetso N, Reitsma JB, Majoie CB, Hulsmans FJ, Peul WC, Bossuyt PM, Heeten GJ, Stam J. Symptomatic and asymptomatic abnormalities in patients with lumbosacral radicular syndrome: Clinical examination compared with MRI. *Clin Neurol Neurosurg* 2006; **108**: 553-557 [PMID: 16289310 DOI: 10.1016/j.clineuro.2005.10.003]

35 **Weishaupt D**, Zanetti M, Hodler J, Boos N. MR imaging of the lumbar spine: prevalence of intervertebral disk extrusion and sequestration, nerve root compression, end plate abnormalities, and osteoarthritis of the facet joints in asymptomatic volunteers. *Radiology* 1998; **209**: 661-666 [PMID: 9844656 DOI: 10.1148/radiology.209.3.9844656]

36 **Rajeswaran G**, Turner M, Gissane C, Healy JC. MRI findings in the lumbar spines of asymptomatic elite junior tennis players. *Skeletal Radiol* 2014; **43**: 925-932 [PMID: 24691895 DOI: 10.1007/s00256-014-1862-1]

37 **Boos N**, Rieder R, Schade V, Spratt KF, Semmer N, Aebi M. 1995 Volvo Award in clinical sciences. The diagnostic accuracy of magnetic resonance imaging, work perception, and psychosocial factors in identifying symptomatic disc herniations. *Spine* (Phila Pa 1976) 1995; **20**: 2613-2625 [PMID: 8747239]

38 **Cavanaugh JM**. Neural mechanisms of lumbar pain. *Spine* (Phila Pa 1976) 1995; **20**: 1804-1809 [PMID: 7502138]

39 **Siddall PJ**, Cousins MJ. Pain mechanisms and management: an update. *Clin Exp Pharmacol Physiol* 1995; **22**: 679-688 [PMID: 8575103]

40 **Igarashi A**, Kikuchi S, Konno S. Correlation between inflammatory cytokines released from the lumbar facet joint tissue and symptoms in degenerative lumbar spinal disorders. *J Orthop Sci* 2007; **12**: 154-160 [PMID: 17393271 DOI: 10.1007/s00776-006-1105-y]

41 **McCarron RF**, Wimpee MW, Hudkins PG, Laros GS. The inflammatory effect of nucleus pulposus. A possible element in the pathogenesis of low-back pain. *Spine* (Phila Pa 1976) 1987; **12**: 760-764 [PMID: 2961088]

42 **Allegri M**, Montella S, Salici F, Valente A, Marchesini M, Compagnone C, Baciarello M, Manferdini ME, Fanelli G. Mechanisms of low back pain: a guide for diagnosis and therapy. *F1000Res* 2016; **5**: pii: F1000 Faculty Rev-1530 [PMID: 27408698 DOI: 10.12688/f1000research.8105.1]

43 **Epstein JA**, Epstein BS, Rosenthal AD, Carras R, Lavine LS. Sciatica caused by nerve root entrapment in the lateral recess: the superior facet syndrome. *J Neurosurg* 1972; **36**: 584-589 [PMID: 5026544 DOI: 10.3171/jns.1972.36.5.0584]

44 **V. M. Facet syndrome**. In: Weinstein JN WS, eds., editor The lumbar spine: The International Society for the Study of the Lumbar Spine. Philadelphia: WB Saunders Company, 1990: 422-441

45 **Werneke M**. A proposed set of metrics for standardized outcome reporting in the management of low back pain. *Acta Orthop* 2016; **87**: 88 [PMID: 26610164 DOI: 10.3109/17453674.2015.1120127]

46 **Smeets R**, Köke A, Lin CW, Ferreira M, Demoulin C. Measures of function in low back pain/disorders: Low Back Pain Rating Scale (LBPRS), Oswestry Disability Index (ODI), Progressive Isoinertial Lifting Evaluation (PILE), Quebec Back Pain Disability Scale (QBPDS), and Roland-Morris Disability Questionnaire (RDQ). *Arthritis Care Res* (Hoboken) 2011; **63** Suppl 11: S158-S173 [PMID: 22588742 DOI: 10.1002/acr.20542]

P- Reviewer: Cerwenka HR, Gao BL **S- Editor**: Song XX
L- Editor: A **E- Editor**: Li D

World Journal of Radiology

Submit a Manuscript: http://www.f6publishing.com

World J Radiol 2017 May 28; 9(5): 230-244

DOI: 10.4329/wjr.v9.i5.230

ISSN 1949-8470 (online)

ORIGINAL ARTICLE

Basic Study

Cystic lesions of peripheral nerves: Are we missing the diagnosis of the intraneural ganglion cyst?

Jyoti Panwar, Anil Mathew, Binu P Thomas

Jyoti Panwar, Department of Radiology, Christian Medical College, Vellore 632004, India

Jyoti Panwar, Joint Department of Medical Imaging, University Health Network, University of Toronto, Toronto, Ontario M5G 2N2, Canada

Anil Mathew, Binu P Thomas, Department of Hand Surgery and Leprosy Reconstructive Surgery, Christian Medical College, Vellore 632004, India

Author contributions: Panwar J and Mathew A participated in the conception, acquisition, analysis, interpretation of the data and drafted the initial manuscript; Panwar J was the guarantor and designed the study; Thomas BP revised the article critically for important intellectual content; language revision and final approval of the version of the article was done by Mathew A and Thomas BP.

Institutional review board statement: The study was reviewed and approved by the Institutional review board, Christian Medical College, Vellore, India.

Informed consent statement: Not applicable given the retrospective design of our study.

Conflict-of-interest statement: There are no conflicts of interest to report.

Data sharing statement: No additional data is available.

Manuscript source: Invited manuscript

Correspondence to: Jyoti Panwar, MD, FRCR, Musculoskeletal Radiology Fellow, Joint Department of Medical Imaging, University Health Network, University of Toronto, 585 University Avenue, Toronto, Ontario M5G 2N2, Canada. drjyoticmch@gmail.com
Telephone: +1-416-3403372

Received: September 26, 2016
Peer-review started: September 28, 2016
First decision: October 20, 2016
Revised: January 17, 2017
Accepted: March 16, 2017
Article in press: March 17, 2017
Published online: May 28, 2017

Abstract

AIM

To highlight the salient magnetic resonance imaging (MRI) features of the intraneural ganglion cyst (INGC) of various peripheral nerves for their precise diagnosis and to differentiate them from other intra and extraneural cystic lesions.

METHODS

A retrospective analysis of the magnetic resonance (MR) images of a cohort of 245 patients presenting with nerve palsy involving different peripheral nerves was done. MR images were analyzed for the presence of a nerve lesion, and if found, it was further characterized as solid or cystic. The serial axial, coronal and sagittal MR images of the lesions diagnosed as INGC were studied for their pattern and the anatomical extent along the course of the affected nerve and its branches. Its relation to identifiable anatomical landmarks, intra-articular communication and presence of denervation changes in the muscles supplied by involved nerve was also studied.

RESULTS

A total of 45 cystic lesions in the intra or extraneural

locations of the nerves were identified from the 245 MR scans done for patients presenting with nerve palsy. Out of these 45 cystic lesions, 13 were diagnosed to have INGC of a peripheral nerve on MRI. The other cystic lesions included extraneural ganglion cyst, paralabral cyst impinging upon the suprascapular nerve, cystic schwannoma and nerve abscesses related to Hansen's disease involving various peripheral nerves. Thirteen lesions of INGC were identified in 12 patients. Seven of these affected the common peroneal nerve with one patient having a bilateral involvement. Two lesions each were noted in the tibial and suprascapular nerves, and one each in the obturator and proximal sciatic nerve. An intra-articular connection along the articular branch was demonstrated in 12 out of 13 lesions. Varying stages of denervation atrophy of the supplied muscles of the affected nerves were seen in 7 cases. Out of these 13 lesions in 12 patients, 6 underwent surgery.

CONCLUSION

INGC is an important cause of reversible mono-neuropathy if diagnosed early and surgically treated. Its classic MRI pattern differentiates it from other lesions of the peripheral nerve and aid in its therapeutic planning. In each case, the joint connection has to be identified preoperatively, and the same should be excised during surgery to prevent further cyst recurrence.

Key words: Intra-neural; Magnetic resonance imaging; Peripheral nerves; Extra-neural; Ganglion cyst

Core tip: This is a retrospective study to emphasize the characteristic magnetic resonance imaging (MRI) features of the intraneural ganglion cyst (INGC) of the peripheral nerves. The radiologist should recognize the classic MRI pattern of the INGC, its joint connection and imaging anatomy of the involved nerve. This would aid surgeons in complete removal of the cyst, prevent its recurrence and hence improved patient outcomes. Both radiologists and surgeons should be aware of other neurogenic lesions and the extra neural ganglion cyst which may also have a joint connection.

Panwar J, Mathew A, Thomas BP. Cystic lesions of peripheral nerves: Are we missing the diagnosis of the intraneural ganglion cyst? *World J Radiol* 2017; 9(5): 230-244 Available from: URL: http://www.wjgnet.com/1949-8470/full/v9/i5/230.htm DOI: http://dx.doi.org/10.4329/wjr.v9.i5.230

INTRODUCTION

Patients presenting with thickened peripheral nerves and nerve palsy are often diagnosed as Hansen's disease (HD) in endemic areas when other diagnostic tests come back inconclusive[1-4]. These patients may be thus treated with long term empirical multi-drug therapy for the same[3-6]. An intraneural ganglion cyst (INGC) is a non-neoplastic mucinous cyst within the epineurium of a nerve and commences from an adjoining joint[7-13]. These cysts are filled with a mucinous material which is walled off by a fibrous layer[7-9]. As these cysts expand within the epineurium, they displace and compress the adjacent nerve fascicles leading to pain, paresthesia, tingling and muscle paralysis in the distribution of the involved nerve[14,15]. It may follow trivial trauma to the joint[7]. The clinical evaluation of an involved nerve will show thickening if superficial and a variable degree of sensory-motor disturbance along its distribution[13-15]. This presentation of variable motor palsy and sensory symptoms of acute onset may mimic other conditions like lumbosacral disc disease, pelvic or shoulder pathologies and may delay early detection[14,16]. The diagnosis of INGC can be confirmed by imaging techniques like magnetic resonance imaging (MRI) and high resolution ultrasonography[14-19]. The nerve paralysis is usually reversible if the nerve is surgically decompressed early. Its articular connection should be identified and disconnected during surgery to prevent recurrence[14,15,20].

MATERIALS AND METHODS

This study was approved by the institutional review board, and consent from all patients was waived. This research did not receive any specific grant from funding agencies in the public, commercial, or not-for-profit sectors.

Patient selection

All MR images of the patients presenting with peripheral nerve palsy from July 2005 to December 2015 were selected from our radiology database. A computer search was also performed for the term "ganglion cyst" of proximal tibiofibular (PTF) joint, "paralabral cyst", "intraneural ganglion cyst", ganglion cyst of knee, shoulder, elbow and hip joints in the radiology information system database. From this cohort of images, all nerves with solid and cystic lesions were first identified. Among the cystic lesions thus identified the images showing elongated cystic lesions of the peripheral nerve along its course and those that fulfilled one or more of the inclusion criteria for INGC (Table 1) were selected. Thirteen such lesions were identified and their MR images, available clinical details, follow-up information and histopathology were reviewed by a musculoskeletal radiologist.

Image acquisition

Images were obtained by a variety of MRI scanners, including 0.5-T units (n = 1; NT Intera, Philips Healthcare, Netherland), 1.5-T units (n = 2; Magnetom Avanto, Siemens Healthcare, Erlangen, Germany), and 3-T units (n = 6; Intera Achieva, Philips Healthcare, Best,

Table 1 Inclusion criteria for intraneural ganglion cyst

Multilocular elongated hyperintense cystic mass on T2 weighted imaging
Distributed along the course of a peripheral nerve and its branches
Extension along the articular branch to the adjacent joint
Denervation changes of the muscles supplied by involved nerve

Netherland). The imaging protocol and parameters also varied from case to case. The images were acquired in all three orthogonal planes including axial, coronal and sagittal in all patients. Fast spin echo T2-weighted axial, coronal and sagittal images with or without fat suppression and T1-weighted axial images were done in all patients scanned in the 0.5-T and 1.5-T MR scanner. Proton density fat suppressed axial, coronal and sagittal images along with T1-weighted axial images were available for all cases done in the 3-T MR scanner.

Image analysis

The MR images of all cystic lesions were reviewed by a musculoskeletal radiologist on a General Electric® (GE) picture archiving and communication system workstation. The images were evaluated, specifically looking for the presence of the following features: (1) the presence of T2/fat suppressed (T2 or proton density) hyperintense cystic lesion, along the nerve or its branches; (2) the exact anatomical site, intra or extra-neural location; (3) any communication to the adjacent joint along an articular branch; (4) the morphology of the cyst in terms of shape and pattern; and (5) denervation changes of the affected muscle compartment was also assessed.

RESULTS

Clinical findings

The mean age of the patients was 38.2 years (range 9-67 years). There were ten males and two females in this series. Pain along the distribution of the involved nerve and weakness of muscles supplied by the same were the most common presenting symptoms and was present in all 12 patients. One lesion was asymptomatic. The same was discovered incidentally on the contralateral side during routine imaging. Four cases of INGCs involving the common peroneal nerve (CPN) were primarily diagnosed as cystic schwannoma and one suprascapular and obturator nerves lesion were labeled as a paralabral and obturator foramen ganglion cysts respectively. However, no labral tear was seen on MR imaging in either case. Of the 13 lesions, 6 cysts were excised or decompressed by surgery. The articular connection was excised during surgery in 4 out of 5 patients with CPN (PTF joint connection) and in one patient with suprascapular nerve (AC joint connection) involvement.

The other cystic lesions included: 9 cases of extra-neural ganglion cyst (ENGC) of PTF joint in close relation with CPN, one ENGC of radio-humeral (elbow) joint impinging upon the deep branch of radial nerve, 6 cases of paralabral cyst impinging upon the suprascapular nerve, 8 cases of cystic schwannoma and 8 cases of nerve abscesses related to HD involving various peripheral nerves. Table 2 summarizes the clinical details of patients with cystic lesions related to and of the nerve.

MRI findings

INGSs: An elongated multi-lobulated cystic lesion, oriented longitudinally along the course of the nerve was seen in all 13 INGC lesions. An extension of the cyst along the articular branch with intra-articular communication was demonstrated in 12 of these lesions (Figures 1 and 2).

Out of the 13 lesions, 7 involved the peroneal nerve with one patient having bilateral lesions of which one side was asymptomatic. The tibial (Figures 3-5) and suprascapular nerves (Figure 6) were involved in 2 patients.

One case each of the obturator (Figures 7 and 8) and proximal sciatic nerves (Figures 9 and 10) were also identified.

A variable extension of cysts along the branches of the parent nerve was seen in 12 cases (Figures 1-5, 8 and 11). Varying stages of denervation of the supplied muscles were seen in 7 cases (Figures 3-5, 8 and 11).

Six patients underwent surgery and their diagnoses were confirmed by histo-pathological evaluation of the biopsied specimens. The intraoperative images of one of these patients are shown in Figure 12.

In one tibial nerve INGC, in addition to PTF joint connection, a second posterior knee joint connection was also noted (Figure 4). In four cases with CPN involvement, the INGC could also be seen extending distally for a variable length along the deep (Figures 2) and superficial peroneal (Figure 11) nerve branches. The obturator nerve cyst also extended along it's anterior branch (Figure 8) the tibial nerve lesions extended along the branch to the popliteus and tibialis posterior muscles (Figure 3-5). Table 3 summarizes the MRI findings of INGC of the peripheral nerves in this series.

Other cystic lesions

ENGC: These are most commonly seen around the PTF joint in close relation with CPN and its branches. Its characteristic MR features are described in Figure 13 and its differentiation from INGC on imaging is illustrated in Figure 14 and summarized in Table 4.

Cystic schwannoma: Schwannomas represent the most common peripheral nerve sheath tumor[21] and are mostly solid or heterogeneous tumors. However, cystic schwannomas of the peripheral nerve are uncommon[22,23] and may mimic other extra or intraneural cystic lesions. MR features of cystic schwannoma of CPN are illustrated in Figure 15.

Paralabral cyst: Paralabral cysts of the shoulder joint are commonly seen in the middle aged men and cause impingement of the suprascapular nerve. They are commonly located at the posterosuperior glenoid region, secondary to a labral tear. They can extend into

Table 2 Epidemiological data of patients diagnosed with cystic lesions related to the nerve

Patient data	Intraneural ganglion cyst	Extraneural ganglion cyst	Para-labral cyst	Cystic schwannoma	Nerve abscess
Total number of lesions	13	10	6	8	8
Mean age (yr)	38.2	30.5	32	42.6	28.2
SD	14.66	16.42	3.94	10.79	12.84
Common symptoms	Pain along distribution of nerve, motor weakness	Pain and swelling	Pain and weakness of external rotators	Parasthesia, pain along distribution of nerve	Parasthesia and weakness
Male:female ratio	10:2	6:4	6:0	5:3	8:0
Nerves involved	CPN 7 Tibial 2 Suprascapular 2 Prox. Sciatic 1 Obturator 1	Near CPN 9 Radial 1	Near SSN 6	CPN 3 Median 2 Sciatic 1 Tibial 1 Radial 1	Ulnar 5[1] CPN 2[1] Median 3 Radial 3[1]
Number who underwent surgery	6/13	10/10	6/6	8/8	3/8
Correct diagnosis on MRI	7/13	8/10	6/6	8/8	8/8

[1]Combined involvement of multiple nerves. MRI: Magnetic resonance imaging; CPN: Common peroneal nerve.

Table 3 Summery of magnetic resonance imaging findings of intraneural ganglion cyst of peripheral nerves

SN	Involved nerve	Extension			Labral or capsular tear	Joint abnormality	Muscle denervation
		Anatomical extent along the parent nerve	Branches	Intra-articular extension			
1	Right CPN	Upto sciatic bifurcation	Recurrent articular	Anterior aspect of PTF joint	Negative	-	Muscles of anterolateral compartment of leg
2	Left CPN	Upto posterolateral fibular head	Recurrent articular, deep peroneal	Anterior aspect of PTF joint	Negative	-	-
3	Right CPN	Upto sciatic bifurcation	Recurrent articular, superficial and deep peroneal	Anterior aspect of PTF joint	Negative	-	Muscles of anterolateral compartment of leg
4	Left CPN	Upto posterolateral fibular head	Recurrent articular, deep peroneal	Anterior aspect of PTF joint	Negative	-	-
5	Left CPN	Upto posterolateral fibular head	Recurrent articular, deep peroneal	Anterior aspect of PTF joint	Negative	-	Muscles of anterolateral compartment of leg
6	Right CPN	Upto posterolateral fibular head	Recurrent articular	Anterior aspect of PTF joint	Negative	-	Muscles of anterolateral compartment of leg
7	Right CPN	Upto neck of fibula	Recurrent articular	Anterior aspect of PTF	Negative		-
8	Right obturator	Along the lateral pelvic wall to pelvic brim	Anterior division	Anteromedial aspect of hip joint	Negative	-	Adductor brevis and magnus
9	Right suprascapular	Suprascapular to spinoglenoid notch	-	-	Negative	-	Supra and infraspinatus
10	Left proximal sciatic	At sciatic notch	Articular	Posteromedial aspect of hip joint	Negative	-	-
11	Right tibial	Upto tibial nerve	Articular, branch to popliteus muscle	Posterior aspect of PTF joint	Negative	-	-
12	Left tibial	Upto sciatic bifurcation	Articular, branch to popliteus muscle, branch to tibialis posterior muscle	Posterior aspect of PTF and knee joints	Negative	-	Popliteus and tibialis posterior
13	Right suprascapular	From the level of AC joint to below the spinoglenoid notch	Articular branch to AC joint	AC joint	Negative	-	-

PTF: Proximal tibiofibular; AC: Acromioclavicular; CPN: Common peroneal nerve.

the spinoglenoid notch and can cause compression of the suprascapular nerve (Figure 16).

Nerve abscess related to HD: Granulomatous nerve lesions of HD may show central breakdown and abscess formation. These are relatively uncommon and are seen in the tuberculoid form of the leprosy (Figure 17).

DISCUSSION

INGC is often referred to as a rare non-neoplastic mucinous cyst located within the epineurium of peripheral

Table 4 Magnetic resonance features differentiating intraneural ganglion cyst from extraneural ganglion cyst

	Intraneural ganglion cyst	Extraneural ganglion cyst
Cyst size	Small	Large
Cyst shape	Tubular beaded configuration	Globular
Cyst pattern and location	It is along the course of the nerve and its branches with no fat plane between the cyst and the nerve	It does not follow the course of the nerve; the nerve is seen separately from the cyst with an intervening preserved fat plane; usually located in between the fibula and peroneus longus muscle, with or without an intramuscular extension
PTF joint connection	Is present and the tail lies anteromedial to proximal fibula between 10-12 o'clock position on axial MR images	Is present but located more superiorly and anterolateral to the proximal fibula at 12-2 o'clock position on axial MR images
Relation with fibula	The extension of the cyst along the articular branch appears to cross the fibula from medial to lateral ("Transverse limb sign")	The cyst never crosses the fibula and always lies anterior, anterolateral or lateral to the fibula (Absent "Transverse limb sign")
Muscle denervation	Common	Uncommon

MR: Magnetic resonance; PTF: Proximal tibiofibular.

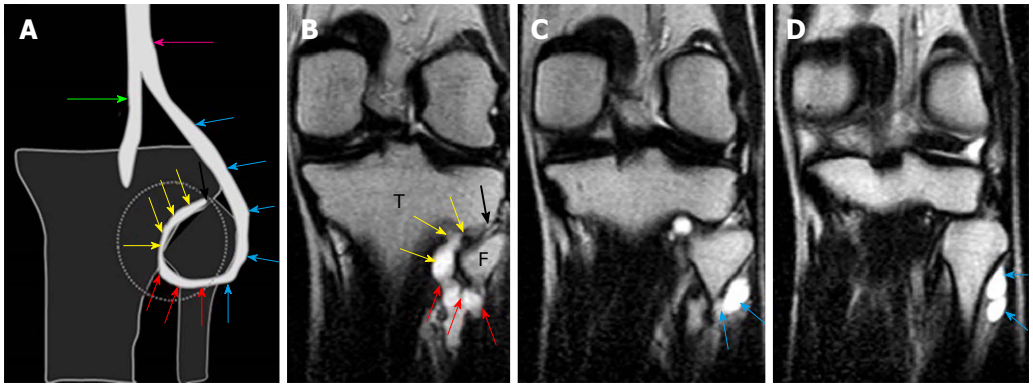

Figure 1 A shows a diagrammatic representation of the intraneural ganglion cyst associated with the proximal tibiofibular joint in the coronal plane; B-D are serial, coronal, T2-weighted, fast spin echo images of the knee show the origin of the lobulated tubular cyst from the proximal tibiofibular joint also called the "tail sign" demonstrated by the black arrows. The further extension along the descending limb (yellow arrows) of the articular branch represents the "vertical limb sign". The ascending limb of the articular branch (red arrows) demonstrates the "transverse limb sign" which continues to the CPN (blue arrows). Extension of the cyst into the two limbs of the articular branch and further ascent into the parent nerve represents the "u-sign". T: Tibia; F: Fibula; CPN: Common peroneal nerve.

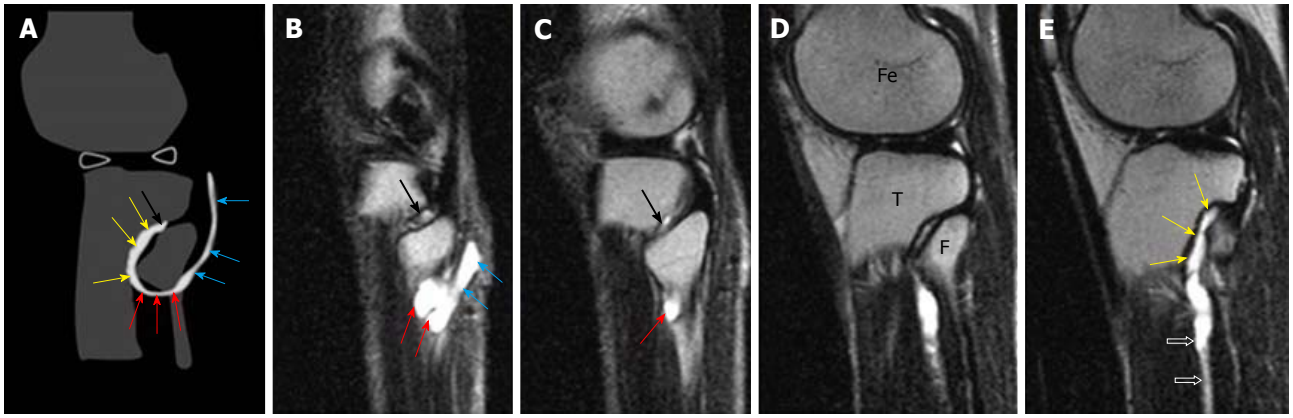

Figure 2 A shows a diagrammatic representation of the intraneural ganglion cyst associated with the proximal tibiofibular joint in the sagittal plane; B-E serial, sagittal, T2-weighted, fast spin echo images of the knee show the origin of the lobulated tubular cyst from the proximal tibiofibular joint represents the "tail sign" (black arrows). The further extension along the descending limb (yellow arrows) represents the "vertical limb sign" and ascending limb (red arrows) of the articular branch demonstrates the "transverse limb sign"; which continues to the CPN (blue arrows). The cyst also extends along the deep peroneal nerve (open arrows) in image E. T: Tibia; F: Fibula; CPN: Common peroneal nerve; Fe: Femur.

nerves and is closely related to an adjoining joint[7-11,20,24,25]. These lesions commonly affect the peroneal nerve at the knee but can involve the other peripheral nerves[7,26,27] as shown in this series. They usually present with mild symptoms and remain undiagnosed initially[27]. MRI plays an important role in diagnosing this condition and can

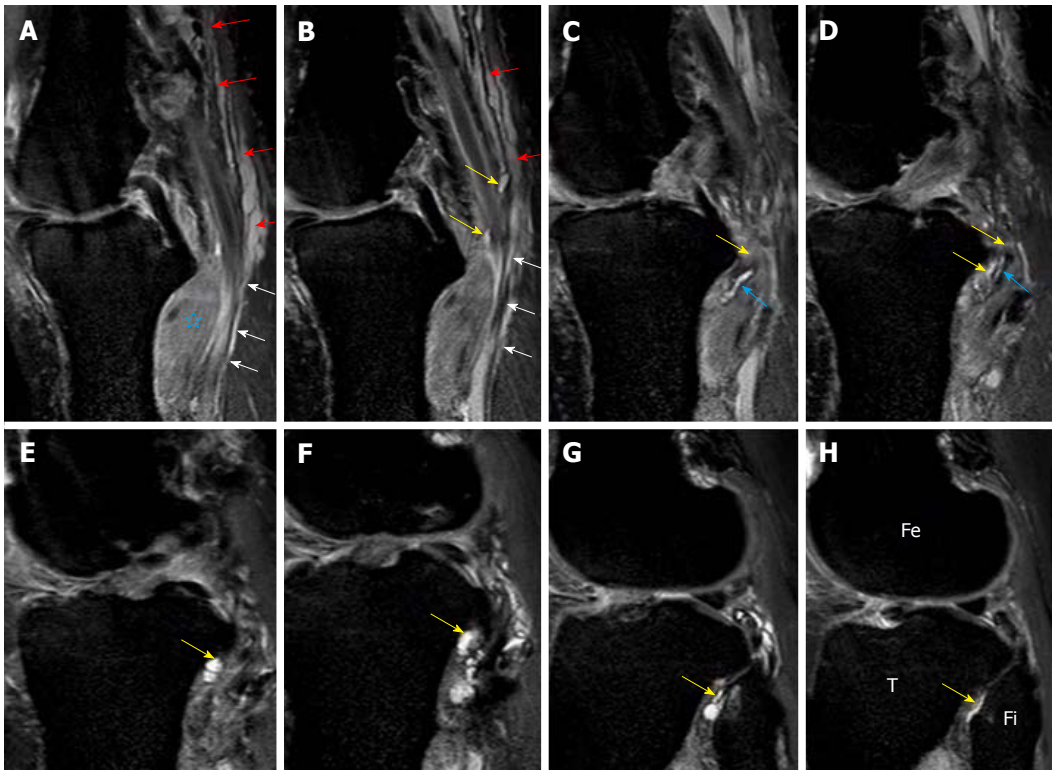

Figure 3 Images A-H show serial, proton density-weighted fat suppressed sagittal sections of the knee demonstrate the longitudinally oriented cystic lesion in the tibial nerve (red arrows) with extension along the articular branch to proximal tibiofibular joint (yellow arrows), branch to popliteus (blue arrows) and tibialis posterior muscles (white arrows). Note the denervation edema in the popliteus muscle (star). T: Tibia; Fi: Fibula; Fe: Femur.

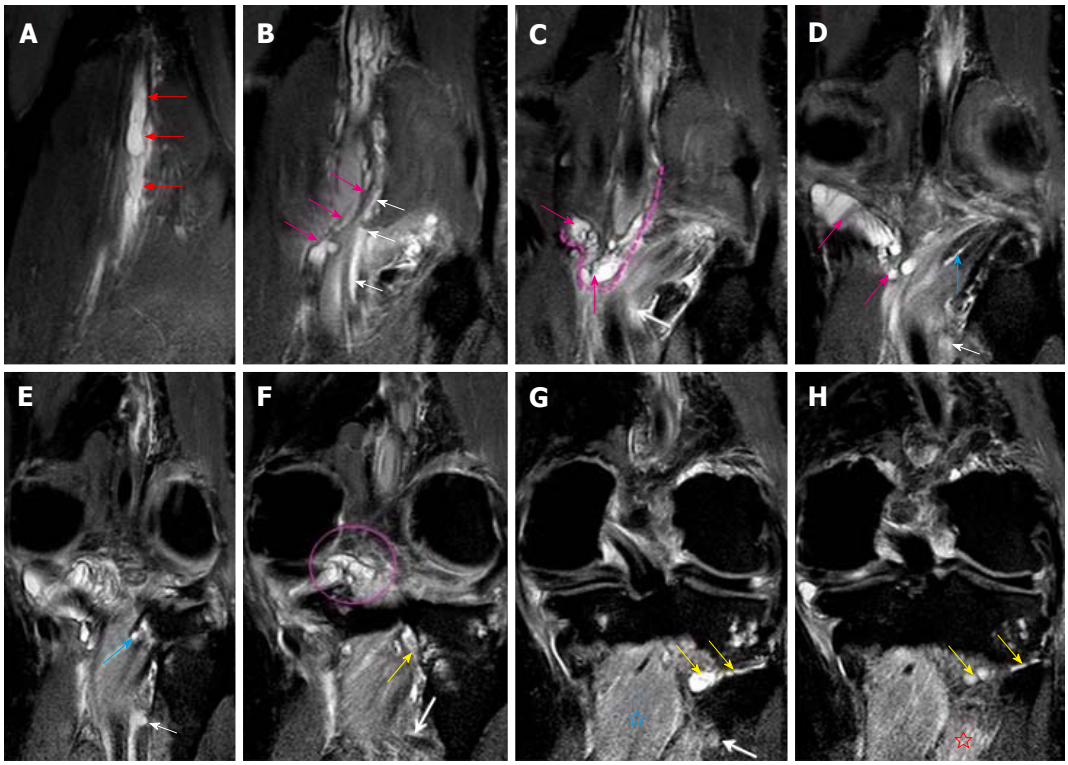

Figure 4 Images A-H show serial, proton density-weighted fat suppressed coronal sections of the knee demonstrate the longitudinal extent of intraneural cyst in the tibial nerve (red arrows), with propagation of cyst along the articular branches that communicate with the posterior aspect of knee joint (pink arrows, dashed line and circle) and to the postero-inferior part of proximal tibiofibular joint (yellow arrows). This represents a dual joint connection (knee and proximal tibiofibular) from the same intraneural ganglion cyst. The cyst also extends along the branch to the popliteus (blue arrows) and tibialis posterior muscles (white arrows). Note the denervation edema in the popliteus (blue star) and tibialis posterior (red star) muscles. Superiorly, the cyst extends up to the bifurcation of the sciatic nerve in the distal third of the thigh.

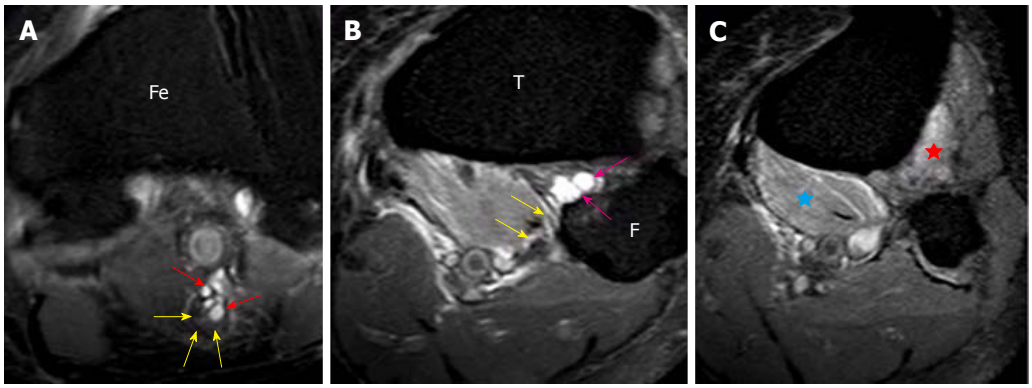

Figure 5 Images A-C show serial, proton density-weighted fat suppressed axial images of the knee demonstrate the eccentric cyst (red arrows) within the epineurium of tibial nerve displacing the nerve fascicles (yellow arrows) which represents the "signet ring sign" (A). The joint connection (pink arrows) is well appreciated where the cyst arises from the posterior aspect of the PTF joint. This represents the "tail sign" (B). The cyst (yellow arrows) extends along the posterior surface of the popliteus muscle into the branch to popliteus muscle. Denervation edema is seen in the popliteus (blue star) and tibialis posterior (red star) muscles. T: Tibia; F: Fibula; Fe: Femur; PTF: Proximal tibiofibular.

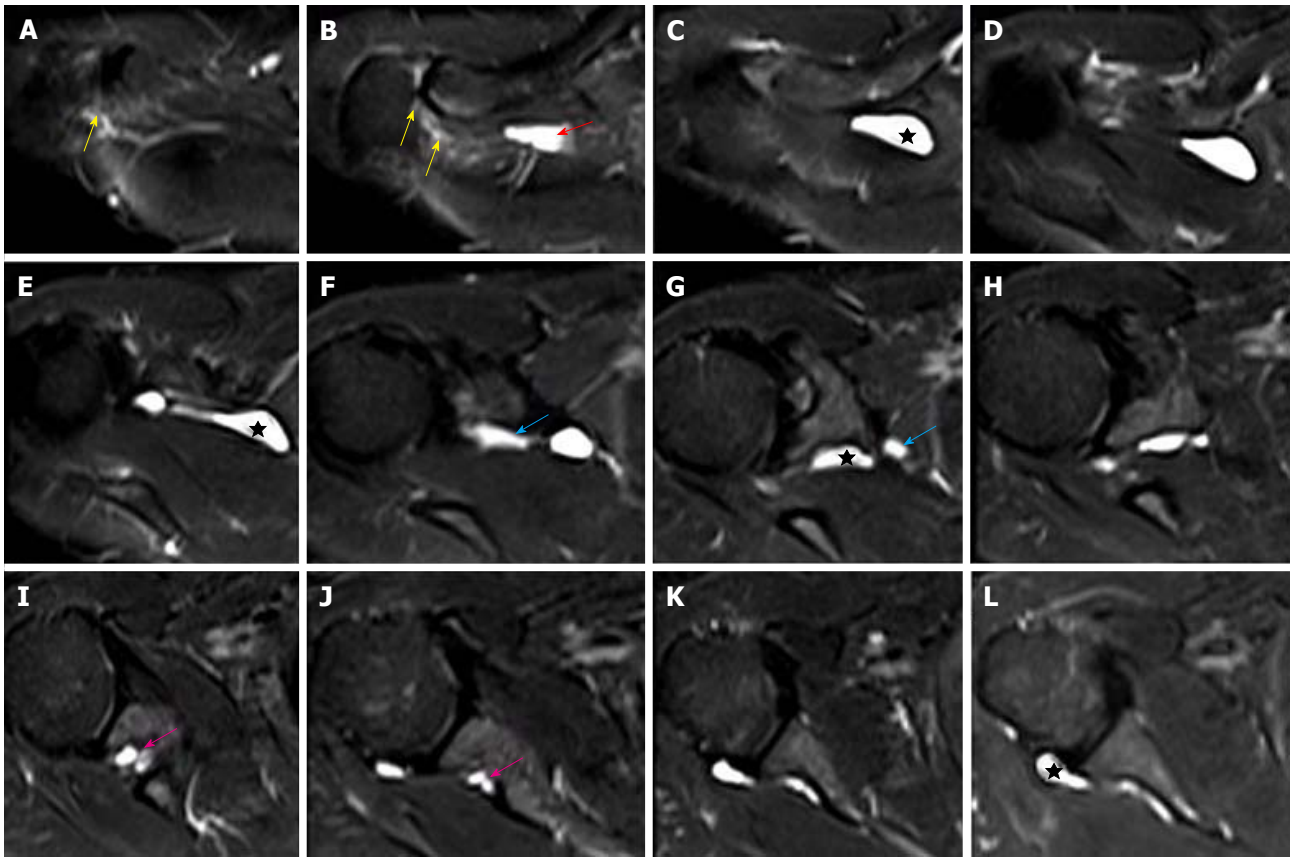

Figure 6 Images A-L show serial T2-weighted fat suppressed axial sections of the right shoulder, outlines the longitudinally oriented cyst (stars) along the course of the suprascapular nerve. The cyst extends from the level of the acromioclavicular joint (B) to the posterior aspect of glenohumeral joint (L). A narrow joint connection extends along the expected course of the articular branch of the suprascapular nerve to the acromioclavicular joint (yellow arrows). Further descend of the intraneural cyst through the posterior triangle into the suprascapular and spinoglenoid notches are demonstrated by red, blue and pink arrows respectively. No obvious labral or capsular tear or degeneration of joint is noted on magnetic resonance imaging.

reliably demonstrate the presence and the pattern of the cystic lesion and the exact level of communication of the cyst to the adjacent joint[8,20,28,29]. This typical imaging pattern and its consistent anatomical location within the nerves and the communication with adjoining joints, distinguish the intraneural cyst from the other neurogenic or extra neural cystic lesions[8,28,29]. Recognition of its articular connection on MR further helps in complete removal of the cyst, thus avoiding cyst recurrences[20,29].

The exact pathogenesis of the INGC is still not known. There are numerous hypotheses for its pathogenesis ranging from recurrent trauma, intra-neural hemorrhage, mucoid degeneration, *de novo* formation from haemartomatous cell rests[7,11,30-32] and the more recent "unified articular theory"[20,29,33,34]. According to the latter, the INGC originates from an adjoining joint and dissects

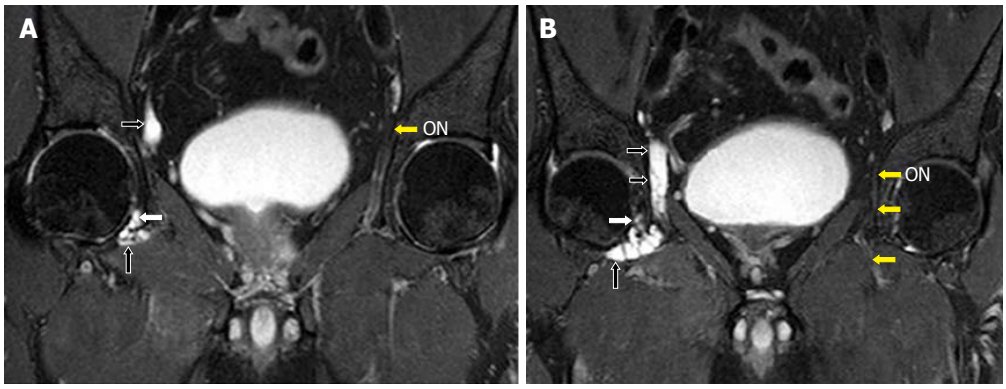

Figure 7 Images A, B show serial, T2-weighted fat suppressed coronal sections of the pelvis that demonstrates the longitudinally oriented intraneural cyst in the right obturator nerve (black arrows). The extension along the articular branch to the anteromedial aspect of right hip joint (white arrows) is also seen. Note the normal left obturator nerve (ON, yellow arrows). Reprinted with permission from Acta Neurologica Belgica.

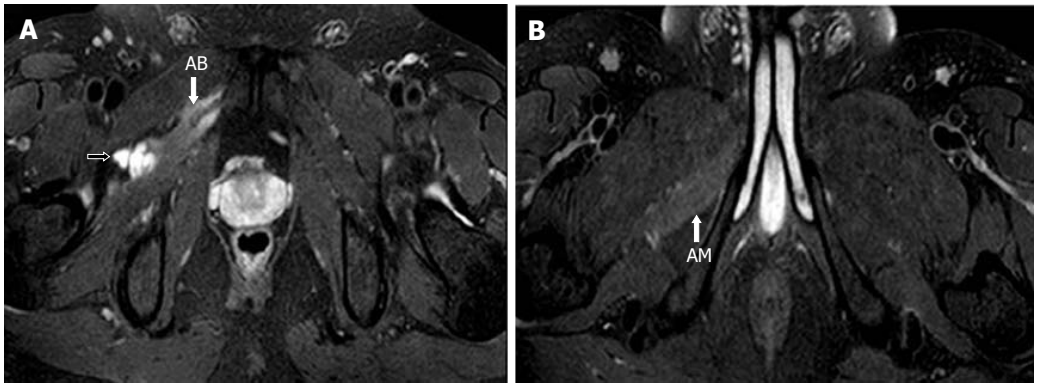

Figure 8 Image A, B show serial, T2-weighted fat suppressed axial images of the pelvis that demonstrates the further inferior extension of the cyst along the anterior branch of the obturator nerve (black arrow). Note the denervation atrophy of adductor brevis (AB) and magnus (AM) muscles. Reprinted with permission from Acta Neurologica Belgica.

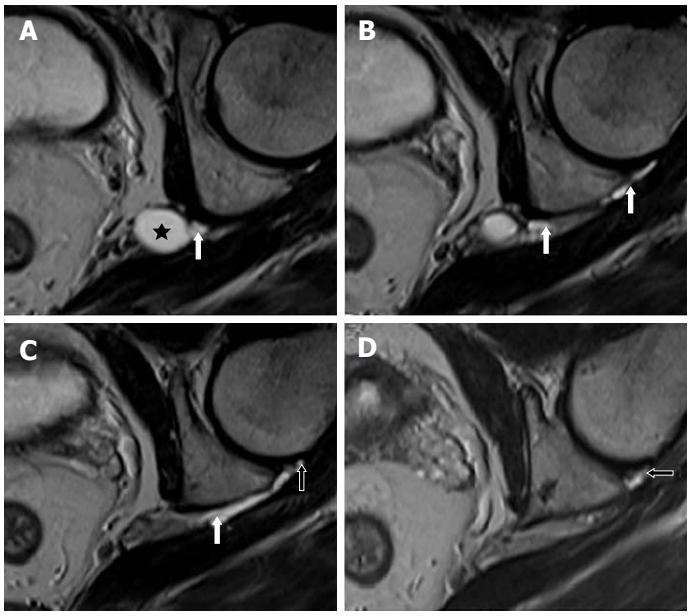

Figure 9 Image A-D show serial, T2-weighted, fast spin echo axial sections of the left hip joint highlighting a cyst (star) at the level of the left sciatic notch. An extension along the expected course of the articular branch of the sciatic nerve (white arrows) communicating with the posteromedial aspect of the ipsilateral hip joint (open arrows) is also seen.

along the articular branch into the parent nerve. The cyst dissects along the path of least resistance, namely the

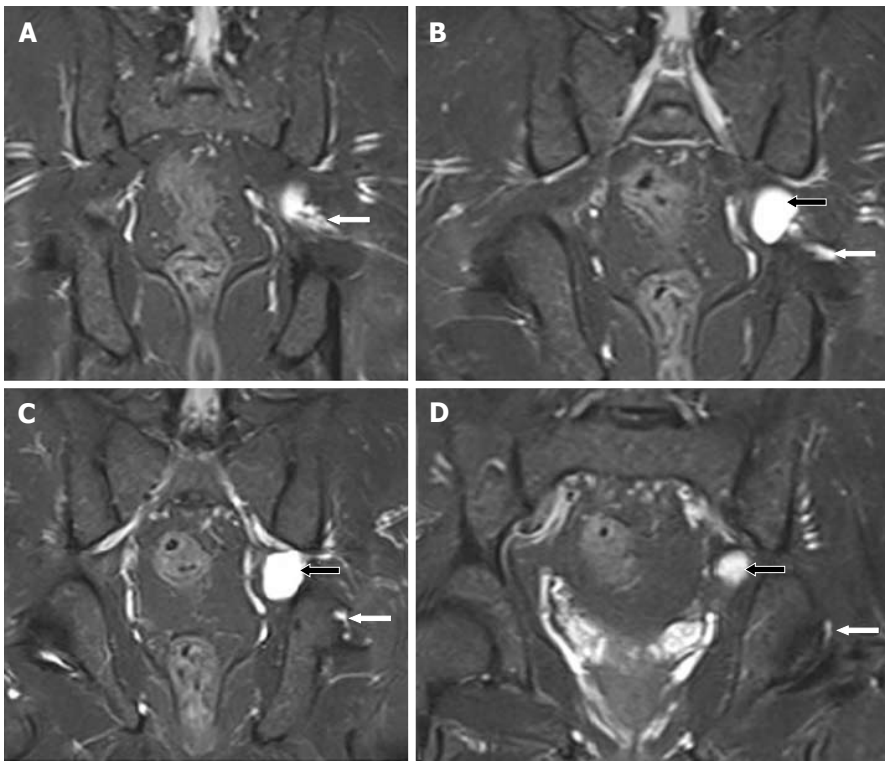

Figure 10 Images A-D show serial, T2-weighted fat suppressed coronal sections of the pelvis, demonstrate a cyst (black arrows) at the level of the left sciatic notch. The cyst extends along the articular branch of the sciatic nerve (white arrows) and communicates with the posteromedial aspect of the ipsilateral hip joint (D). No obvious labral or capsular tear or degeneration of joint is noted.

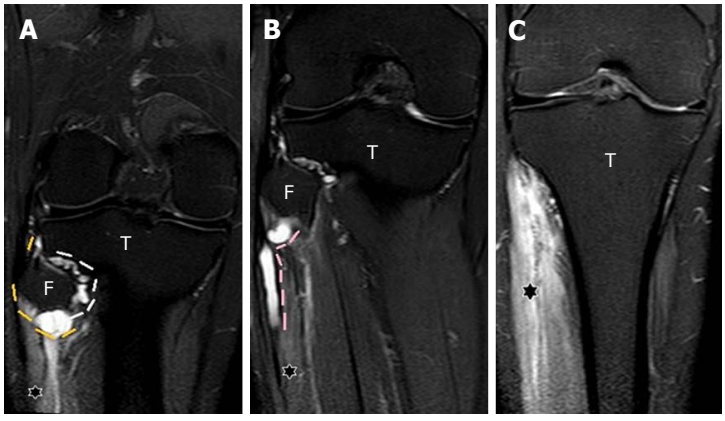

Figure 11 Images A-C show serial, coronal, proton density fat suppressed sections of the knee and proximal leg. The entire extent of the cyst within the articular branch (white dashes) to the PTF joint extending to the CPN (yellow dashes) at the posterolateral fibular neck is seen, demonstrating the "u-sign" (A). The cyst extends into the proximal portion of the superficial peroneal nerve (pink dashes) for a length of approximately 5 cm (B). Denervation hyperintensity of the muscles (stars) of anterior and peroneal compartments of the leg is also seen. T: Tibia; F: Fibula; PTF: Proximal tibiofibular; CPN: Common peroneal nerve.

perineural tissue of the nerve[11,30,31].

The diagnostic work-up includes clinical examination, electrophysiological studies and imaging. The ganglion cyst usually presents with pain, motor weakness and paraesthesia along the distribution of involved nerve[13-15,35]. Electrophysiological studies including electromyography and nerve conduction studies may indicate muscle denervation and conduction latency, respectively[35-38]. MRI is the imaging of choice for the nerve and its surrounding soft tissues[37,39-41]. It helps in defining the lesion along the course of the nerve.

On MR, these cysts are small in size and demonstrate the typical, tubular beaded configuration oriented longitudinally along the course of the involved nerve and its branches[8,9,19,38,40]. They appear as low signal on T1-weighted and high signal on T2-weighted images[42,43]. The joint connection and the extension of the cyst along the articular branch of nerve when present, can be well demonstrated[20,29,30,36,38,39]. Further denervation muscle edema as T2 hyperintensity and muscle atrophy as T1 hyperintensity can be seen[8,10,38]. In the peroneal intraneural cyst, the PTF joint connection and a cyst

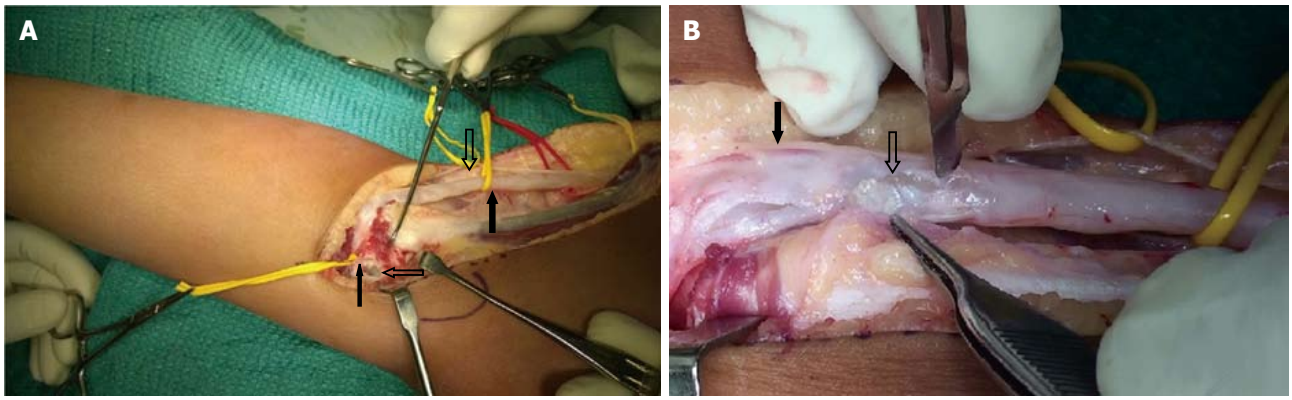

Figure 12 The intraoperative images of one of these patients. A: Surgical exposure and decompression of the CPN in a 9-year-old girl presenting with foot drop. The intraoperative picture shows a thickened CPN (thick block arrow); the sural communicating branch of the CPN (thick hollow arrow); the articular branch of the CPN (thin block arrow) and the arthrotomy of the PTF joint and a mucinous cyst within it (thin hollow arrow); B: Close up of the CPN, being decompressed with multiple stab incisions with mucin (hollow arrow) within the substance of the nerve. The superficial peroneal branch of the nerve (block arrow) appeared unaffected which correlated clinically. PTF: Proximal tibiofibular; CPN: Common peroneal nerve.

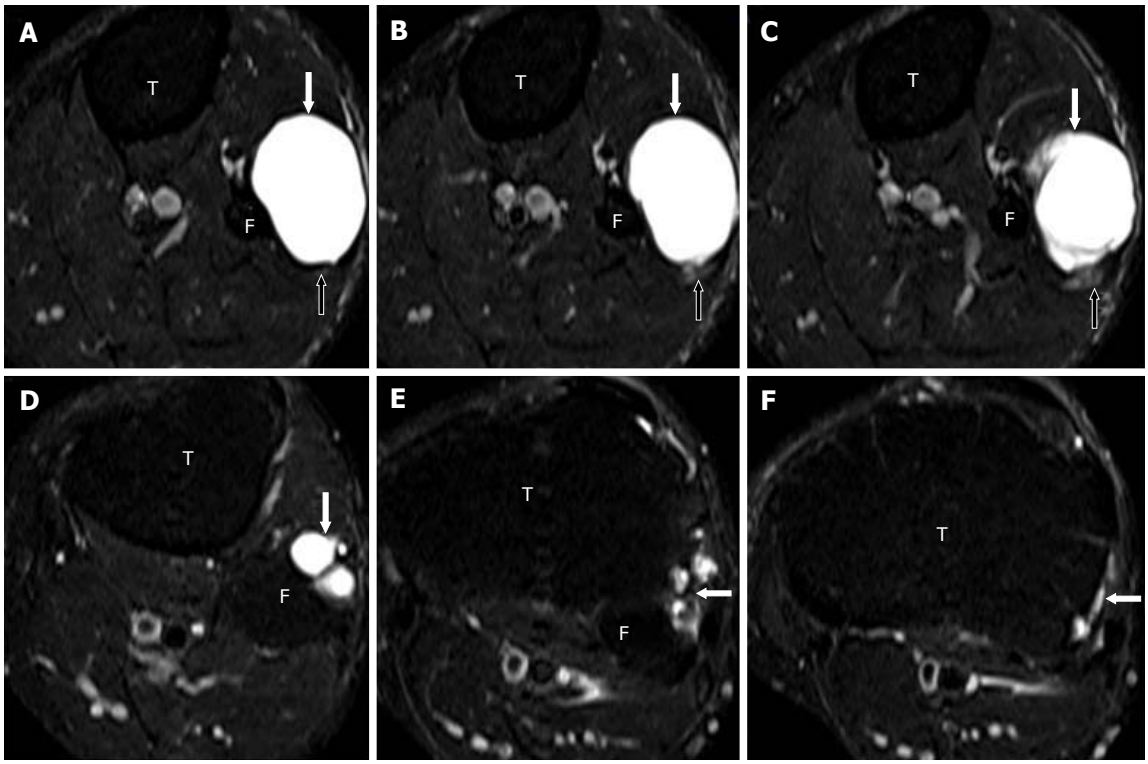

Figure 13 Images A-F show serial, T2-weighted fat suppressed axial sections of the proximal leg and demonstrate a large multilobulated globular extra-neural ganglion cyst (block arrows). The ENGC is antero-lateral to the proximal fibula and indenting the peroneus longus muscle anteriorly (A-C). The CPN (open arrows) lies posterior to the cyst but is seen separate from it. The tail of the cyst (arrows in D-F) extends superiorly and communicates with the superior aspect of the PTF joint. PTF: Proximal tibiofibular; CPN: Common peroneal nerve; ENGC: Extraneural ganglion cyst; T: Tibia; F: Fibula.

along the descending and ascending limb of articular branch of CPN can be seen in all the three orthogonal planes[20,24,29,38,39]. As described by Spinner *et al*[24,29,30] in 2008, on serial axial sections, the joint connection is interpreted as the "tail sign" (Figures 1-5 and 14) and the extension of the cyst in the ascending limb of the articular branch as the "transverse limb sign" (Figures 1, 2 and 14). An eccentric cyst within the outer epineurium of the CPN is interpreted as the "signet ring sign" (Figures 3-5 and 14). In all our seven CPN lesions, we found that they had evidence of joint connection; presence of cysts along the articular branch; variable proximal ascent of the intra-neural cyst along the CPN and distal descent along its branches. On coronal images this extension of the cyst along the descending and ascending portions of the articular branch is interpreted as "u-sign" (Figures 1, 2 and 11).

In the lower extremity, less commonly, they can involve the lumbosacral plexus, sciatic, obturator and tibial nerves[9,12,28,44]. The sciatic nerve can be involved in its

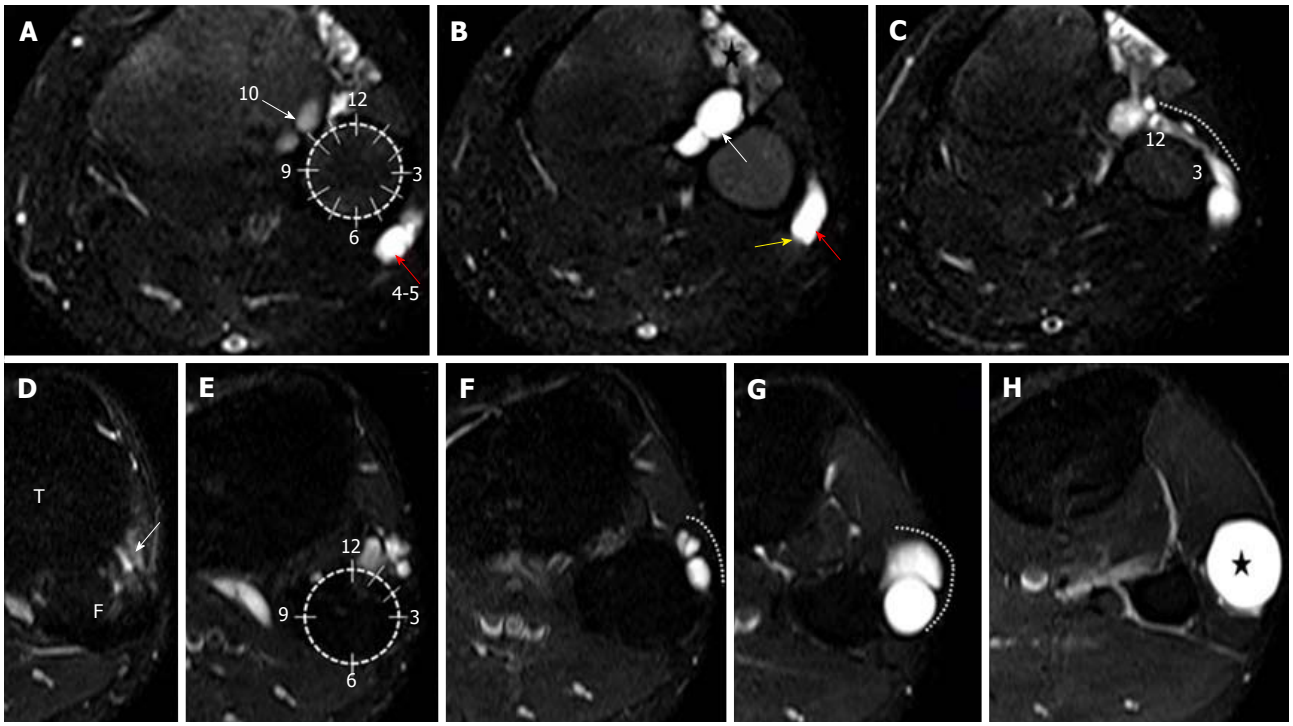

Figure 14 Axial, T2-weighted fat suppressed images A-H of the proximal leg show the left clock face model to differentiate intraneural ganglion cyst from extraneural ganglion cyst. A-C represent INGC where images A, B (at the upper-mid fibular head level) depict the joint connection of the cyst at the 10 o'clock (white arrows) which signifies the "tail sign". The cyst (red arrows) within the outer epineurium of the CPN (yellow arrow), between the 4 and 5 o'clock position represents the "signet ring sign". Image C, (at the level of fibular neck) shows the extension of the cyst along the ascending limb of the articular branch (dotted white line) depicting the "transverse limb sign". It crosses the anterior surface of fibula from the PTF joint and progresses clockwise from 12-3 o'clock position around the fibular head. On the other hand, images D-H, depicting ENGC show a more superiorly located joint connection (white arrow) in between 12-2 o'clock position in images D, E. It lies anterolateral to the fibula (dotted white line) and never crosses it as seen in images F, G. The cyst (star) is more globular and lying in the intermuscular plane as seen in the image H. INGC: Intraneural ganglion cyst; CPN: Common peroneal nerve; ENGC: Extraneural ganglion cyst; T: Tibia; F: Fibula.

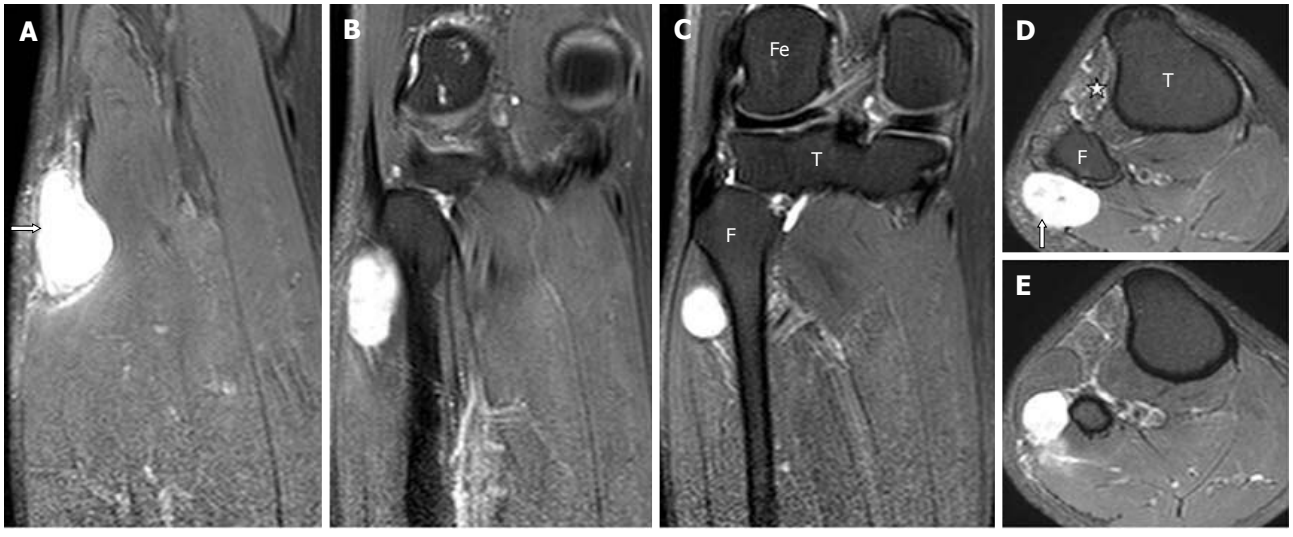

Figure 15 Serial, coronal (images A-C), and axial (images D-E), proton density fat suppressed sections show a well-defined oval cystic lesion at the posterolateral aspect of upper fibula along the expected course of common peroneal nerve which does not communicate within the proximal tibiofibular joint. Mild denervation edema is seen in the anterior compartment muscles (star). This is a case of cystic schwannoma involving the CPN. T: Tibia; F: Fibula; Fe: Femur; CPN: Common peroneal nerve.

proximal or distal portion. We have seen in our case, the presence of intra-neural sciatic ganglion cyst at the sacral notch, with characteristic tubular connection to the posteromedial hip joint on MR. There were no obvious degenerative changes in the joint, labral tears or other structural problems on both the conventional MR and radiographs in the case reported herein. However, intra-articular contrast was not given and hence, the common underlying pathology of labral tear or capsular rent with intra-neural extension from a paralabral or para-articular

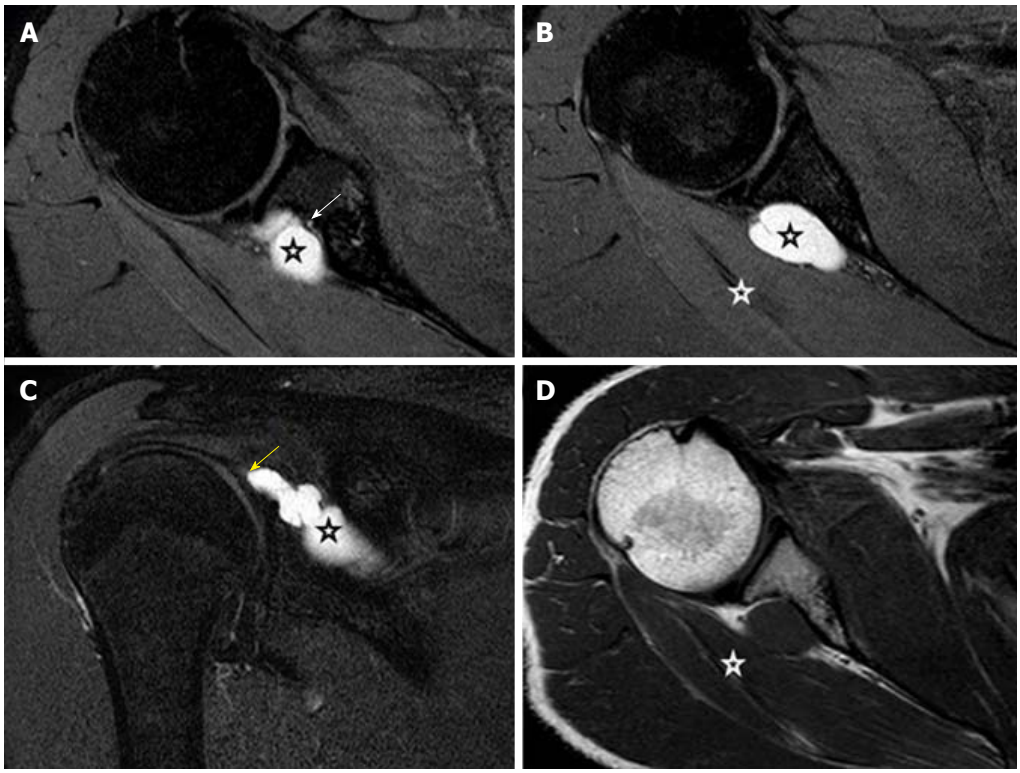

Figure 16 Proton density fat suppressed, serial axial (A, B), coronal (C) and T1-weighted, axial (D) show a well-defined lobulated slightly elongated cystic lesion (black stars) at the spinoglenoid notch compressing upon the suprascapular nerve (white arrow), which is seen separately from the cyst with preserved fat plane. There is a tail like communication (yellow arrow) of the cyst with the posterior labrum. This suggests labral tear with paralabral cyst formation. Denervation edema and mild volume loss in the infraspinatus muscle (white stars) is seen.

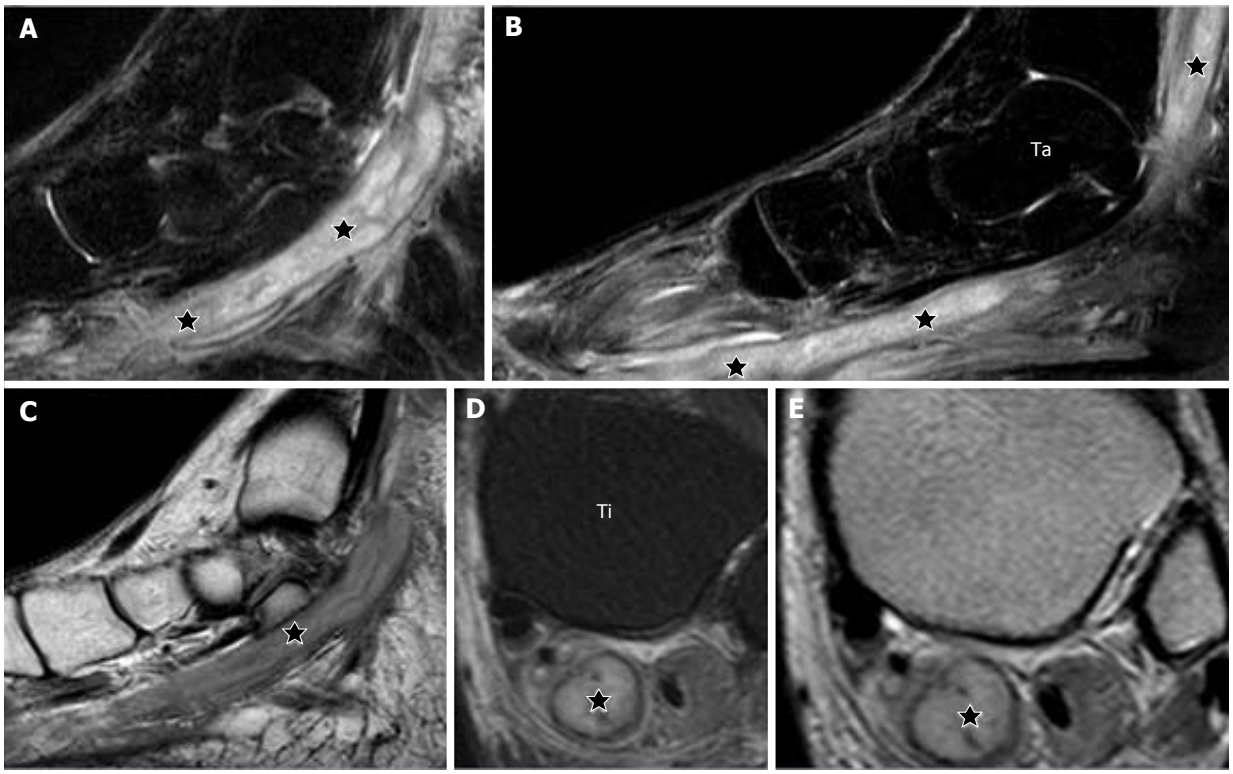

Figure 17 T2-weighted fat suppressed, serial sagittal (A, B); T1-weighted, sagittal (C); T2-weighted fat suppressed, axial (D) and proton density-weighted, axial (E) show an elongated tubular cystic lesion (stars) along the posterior tibial nerve at the lower leg, ankle and foot. The lesion is seen within the substance of the nerve and has a central cystic component (stars) and a peripheral thin wall consistent with an abscess (D, E). This is a case of Hansen's disease with posterior tibial nerve abscess; Ta: Talus; Ti: Tibia.

cyst cannot be completely excluded. In Spinner's series of INGC around the hip and pelvic region[44], four out of five cases showed a cyst at the sciatic notch with an articular communication with the ipsilateral hip joint and further extension of the same into the sciatic nerve. Likewise, the obturator INGC also has a known joint connection with the anteromedial hip joint[44,45] as seen in our case. The propagation of the cyst along the articular branch and further dissection of the cyst along the parent nerve and its anterior and posterior branches has been described[45] and is demonstrated in the current case. Variable atrophy and denervation hyperintensity of ipsilateral adductor brevis and magnus muscles was also seen in our case.

Various case reports have described the involvement of tibial nerve in the popliteal fossa by the INGC[7,12,36,40,46,47]. These tibial INGCs are the posterior counterpart of the peroneal INGCs and demonstrate an intraneural cyst and its connection to the adjacent joint *via* the articular branch to the PTF joint[40,47,48]. In one of our cases there was evidence of dual communication of the tibial intra-neural cyst to both the knee and PTF joint through its corresponding articular branches (Figures 3-5) and further extension of cyst into the popliteus and tibialis posterior nerve branches (Figures 3-5). Denervation edema was noted in both popliteus and tibialis posterior muscles (Figures 3-5).

In the upper extremity, less commonly, they can involve the suprascapular, ulnar or median nerves[8,49]. INGC is a common cause of suprascapular nerve im-pingement at the suprascapular and more commonly at the spino-glenoid notch originating from gleno-humeral joint and often associated with tears of the glenoid labrum[50,51]. It may also arise from the acromioclavicular (AC) joint as articular branch of the suprascapular nerve innervate the AC joint[52]. They track along the articular branch into the parent nerve and can be associated with a labral tear or capsular rent[53]. However, in one of our cases, the joint connection could not be demonstrated. In the other case there was an AC joint connection (Figure 6). In contrast to this extra neural paralabral cyst where the nerve is seen separately from the cyst with a preserved fat plane in between, an INGC affecting the suprascapular nerve evolves within the epineurium of the nerve as seen in other peripheral nerve INGCs[53-55].

In our series of 245 cases of peripheral nerve palsy for which imaging was done, 45 cases of cystic lesions were identified. Of these 45 cystic lesions, more than a fourth (13 cases), were diagnosed to be INGC retrospectively. Although the exact incidence of INGC is not known, in our series it was the commonest cause for the cystic nerve lesions. The fact that these lesions are reported as rare[7-11] may be incorrect since they are often underdiagnosed as shown in our series. The primary radiological diagnosis of INGC in our series was correct in only 60% of the cases, *i.e.*, the last 7 cases in this series. Lack of knowledge of this pathological entity and absence of this entity in standard radiological textbooks were probable reasons for its under-diagnosis among the early cases in this series. INGC as an entity was little known before the 90s even in western literature, being reported as rare case reports or case series prior to that[14,56,57]. The others cystic lesions in this series varied from cystic schwannoma, extra-neural ganglion cysts, paralabral cysts and nerve abscesses. All of these cystic lesions were correctly diagnosed primarily except two ENGCs which were mistaken as cystic schwannoma.

This article endeavors to describe different INGCs at varying anatomical locations, to emphasize the fact that it is the single largest cause of surgically treatable mono-neuropathy due to a cystic nerve lesion. These lesions have a classic configuration, anatomical location within the nerve and extensions along its branches. Most have defined communications to the nearby joint and the innervated muscles show signs of denervation. Identification of the articular branch and disconnecting it is important to prevent recurrence. The youngest patient in this series had surgery, 7 mo after the onset of nerve palsy due to the late presentation at the hospital. The cysts were decompressed and the articular branch disconnected during the surgery. The innervated muscles showed MRC grade 4 recovery about one year after surgery, in spite of the late intervention.

In conclusion, over the past years, INGC has been increasingly recognized as a radio-pathologic entity. It is a cause of peripheral neuropathy that can be treated by surgery, but is often under-diagnosed. This research looked at a historic cohort of patients that were imaged for mono-neuropathy and within that the subsets of patients with cystic lesions were looked at, in greater detail. We were certainly missing the diagnosis of the INGC until recently. The surgical treatment of a cystic schwannoma is enucleation as opposed to the INGC where the nerve is decompressed and the articular branch is excised. This study re-emphasizes that any elongated cystic lesion along the course of a peripheral nerve and in the vicinity of a joint should be considered as an INGC unless proved otherwise. This will ensure that both the radiologist and the surgeon would diligently search for the articular (branch) connection and hence prevent a misdiagnosis and a possible recurrence.

COMMENTS

Background

Intraneural ganglion cysts (INGCs) of peripheral nerves occur within the epineurium and related to the adjoining joint were thought of as a relatively uncommon entity. They are generally formed when the joint fluid tracks into the epineural sheath of the articular branch of the nerve and further along the path of least resistance. They commonly present with sensory-motor symptoms along the distribution of the involved nerve. If these are identified and treated early, symptoms are reversible. The articular branch disconnection of the cyst will avoid the recurrence of the cyst. In this study, they evaluated 13 such cases involving the different peripheral nerves.

Research frontiers

Magnetic resonance imaging (MRI) is the most important modality to diagnose this condition. It also allows differentiating it from other intra or juxtra-neural

lesions like neurogenic tumors and the extra-neural ganglion cyst. Though it has been described as a rare disease in literature, the results of this study showed that it is the single largest cause of surgically treatable mono-neuropathy caused by a cystic nerve lesion.

Innovations and breakthroughs

In this study, the classic MRI pattern of the INGC was a useful tool in diagnosing this condition and to differentiate it from other intra or extraneural cystic lesions. These results agree with prior literature. However, in this study, 40% of cases representing the initial cases in this series were misdiagnosed preoperatively and were mistaken for neurogenic tumor. This emphasizes the diagnostic knowledge of this condition. An early diagnosis and surgical intervention will improve patient outcomes.

Applications

In the order of differential diagnosis of cystic nerve lesions arising in the vicinity of a joint, the INGC comes first. This research re-emphasizes that the knowledge of the classic MRI pattern is paramount in diagnosing the INGC. An early surgical intervention will cause significant reversal of neurologic symptoms.

Terminology

INGC: Intraneural ganglion cyst, cyst occurring within the epineurium of nerve; ENGC: Extraneural ganglion cyst, cyst adjacent to nerve but outside the epineural sheath; CPN: Common peroneal nerve, a nerve in the lower leg that provides sensation and motor function to parts of the lower leg.

Peer-review

This review article has well described the use and dose optimisation of computed tomography in patients with cystic nerve lesions, it is well-organized and useful for clinical practice, especially for the western radiology society.

REFERENCES

1 **van Brakel WH**, Nicholls PG, Das L, Barkataki P, Suneetha SK, Jadhav RS, Maddali P, Lockwood DN, Wilder-Smith E, Desikan KV. The INFIR Cohort Study: investigating prediction, detection and pathogenesis of neuropathy and reactions in leprosy. Methods and baseline results of a cohort of multibacillary leprosy patients in north India. *Lepr Rev* 2005; **76**: 14-34 [PMID: 15881033]

2 **de Freitas MR**, Nascimento OJ, Quaglino EA, Oliveira A, Hahn MD. Small-fiber polyneuropathy in leprosy without skin changes: study of 17 cases. *Arq Neuropsiquiatr* 2003; **61**: 542-546 [PMID: 14513154 DOI: 10.1590/S0004-282X2003000400003]

3 World Health Organization, Global leprosy situation, Relevé Épidémiologique Hebd. Sect. Hygiène Secrétariat Société Nations Wkly Epidemiol Rec Health Sect Secr Leag Nation 2005; **80**: 289-295

4 **Scollard DM**, Adams LB, Gillis TP, Krahenbuhl JL, Truman RW, Williams DL. The continuing challenges of leprosy. *Clin Microbiol Rev* 2006; **19**: 338-381 [DOI: 10.1128/CMR.19.2.338-381.2006]

5 **Joyce M**, Scollard D. Lepr. Hansens Dis. Conns Curr. Ther., edition 1, Saunders, Philadelphia, 2004: 100-105

6 **Ustianowski AP**, Lockwood DN. Leprosy: current diagnostic and treatment approaches. *Curr Opin Infect Dis* 2003; **16**: 421-427 [PMID: 14501994 DOI: 10.1097/01.qco.0000092813.64370.be]

7 **Patel P**, Schucany WG. A rare case of intraneural ganglion cyst involving the tibial nerve. *Proc* (Bayl Univ Med Cent) 2012; **25**: 132-135 [PMID: 22481843]

8 **Uetani M**, Hashmi R, Hayashi K, Nagatani Y, Narabayashi Y, Imamura K. Peripheral nerve intraneural ganglion cyst: MR findings in three cases. *J Comput Assist Tomogr* 1998; **22**: 629-632 [PMID: 9676458 DOI: 10.1097/00004728-199807000-00023]

9 **Harbaugh KS**, Tiel RL, Kline DG. Ganglion cyst involvement of peripheral nerves. *J Neurosurg* 1997; **87**: 403-408 [PMID: 9285606 DOI: 10.3171/jns.1997.87.3.0403]

10 **Spinner RJ**, Desy NM, Rock MG, Amrami KK. Peroneal intraneural ganglia. Part I. Techniques for successful diagnosis and treatment. *Neurosurg Focus* 2007; **22**: E16 [PMID: 17613207 DOI: 10.3171/foc.2007.22.6.17]

11 **Jacobs RR**, Maxwell JA, Kepes J. Ganglia of the nerve. Presentation of two unusual cases, a review of the literature, and a discussion of pathogenesis. *Clin Orthop Relat Res* 1975: 135-144 [PMID: 172271 DOI: 10.1097/00003086-197511000-00020]

12 **Adn M**, Hamlat A, Morandi X, Guegan Y. Intraneural ganglion cyst of the tibial nerve. *Acta Neurochir* (Wien) 2006; **148**: 885-889; discussion 889-890 [PMID: 16775659 DOI: 10.1007/s00701-006-0803-8]

13 **Johnston JA**, Lyne DE. Intraneural ganglion cyst of the peroneal nerve in a four-year-old girl: a case report. *J Pediatr Orthop* 2007; **27**: 944-946 [PMID: 18209620 DOI: 10.1097/BPO.0b013e3181558c05]

14 **Tehli O**, Celikmez RC, Birgili B, Solmaz I, Celik E. Pure peroneal intraneural ganglion cyst ascending along the sciatic nerve. *Turk Neurosurg* 2011; **21**: 254-258 [PMID: 21534214 DOI: 10.5137/1019-5149.JTN.2660-09.1]

15 **Liang T**, Panu A, Crowther S, Low G, Lambert R. Ultrasound-guided aspiration and injection of an intraneural ganglion cyst of the common peroneal nerve. *HSS J* 2013; **9**: 270-274 [PMID: 24426879 DOI: 10.1007/s11420-013-9345-9]

16 **Lang CJ**, Neubauer U, Qaiyumi S, Fahlbusch R. Intraneural ganglion of the sciatic nerve: detection by ultrasound. *J Neurol Neurosurg Psychiatry* 1994; **57**: 870-871 [PMID: 8021688 DOI: 10.1136/jnnp.57.7.870-a]

17 **Leijten FS**, Arts WF, Puylaert JB. Ultrasound diagnosis of an intraneural ganglion cyst of the peroneal nerve. Case report. *J Neurosurg* 1992; **76**: 538-540 [PMID: 1310730 DOI: 10.3171/jns.1992.76.3.0538]

18 **Masciocchi C**, Innacoli M, Cisternino S, Barile A, Rossi F, Passariello R. Myxoid intraneural cysts of external popliteal ischiadic nerve. Report of 2 cases studied with ultrasound, computed tomography and magnetic resonance imaging. *Eur J Radiol* 1992; **14**: 52-55 [PMID: 1314178 DOI: 10.1016/0720-048X(92)90062-E]

19 **McCarthy CL**, McNally EG. The MRI appearance of cystic lesions around the knee. *Skeletal Radiol* 2004; **33**: 187-209 [PMID: 14991250 DOI: 10.1007/s00256-003-0741-y]

20 **Spinner RJ**, Atkinson JL, Scheithauer BW, Rock MG, Birch R, Kim TA, Kliot M, Kline DG, Tiel RL. Peroneal intraneural ganglia: the importance of the articular branch. Clinical series. *J Neurosurg* 2003; **99**: 319-329 [PMID: 12924707 DOI: 10.3171/jns.2003.99.2.0319]

21 **Martinez Algarra JC**, Gastaldi Rodrigo P, Palomares Talens E. [Multiple schwannoma of the sciatic nerve. Apropos of a case]. *Rev Chir Orthop Reparatrice Appar Mot* 1999; **85**: 632-635 [PMID: 10575727]

22 **Parmar H**, Patkar D, Gadani S, Shah J. Cystic lumbar nerve sheath tumours: MRI features in five patients. *Australas Radiol* 2001; **45**: 123-127 [PMID: 11380354 DOI: 10.1046/j.1440-1673.2001.00891.x]

23 **Wu D**, Ba Z, Huang Y, Zhao W, Shen B, Kan H. Totally cystic schwannoma of the lumbar spine. *Orthopedics* 2013; **36**: e679-e682 [PMID: 23672923 DOI: 10.3928/01477447-20130426-36]

24 **Spinner RJ**, Carmichael SW, Wang H, Parisi TJ, Skinner JA, Amrami KK. Patterns of intraneural ganglion cyst descent. *Clin Anat* 2008; **21**: 233-245 [PMID: 18330922 DOI: 10.1002/ca.20614]

25 **Nicholson TR**, Cohen RC, Grattan-Smith PJ. Intraneural ganglion of the common peroneal nerve in a 4-year-old boy. *J Child Neurol* 1995; **10**: 213-215 [PMID: 7642891 DOI: 10.1177/088307389501000310]

26 **Kim TS**, Jo YH, Paik SS, Kim SJ. Intraneural Ganglion Cyst of the Peripheral Nerve: Two Cases Report. *J Korean Bone Jt Tumor Soc* 2013; **19**: 83 [DOI: 10.5292/jkbjts.2013.19.2.83]

27 **Haller JM**, Potter MQ, Sinclair M, Hutchinson DT. Intraneural ganglion in superficial radial nerve mimics de quervain tenosynovitis. *J Wrist Surg* 2014; **3**: 262-264 [PMID: 25364639 DOI: 10.1055/s-0034-1384746]

28 **Swartz KR**, Wilson D, Boland M, Fee DB. Proximal sciatic nerve intraneural ganglion cyst. *Case Rep Med* 2009; **2009**: 810973 [PMID: 20069041 DOI: 10.1155/2009/810973]

29 **Spinner RJ**, Luthra G, Desy NM, Anderson ML, Amrami KK. The clock face guide to peroneal intraneural ganglia: critical "times" and sites for accurate diagnosis. *Skeletal Radiol* 2008; **37**:

1091-1099 [PMID: 18641980 DOI: 10.1007/s00256-008-0545-1]
30 **Spinner RJ**, Amrami KK, Wang H, Kliot M, Carmichael SW. Cross-over: a generalizable phenomenon necessary for secondary intraneural ganglion cyst formation. *Clin Anat* 2008; **21**: 111-118 [PMID: 18220283 DOI: 10.1002/ca.20590]
31 **Krishnan KG**, Schackert G. Intraneural ganglion cysts: a case of sciatic nerve involvement. *Br J Plast Surg* 2003; **56**: 183-186 [PMID: 12791372 DOI: 10.1016/S0007-1226(03)00036-5]
32 **Colbert SH**, Le MH. Case report: intraneural ganglion cyst of the ulnar nerve at the wrist. *Hand* (NY) 2011; **6**: 317-320 [PMID: 22942857 DOI: 10.1007/s11552-011-9329-5]
33 **Spinner RJ**, Amrami KK, Wolanskyj AP, Desy NM, Wang H, Benarroch EE, Skinner JA, Rock MG, Scheithauer BW. Dynamic phases of peroneal and tibial intraneural ganglia formation: a new dimension added to the unifying articular theory. *J Neurosurg* 2007; **107**: 296-307 [PMID: 17695383 DOI: 10.3171/JNS-07/08/0296]
34 **Elangovan S**, Odegard GM, Morrow DA, Wang H, Hébert-Blouin MN, Spinner RJ. Intraneural ganglia: a clinical problem deserving a mechanistic explanation and model. *Neurosurg Focus* 2009; **26**: E11 [PMID: 19435441 DOI: 10.3171/FOC.2009.26.2.E11]
35 **Greer-Bayramoglu RJ**, Nimigan AS, Gan BS. Compression neuropathy of the peroneal nerve secondary to a ganglion cyst. *Can J Plast Surg* 2008; **16**: 181-183 [PMID: 19721802 DOI: 10.4172/plastic-surgery.1000570]
36 **Spinner RJ**, Desy NM, Amrami KK. Sequential tibial and peroneal intraneural ganglia arising from the superior tibiofibular joint. *Skeletal Radiol* 2008; **37**: 79-84 [PMID: 17968541 DOI: 10.1007/s00256-007-0400-9]
37 **Kukreja MM**, Telang VG. Common Peroneal Nerve Palsy Secondary to a Proximal Tibiofibular Joint "Ganglion Cyst"—A Case Report and Review of Literature. [accessed 2016 Jun 19]. Available from: URL: http://file.scirp.org/pdf/OJO_2015112014185133.pdf
38 **Coakley FV**, Finlay DB, Harper WM, Allen MJ. Direct and indirect MRI findings in ganglion cysts of the common peroneal nerve. *Clin Radiol* 1995; **50**: 168-169 [PMID: 7889707 DOI: 10.1016/S0009-9260(05)82993-9]
39 **Spinner RJ**, Amrami KK, Rock MG. The use of MR arthrography to document an occult joint communication in a recurrent peroneal intraneural ganglion. *Skeletal Radiol* 2006; **35**: 172-179 [PMID: 16333654 DOI: 10.1007/s00256-005-0036-6]
40 **Spinner RJ**, Atkinson JL, Harper CM, Wenger DE. Recurrent intraneural ganglion cyst of the tibial nerve. Case report. *J Neurosurg* 2000; **92**: 334-337 [PMID: 10659022 DOI: 10.3171/jns.2000.92.2.0334]
41 **Leon J**, Marano G. MRI of peroneal nerve entrapment due to a ganglion cyst. *Magn Reson Imaging* 1987; **5**: 307-309 [PMID: 3657403 DOI: 10.1016/0730-725X(87)90009-9]
42 **Dubuisson AS**, Stevenaert A. Recurrent ganglion cyst of the peroneal nerve: radiological and operative observations. Case report. *J Neurosurg* 1996; **84**: 280-283 [PMID: 8592235 DOI: 10.3171/jns.1996.84.2.0280]
43 **Iverson DJ**. MRI detection of cysts of the knee causing common peroneal neuropathy. *Neurology* 2005; **65**: 1829-1831 [PMID: 16344535 DOI: 10.1212/01.wnl.0000187098.42938.b6]
44 **Spinner RJ**, Hébert-Blouin MN, Trousdale RT, Midha R, Russell SM, Yamauchi T, Sasaki S, Amrami KK. Intraneural ganglia in the hip and pelvic region. Clinical article. *J Neurosurg* 2009; **111**: 317-325 [PMID: 19374493 DOI: 10.3171/2009.2.JNS081720]
45 **Sureka J**, Panwar S, Mullapudi I. Intraneural ganglion cysts of obturator nerve causing obturator neuropathy. *Acta Neurol Belg* 2012; **112**: 229-230 [PMID: 22426671 DOI: 10.1007/s13760-012-0041-1]
46 **Spinner RJ**, Hébert-Blouin MN, Amrami KK, Rock MG. Peroneal and tibial intraneural ganglion cysts in the knee region: a technical note. *Neurosurgery* 2010; **67**: ons71-ons8; discussion ons78 [PMID: 20679946 DOI: 10.1227/01.NEU.0000374683.91933.0E]
47 **Davis GA**, Cox IH. Tibial intraneural ganglia at the ankle and knee: incorporating the unified (articular) theory in adults and children. *J Neurosurg* 2011; **114**: 236-239 [PMID: 20415523 DOI: 10.3171/2010.3.JNS10427]
48 **Jerath NU**, Chen JJ, Miller BJ, Reddy CG. Teaching NeuroImages: intraneural ganglion cyst of the tibial nerve. *Neurology* 2014; **82**: e174-e175 [PMID: 24843041 DOI: 10.1212/WNL.0000000000000429]
49 **Wang H**, Terrill RQ, Tanaka S, Amrami KK, Spinner RJ. Adherence of intraneural ganglia of the upper extremity to the principles of the unifying articular (synovial) theory. *Neurosurg Focus* 2009; **26**: E10 [PMID: 19435440 DOI: 10.3171/FOC.2009.26.2.E10]
50 **Lee BC**, Yegappan M, Thiagarajan P. Suprascapular nerve neuropathy secondary to spinoglenoid notch ganglion cyst: case reports and review of literature. *Ann Acad Med Singapore* 2007; **36**: 1032-1035 [PMID: 18185886]
51 **Limbucci N**, Rossi F, Salvati F, Pistoia LM, Barile A, Masciocchi C. Bilateral suprascapular nerve entrapment by glenoid labral cysts associated with rotator cuff damage and posterior instability in an amateur weightlifter. *J Sports Med Phys Fitness* 2010; **50**: 64-67 [PMID: 20308974]
52 **Ebraheim NA**, Whitehead JL, Alla SR, Moral MZ, Castillo S, McCollough AL, Yeasting RA, Liu J. The suprascapular nerve and its articular branch to the acromioclavicular joint: an anatomic study. *J Shoulder Elbow Surg* 2011; **20**: e13-e17 [PMID: 21194975 DOI: 10.1016/j.jse.2010.09.004]
53 **Spinner RJ**, Amrami KK, Kliot M, Johnston SP, Casañas J. Suprascapular intraneural ganglia and glenohumeral joint connections. *J Neurosurg* 2006; **104**: 551-557 [PMID: 16619659 DOI: 10.3171/jns.2006.104.4.551]
54 **Spinner RJ**, Amrami KK. Intraneural ganglion of the suprascapular nerve: Case report. *J Hand Surg Am* 2006; **31**: 1698-1699 [PMID: 17145396 DOI: 10.1016/j.jhsa.2006.09.015]
55 **Sanger J**, Cortes W, Yan JG. Intraneural ganglion of the suprascapular nerve: case report. *J Hand Surg Am* 2006; **31**: 40-44 [PMID: 16443102 DOI: 10.1016/j.jhsa.2005.08.010]
56 **Parkes A**. Intraneural ganglion of the lateral popliteal nerve. *J Bone Joint Surg Br* 1961; **43-B**: 784-790 [PMID: 14038186]
57 **Bacigalupo LE**, Damasio MB, Zuccarino F, Succio G, Silversti E, Bianchi S, Martinoli C. US and MR imaging of peroneal intraneural ganglia: Emphasis on the articular branch. *Skeletal Radiol* 2005; **34**: 588 [DOI: 10.1007/s00256-005-0959-y]

P- Reviewer: Ju CI, Reddy CG, Squires JH **S- Editor**: Song XX
L- Editor: A **E- Editor**: Li D

World Journal of Radiology

Submit a Manuscript: http://www.f6publishing.com

World J Radiol 2017 May 28; 9(5): 245-252

DOI: 10.4329/wjr.v9.i5.245

ISSN 1949-8470 (online)

ORIGINAL ARTICLE

Retrospective Study

Transarterial chemoembolization using 40 μm drug eluting beads for hepatocellular carcinoma

Giorgio Greco, Tommaso Cascella, Antonio Facciorusso, Roberto Nani, Rodolfo Lanocita, Carlo Morosi, Marta Vaiani, Giuseppina Calareso, Francesca G Greco, Antonio Ragnanese, Marco A Bongini, Alfonso V Marchianò, Vincenzo Mazzaferro, Carlo Spreafico

Giorgio Greco, Tommaso Cascella, Rodolfo Lanocita, Carlo Morosi, Marta Vaiani, Giuseppina Calareso, Francesca G Greco, Alfonso V Marchianò, Carlo Spreafico, Department of Radiology, Interventional Radiology, Nuclear Medicine and Radiotherapy, National Cancer Institute, 20133 Milan, Italy

Antonio Facciorusso, Gastroenterology Unit, Ospedali Riuniti Foggia, University of Foggia, 71122 Foggia, Italy

Roberto Nani, Antonio Ragnanese, Radiology and Interventional Radiology Unit, Azienda Ospedaliera Giovanni Paolo XXIII, 24128 Bergamo, Italy

Marco A Bongini, Vincenzo Mazzaferro, Hepato-biliary Surgery and Liver Transplantation Unit, National Cancer Institute, 20133 Milan, Italy

Author contributions: Greco G collected data, performed the research, wrote the manuscript and made the revision; Greco G, Cascella T, Lanocita R, Morosi C, Marchianò AV, Spreafico C and Nani R performed TACEs and designed the study; Ragnanese A, Calareso G, Vaiani M and Greco FG collected data; Facciorusso A performed statistical analysis; Bongini MA and Mazzaferro V selected the patients, performed clinical support and follow-up, performed liver transplantation; Greco G and Spreafico C evaluated imaging follow-up; Spreafico C supervised the report.

Institutional review board statement: The study was reviewed and approved by the Ethics Committee of the National Cancer Institute of Milan.

Informed consent statement: Patients were not required to give informed consent to the study because the analysis used anonymous clinical data that were obtained after each patient agreed to treatment by written consent.

Conflict-of-interest statement: We have no financial relationships to disclose.

Data sharing statement: No additional data are available.

Manuscript source: Unsolicited manuscript

Correspondence to: Giorgio Greco, MD, Department of Radiology, Interventional Radiology, Nuclear Medicine and Radiotherapy, National Cancer Institute, Via Giacomo Venezian 1, 20133 Milan, Italy. giorgio.greco@istitutotumori.mi.it
Telephone: +39-02-23903384
Fax: +39-02-23902060

Received: December 10, 2016
Peer-review started: December 13, 2016
First decision: January 16, 2017
Revised: February 23, 2017
Accepted: March 12, 2017
Article in press: March 13, 2017
Published online: May 28, 2017

Abstract

AIM

To assess the safety and efficacy of transarterial chemoembolization (TACE) of hepatocellular carcinoma (HCC) using a new generation of 40 μm drug eluting beads in patients not eligible for curative treatment.

METHODS

Drug eluting bead TACE (DEB-TACE) using a new generation of microspheres (embozene tandem, 40 μm) preloaded with 100 mg of doxorubicin was performed on 48 early or intermediate HCC patients with compensated

cirrhosis. Response to therapy was assessed with Response Evaluation Criteria in Solid Tumors (RECIST) and modified RECIST (mRECIST) guidelines applied to computed tomography or magnetic resonance imaging. Eleven out of the 48 treated patients treated progressed on to receive liver orthotopic transplantation (OLT). This allowed for histological analysis on the treated explanted nodules.

RESULTS

DEB-TACE with 40 μm showed a good safety profile without major complications or 30-d mortality. The objective response rate of treated tumors was 72.6% and 26.7% according to mRECIST and RECIST respectively. Histological examination in 11 patients assigned to OLT showed a necrosis degree > 90% in 78.6% of cases. The overall time to progression was 13 mo (11-21).

CONCLUSION

DEB-TACE with 40 μm particles is an effective treatment for the treatment of HCC in early-intermediate patients (Barcelona Clinic Liver Cancer stage A/B) with a good safety profile and good results in term of objective response rate and necrosis.

Key words: Embozene tandem; Drug eluting beads; Drug eluting bead transarterial chemoembolization; Transarterial chemoembolization; Hepatocellular carcinoma

Core tip: This is the first study exploring the safety and efficacy of 40 μm drug eluting bead transarterial chemoembolization for the treatment of hepatocellular carcinoma (HCC) in a series of 48 patients not suitable for ablation or surgical therapies. The use of microspheres smaller than 100 μm is not common practice in the western countries due to skepticism and fear of non-target embolization. Our aim is to present our initial experiences when treating with smaller microspheres so we all can test the potential advantages inherent to them and evaluate the effectiveness in the treatment of HCC nodules.

Greco G, Cascella T, Facciorusso A, Nani R, Lanocita R, Morosi C, Vaiani M, Calareso G, Greco FG, Ragnanese A, Bongini MA, Marchianò AV, Mazzaferro V, Spreafico C. Transarterial chemoembolization using 40 μm drug eluting beads for hepatocellular carcinoma. *World J Radiol* 2017; 9(5): 245-252 Available from: URL: http://www.wjgnet.com/1949-8470/full/v9/i5/245.htm DOI: http://dx.doi.org/10.4329/wjr.v9.i5.245

INTRODUCTION

Transarterial chemoembolization (TACE) is the current standard of care for hepatocellular carcinoma (HCC) in patients with multinodular disease, classified as intermediate stage (stage B) of the Barcelona Clinic Liver Cancer (BCLC) staging system[1]. Furthermore, in clinical practice, a number of patients with early stage (stage A) disease, not eligible for curative treatment (surgery, transplantation or ablation) are commonly treated with TACE[2,3].

Conventional TACE (c-TACE) has shown superiority over basic supportive care in unresectable HCC in two randomised studies published in the early 2000s[4,5] and in a meta-analysis published in 2003[6].

Recently developed drug eluting beads (DEB) have the ability to bind and carry up to double the doxorubicin dose[7,8] thus overcoming the common drawbacks of c-TACE such as the release of the chemotherapeutic agent into the systemic circulation.

DEB-TACE superiority over c-TACE or TACE superiority over transarterial embolization has not been proven in recent studies[9,10] both in terms of survival and as objective response to treatment. These new microspheres have ensured a reduction in the systemic concentration of the loaded chemotherapeutic agent, with a lower rate of post-procedural toxicity compared to c-TACE[11-13]. The first available microspheres had a diameter ranging between 500 and 900 μm that has gradually reduced over the years to let DEB penetrate deeper into tumor circulation arterioles. This theory is supported by recently published controlled studies on smaller microspheres that show encouraging preliminary data on the radiological response in terms of extensive intratumoral necrosis[14,15].

Embozene tandem 40 μm (Boston Scientific, Minneapolis, MA, United States) are a new size of tightly calibrated spherical drug-eluting beads able to load up 100 mg of doxuribicin in a 2 mL syringe, or 150 mg in a 3 mL syringe. These biocompatible, non-resorbable, hydrogel microspheres are coated with an inorganic perfluorinated polymer (Polyzene®-F). They show a small increase in size (< 5% of the original diameter) during drug loading and storage if compared with similar DEB on the market. Dc-Beads M1 (initial diameter 70-150 μm) show a dehydration and loss in size after loading drug; Hepashere (initial diameter 30-60 μm), instead, show an increase in size up to 4 times of the initial diameter, resulting in a final diameter between 120-240 μm after loading drug. Smaller microspheres theoretically allow for more distal vascular penetration and more homogeneous intratumoral drug distribution, with no meaningful evidence of better results in terms of objective response if compared to 100-300 μm particles[16].

The aim of this study was to assess the efficacy and safety of 40 μm DEB-TACE in a series of 48 early-intermediate HCC patients complying with eligibility criteria. Primary endpoint was the evaluation of adverse events and complications related to TACE as well as the tumor response rate, considered as best achieved response. Secondary outcomes were the time to progressions (TTP) and time to response (TTR).

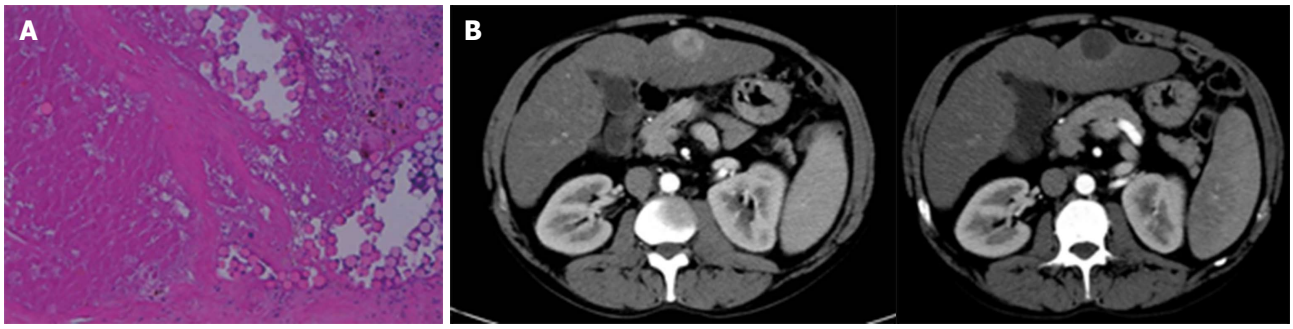

Figure 1 Patient with evidence of a ca. 32 mm tumor with arterial blood flow typical of hepatocellular carcinoma (wash-in phase at the centre of the image) in segment 3 treated with a single cycle of transarterial chemoembolization. A: Corresponding histological image of the tumor after transplantation: Particles can be seen inside the afferent arterioles of the tumor, documenting 100% necrosis; B: The follow-up CT scan after TACE observed complete response according to mRECIST. TACE: Transarterial chemoembolization; mRECIST: Modified Response Evaluation Criteria in Solid Tumors; CT: Computed tomography.

MATERIALS AND METHODS

Study population

Data from 48 early-intermediate HCC patients (BCLC stage A/B) referred to our two tertiary centers between May 2013 and May 2015 and treated with DEB-TACE using 40 μm microspheres were retrospectively analysed (Table 1). All patients signed a dedicated informed consent form. A multidisciplinary team made up of interventional radiologists, oncologists, hepatologists, pathologists and hepatic surgeons selected candidates for the treatment.

All patients were asymptomatic at enrolment (performance status 0) with cirrhotic disease related to hepatitis C in 56.2% of cases (27/48). Fifty-six point two percent of patients were in BCLC B stage, while 43.8% were in early stage A. All patients presented with a preserved liver function (93.4% Child-Pugh A and 6.6% Child-Pugh B7). Other comorbidities were reported in approximately half of the study population (notably Diabetes, Arterial Hypertension and Chronic Obstructive Pulmonary Disease). No tumors receiving DEB-TACE had been previously treated. The mean number of tumors was 2 (range 1-4) with 30 mm (range 10-96) maximum mean diameter, and the mean sum of all maximum diameters came up to 44 mm (range 13-130).

Patient eligibility was established with the following inclusion criteria: Age > 18 years; HCC diagnosis according to the current guidelines[1-3]: Early/intermediate patients not eligible for percutaneous or surgical ablative therapies; well compensated cirrhosis with Child-Pugh Score up to B7; performance status 0 according to the Eastern Cooperative Oncology Group.

Exclusion criteria included bilirubin > 2 mg/dL; principal (main trunk) or segmental portal thrombosis; previous treatments on target tumors (ablation, TACE, Sorafenib); intolerance to doxorubicin (leukocyte count < 3000/mm^3; cardiac ejection fraction < 50%); aspartate amino transferase and alanine amino transferase levels > 270 IU/mL, and patients receiving angiogenesis agents or affected by uncorrectable coagulation disorders.

Imaging study protocols

To assess the disease extent in the liver, its vascular pattern and possible intrahepatic vascular invasions, all patients received pre-treatment abdominal imaging with computed tomography (CT) 128 slices (Somaton Definition Flash, Siemens Healthcare, Erlangen, Germany) or with magnetic resonance imaging (MRI) 1.5 T (Achieva, Philips Healthcare, Best, the Netherlands). In addition to that, they received a CT scan of the chest for a complete staging of the extrahepatic disease.

CT image acquisition technique, before and after treatment, required both a baseline abdominal scan and the arterial, portal and late venous phase study after intravenous administration of a 120-140 mL bolus of iodinated contrast medium (Iopamiro 370 mg/dL, Bracco, Milan, Italy) at an injection flow of 4 mL/s with the Bolus Tracking technique.

The protocol for abdominal MRI required the acquisition of in-phase and out-of-phase T1 weighted sequences, T2 weighted Half-Fourier acquisition Single-shot Turbo-spin Echo (HASTE) and Fat-Saturated (FAT-SAT) sequences, diffusion study and Tissue High Resolution Isotropic Voxel Excitation sequences [T1 weighted FAT-SAT and 3D GRE (3D GradientEcho)] both before and after infusion of Gadolinium-EthOxyBenzyl-Diethylene Triamine Pentaacetic Acid (Gd-EOB-DTPA) 0.025 mmol/mL (Primovist, Bayer, Leverkusen, Germany) with acquisitions up to 20 min during the hepatospecific phase.

DEB-TACE

TACE was performed using transfemoral arterial access route with a micro-puncture system by placing a 5F vascular introducer (Boston Scientific, Natick, MA, United States). The angiographic study of the superior mesenteric artery and the celiac trunk for the characterisation of hepatic vascular anatomy was performed using an angiography unit (Axiom Angiographic Unit, Siemens Healthcare, Erlanger, Germany), and a 5F catheter (Cobra or Simmons, Boston Scientific, Natick, MA, United States). The angiographic study of extrahepatic pathological branches in some HCC tumors (usually peripheral tumors) was based on a careful study of pre-TACE imaging or on missing parts of the pathological tumor vascularization at the selective angiographic study.

Selective studies of segmental and pathological feeding vessels were also performed using a coaxial

micro catheter (Progreat 2.7F, Terumo, Tokyo, Japan), with a highly selective administration of the treatment.

In cases presenting multifocal disease, the treatment never targeted more than three hepatic segments per session. DEB-TACE was performed using a 2 mL/100 mg of doxorubicin (Adriblastina, Pfizer, New York, NY, United States) loaded dose on embozene tandem 40 μm microspheres.

In all performed DEB-TACE treatments embozene tandem 40 μm microspheres were diluted in 20-30 mL of iodinated contrast medium (Iopamiro 370 mg/dL), slowly injected manually with a 3 mL syringe, applying gentle pressure, until blood flow stasis was induced[17].

Vasodilator drugs *via* transcatheter intra-arterial were not administered before starting chemoembolization with a view to expand to the maximum the neoplastic vascular network and theoretically increase the penetration of the particles and, accordingly, the potential effectiveness of the treatment as reported by some authors[18]. Permanent or temporary embolizing materials were not used to complete DEB-TACE in some tumors of greater dimensions where vascular stasis with only 40 μm drug eluting beads was not achieved. In such cases, a second treatment session has been scheduled after performing a CT/MRI investigation to assess that some conditions leading to the impossibility of repeating the treatment, such as the onset of ascites or portal vein thrombosis, had not occurred.

Access haemostasis was achieved by a mechanical system, as Exoseal (Cordis, Miami Lakes, FL, United States), and a subsequent manual compression for about 3-5 min until haemostasis was achieved.

Premedication included 100 mg of paracetamol (Paracetamolo 10 mg/mL S.A.L.F., Bergamo, Italy), 8 mg of ondansetron (Ondansetron 8 mg/4 mL Hikma, Fervença, Portugal) and 50 mg of ranitidine (Ranitidina 50 mg/5 mL, S.A.L.F., Bergamo, Italy). Intravenous antibiotic prophylaxis was administered with 2 g of cefazolin (Cefamizin, Pfizer, New York, NY, United States) consistent with the hospital internal guidelines.

Hospitalization, adverse events and toxicity

Patients were discharged after a brief observation period (48-72 h). Clinical evaluation and assessment of treatment-related toxicity were performed on an outpatient basis with physician's visits and laboratory tests 12, 24 and 48 h after TACE, 4 wk later and every 3 mo thereafter. AE were defined as treatment related if occurred during hospital stay or within 30 d from treatment. Safety parameters were classified according to the Common Terminology Criteria for Adverse Events 4.0[19] at each follow-up visit.

Imaging evaluation and follow-up

Two radiologists (Dr. Carlo Spreafico and Dr. Giorgio Greco) both experienced in interventional radiology and interventional hepatic imaging performed all radiological assessments independently.

Tumoral response to treatment was assessed according to RECIST and mRECIST with a CT scan or MRI investigation performed 4 wk after DEB-TACE and, then, every 3 mo during the follow-up period[20].

A second treatment session, according to the "on demand" policy, was scheduled in case of partial response (PR) or stable disease (SD) after performing blood chemistry tests documenting good preserved hepatic function and continuity in the eligibility criteria for treatment.

In case of repeated DEB-TACE sessions, only the best response was considered for analytical purposes since this has been recently proved a better predictor of survival than the initial response[21]. In patients submitted to OLT, the treated tumors were histologically analysed during the months after treatment with targeted definition of necrosis induced by TACE.

Statistical analysis

The descriptive statistical analysis was expressed as median and range in the case of continuous variables and absolute numbers and percentage in the case of categorical ones. Time to best response and TTP were calculated with the Kaplan-Meyer method, computed from the time of the first treatment and censored to the day of transplantation in transplant patients. All calculations were obtained with the SPSS software (IBM, Armonk, NY, United States). The statistical review of the study was performed by a biomedical statistician.

RESULTS

DEB-TACE and radiological tumor response

All procedures were performed without technical impediments that would prevent treatment of the target tumor. The two study sites performed an overall number of 73 TACE (47 segmental, 22 bisegmental and 4 trisegmental) on a total number of 128 tumors. 31 patients (64.7%) underwent one treatment cycle, 10 patients (20.8%) to 2 treatment cycles, 6 patients (12.5%) to 3 treatment cycles, and 1 patient to 4 treatment cycles (2%), with a mean number of treatments per patient of 1.45.

Response to treatment was assessed by classifying the tumors into three classes according to dimensional criteria, as specified in Table 2 (according to mRECIST) and Table 3 (according to RECIST). The objective response rate (CR + PR) was 26.8% and 69% for tumors smaller than 3 cm, 32.1% and 85.7% for tumors with diameters between 3 and 5 cm, 10% and 70% for tumors with diameter over 5 cm according to RECIST and mRECIST, respectively.

Considering all the treated tumors, the overall objective response rate (CR + PR) was 26.7% according to RECIST and 72.6% according to mRECIST. These data include all the 48 patients of our series. These results were calculated with RECIST and mRECIST criteria, based on the last available CT scan/MRI, with an overall mean follow-up period of 357 d (range 30-810).

Hystological tumor response in transplanted patients

Eleven patients qualified for OLT after 15 overall cycles of DEB-TACE, with a mean number of treatments per

Table 1 Demographic characteristics and tumoral parameters of the study population, *n* (%)

Age (yr)	67 (49-95)
Sex	
Male	42 (87.5)
Female	6 (13.5)
Aetiology	
HCV	27 (56.2)
HBV	9 (18.75)
Alcohol	6 (12.5)
Cryptogenetic	3 (6.25)
NASH	3 (6.25)
Child-Pugh	
A	45 (93.4)
B	3 (6.6)
MELD	8 (6-14)
BCLC	
A	21 (43.8)
B	27 (56.2)
ECOG 0	48 (100)
Portal hypertension	
Yes	22 (45.9)
No	26 (54.1)
Tumour extension	
Unilobar	29 (60.4)
Bilobar	19 (39.6)
No. of tumors (target)	
Total	128
Median	2 (1-4)
Max. diameter (mm)	30 (10-96)
Sum of diameters (mm)	44 (13-130)
TACE	
Total cycles	73
Segmental	47 (64.4)
Bisegmental	22 (30.1)
Trisegmental	4 (5.5)

TACE: Transarterial chemoembolization; HBV; Hepatitis B virus; HCV: Hepatitis C virus; NASH: Nonalcoholic steatohepatitis; MELD: Model for end-stage liver disease; BCLC: Barcelona Clinic Liver Cancer; ECOG: Eastern Cooperative Oncology Group.

Table 2 Target lesions: Modified Response Evaluation Criteria in Solid Tumors response rate

Ø nodules	No. of nodules	CR	PR	SD	PD
Ø < 3 cm	77	47.4%	21.6%	27.8%	3.2%
3 ⩽ Ø ⩽ 5 cm	22	42.8%	42.8%	10.8%	3.6%
Ø > 5 cm	3	40%	30%	30%	0%
Overall response	102	46%	26.6%	24.4%	3%

CR: Complete response; PR: Partial response; SD: Stable disease; PD: Progressive disease.

Table 3 Target lesions: Response Evaluation Criteria in Solid Tumors response rate

Ø nodules	No. of nodules	CR	PR	SD	PD
Ø < 3 cm	77	6.2%	20.6%	66%	7.2%
3 ⩽ Ø ⩽ 5 cm	22	3.5%	28.6%	64.4%	3.5%
Ø > 5 cm	3	0%	10%	90%	0%
Overall response	102	5.2%	21.5%	67.4%	5.9%

CR: Complete response; PR: Partial response; SD: Stable disease; PD: Progressive disease.

Table 4 Histological response rate of treated nodules in patients submitted to orthotopic transplantation

Ø nodules	Degree of necrosis		
	100%	> 90%	< 50%
Ø < 3 cm	7	-	3
3 ⩽ Ø ⩽ 5 cm	2	2	-
Overall necrosis	9 (64.3%)	2 (14.3%)	3 (21.4%)

patient of 1.36. Seven out of 11 patients received 1 treatment, with remaining 4 receiving 2 treatments. Median time elapsed between TACE and OLT was 4.8 mo (95%CI: 2.3-6.5). The histological examination (Table 4) performed on 11 explanted livers reported a total number of 14 tumors of HCC, 10 of which were ⩽ 3 cm and 4 were between 3 and 5 cm.

Among the tumors smaller than 3 cm, 7 presented 100% necrosis and 3 presented a necrosis rate below 50%. Two out of 4 tumors > 3 cm presented a 100% necrosis rate (Figure 1), while the other 2 were above 90%.

DEB-TACE: Adverse events and toxicity

Toxicity data are reported in Table 5. All the observed AE were mild and transient, with no grade 3/4 toxicity reported. There were no cases of post procedure mortality within 30 d.

No major AE were recorded, neither systemically (pulmonary embolism, splenic infarction, gastrointestinal mucosal tumors, acute pancreatitis or cholecystitis, spinal cord injury) related to non-target embolization nor locally (hepatic infection or abscesses, ischemic hepatitis and bile duct injuries) due to local toxicity or ischemia[22]. Median hospital stay was 2 d (range 2-4). Post-embolization syndrome (PES) occurred in 15% of treatments (11/73). Other common AE were abdominal pain (24.6%) and nausea/vomiting (12.3%), which were treated with analgesic drugs and anti-emetics, and mild ascites (4.1%). Transient post procedure increase in transaminase levels occurred in 13.7% of cases (10/73). Other 1/2 grade laboratory tests alterations included a transient increase in bilirubin levels (6.8%).

TTR, TTP and progression free survival

The TTR for all patients was of 4 mo (95%CI: Range 1-4). Overall 24 patients (50%) experienced tumor progression through the study period. One-year progression free survival (PFS) was 64.5% whereas 2-year PFS was 52%. Median TTP was 13 mo (95%CI: Range: 11-21), calculated on mRECIST, as described in Figure 2.

DISCUSSION

DEB-TACE is the standard of care for HCC intermediate stage patients and a valuable therapeutic option in

Table 5 Adverse events

Toxicity	Grade 1/2	Grade 3/4
Clinical findings		
Post embolization syndrome	11/73 (15%)	-
Ascites	3/73 (4.1%)	-
Abdominal pain	18/73 (24.6%)	-
Nausea/vomiting	9/73 (12.3%)	-
Laboratory tests		
Bilirubin	5/73 (6.8%)	-
Transaminase	10/73 (13.7%)	-

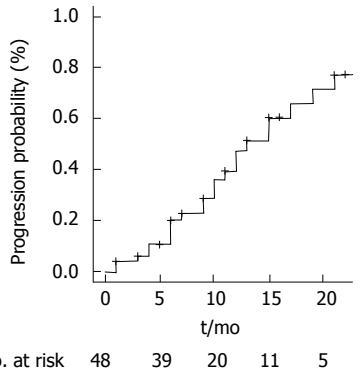

Figure 2 Time to progression.

BCLC A stage when curative approach is unfeasible[1,23]. Several consecutive sessions are usually needed for DEB-TACE to be effective, *i.e.,* the complete tumor response, so that the optimal treatment should lead to higher tumor necrosis rate with the lowest incidence of adverse event. DEB-TACE showed a low incidence of PES[13] and systemic toxicity than in previous reports[8], but its superiority over c-TACE is still a matter of debate[10,24-26].

Since the diameter of chemo loaded microspheres seems to be related to their therapeutic action[17,18], studies on pharmacological kinetics have focused on producing smaller particles that could penetrate deeper into the tumor's vascular network. The most distal penetration of these microspheres reduces the phenomenon of hypoxic-ischaemic neoangiogenesis[27,28]. However, for embolization not associated with any drug (bland embolization), the use of particles with a diameter < 100 μm presented a concerning rate of complications, especially in the treatment of large tumors[29,30]. Some complications in this type of procedures are related to the "non-target embolization" that is, the unwanted escape of microspheres outside the optimal area for treatment, which can affect other organs or unwanted areas of the same organ. Acute pancreatitis (0.88%-15.2%), acute cholecystitis (0.2%-5.4%), pulmonary embolism (0.17%-2.7%), splenic infarction (0.08%-1.4%), gastro-intestinal mucosal tumors (0.22%-0.7%), spinal cord injury (0.3%-1.2%) are among the possible extrahepatic complications[31]. Unwanted hepatic complications such as ischemic hepatitis (0.26%-15.4%), liver infarction or abscess (0.5%-2.7%) or bile duct injuries[31] are connected to local ischemic damages. Some recent studies have proven a very high degree of safety in the use of loadable particles with diameters below 100 μm, with good preliminary efficacy results in terms of radiological and histological response to treatment[14,15,18].

A new generation of microspheres (embozene tandem 40 μm) has been recently marketed for selective intra-arterial treatment even though data on the efficacy and safety profile of the product is yet to be published. To our knowledge, this is the first report on the safety and efficacy of 40 μm particles preloaded with doxorubicin in the treatment of HCC with DEB-TACE. The overall objective response rate (CR + PR) obtained has been of 26.7% to RECIST and 72.6% to mRECIST. This is comparable to the rates according to mRECIST of two recent series carried out with 70-150 μm[14,15] and 30-60 μm[18] (initial diameters) particles loaded with doxorubicin by Spreafico *et al*[14] and Malagari *et al*[18] respectively.

Cases of failed response to locoregional therapy, defined as progressive disease, were around 5.9% and 3% with RECIST and mRECIST, respectively. Median TTP was 13 mo (11-21), an interesting and slightly better result if compared with previous published trials using other microspheres. Moreover, it is to be considered that we did not restrict progression analysis only to local progression of target tumors, but also distant intrahepatic progressions and/or metastases occurrence were investigated.

In 11 patients out of the recruited 48, DEB-TACE was used as bridging therapy for OLT with a complete pathologic response (meant as a 100% necrosis in the histological evaluation) in 64.3% cases (9/14 tumors). Tumors smaller than 3 cm shown a better response in term of histological necrosis (70% complete necrosis), compared to those larger than 3 cm (50% complete necrosis). These histological results are consistent with those reported elsewhere[32,33].

The best radiological response was obtained with a single cycle in 60% of patients, with two cycles in 30% of cases and with three cycles in 10% of patients, with a TTR of about 4 mo (95%CI: Range: 4-6). The effectiveness of HCC treatment using TACE on demand has been proved in our series in the event of detection of SD or PR during the follow-up by CT or MRI, in line with data in the literature. The very low toxicity rates observed in our series are probably a consequence of the high selectivity of the procedure ensured by the use of smaller particles.

The procedures were generally well tolerated. Recorded toxicity levels were lower than recent studies using larger diameter microspheres and consistent with two other studies concerning microspheres with a pre-loading diameter between 70-150 μm[14,15] and 30-60 μm[18].

The incidence of PES was to be lower than the percentages published in other series[11,12,14,18] with particles having similar or larger dimensions, most likely due to the selectivity of the procedure and possible sparing of a larger area of peritumoral hepatic parenchyma.

To our knowledge this is the first series regarding the use of 40 μm DEB in HCC treatment. This is interesting

for world community and especially for western countries where there is skepticism about using particles smaller than 100 μm for DEB-TACE due to the non-target embolization danger. Our preliminary experience shows that 40 μm DEB-TACE is a highly effective and safe technique for HCC non suitable to ablation or surgery therapies with a low rate of PES and no major complications, either local or systemic. The results are complete for all the 48 patients and for 11 of them a histologically proven response to DEB-TACE on surgical specimen is available. Objective local response reached 72.6% and 26.7% according to mRECIST and RECIST without damage to adjacent healthy liver as evidenced by imaging, histology and liver biochemistry. The study has some limitations such as the retrospective nature, the single series and the small sample of patients. Further studies with a longer follow-up period and a bigger sample should be planned to confirm our results.

The results of this retrospective study indicate that DEB-TACE with 40 μm particles is an effective and safe treatment for early-intermediate HCC patients not eligible for curative treatment with good results in term of objective response rate and necrosis.

COMMENTS

Background

Transarterial chemoembolization (TACE) is the current standard of care for hepatocellular carcinoma (HCC) in patients with multinodular disease, classified as intermediate stage (stage B) to Barcelona Clinic Liver Cancer (BCLC) Staging System or in patients in early stage (stage A) not eligible for curative treatment (surgery, liver transplantation or percutaneous ablative treatments). Conventional TACE (c-TACE) has shown superiority over basic supportive care in unresectable HCC in literature since the early 2000s. Actually there is no evidence of superiority of drug eluting bead TACE (DEB-TACE) on c-TACE or transarterial embolization in literature. In the last fifteen years many particles with diameters gradually smaller have been developed for DEB-TACE. These new 40 μm diameter drug eluting beads theoretically penetrate deeper into tumor circulation arterioles reducing the phenomenon of hypoxic-ischaemic neoangiogenesis due to transarterial embolization. There is no evidence in literature of DEB-TACE superiority over c-TACE in terms of efficacy. The only demonstrated vantage is the reduced rate of post embolic syndrome.

Research frontiers

The authors' report on 40 μm DEB-TACE for HCC is the first experience in literarature. The weakness points are the small sample of patients and the retrospective design of the study but it can represent an interesting report for scientific community as first evaluation of safety and efficacy of this new generation of microparticles. Further studies with a larger number of patients will be needed to confirm data and confirm or deny the theoretical benefits of this new generation of micro-particles in the treatment of HCC.

Innovations and breakthroughs

The study confirms a degree of objective response to treatment, defined as complete or partial response according to Response Evaluation Criteria in Solid Tumors (RECIST) and modified RECIST applied to computed tomography and magnetic resonance imaging, consistent with that of previous studies in the literature with a slightly higher caliber particles (40-60 and 70-150 μm). The data is comforting when you consider the lack of intra or extrahepatic complications due to the phenomenon of non-target embolization, cause for concern in Western countries where the DEBTACE is widespread with larger gauge particles.

Applications

This study suggests that 40 μm DEBTACE is safe and effective in early-intermediate HCC patients with compensated cirrhosis.

Terminology

DEB-TACE: Drug eluting bead TACE; Nontarget embolization: Unwanted escape of particles outside the territory seat of treatment.

Peer-review

This paper presented about the efficacy of TACE using drug eluting beads for HCC patients. This topic could be interesting for readers.

REFERENCES

1 EASL-EORTC clinical practice guidelines: management of hepatocellular carcinoma. *J Hepatol* 2012; **56**: 908-943 [PMID: 22424438 DOI: 10.1016/j.jhep.2011.12.001]

2 **Llovet JM**, Bruix J. Systematic review of randomized trials for unresectable hepatocellular carcinoma: Chemoembolization improves survival. *Hepatology* 2003; **37**: 429-442 [PMID: 12540794 DOI: 10.1053/jhep.2003.50047]

3 **Bruix J**, Sherman M. Management of hepatocellular carcinoma: an update. *Hepatology* 2011; **53**: 1020-1022 [PMID: 21374666 DOI: 10.1002/hep.24199]

4 **Llovet JM**, Real MI, Montaña X, Planas R, Coll S, Aponte J, Ayuso C, Sala M, Muchart J, Solà R, Rodés J, Bruix J. Arterial embolisation or chemoembolisation versus symptomatic treatment in patients with unresectable hepatocellular carcinoma: a randomised controlled trial. *Lancet* 2002; **359**: 1734-1739 [PMID: 12049862 DOI: 10.1016/S0140-6736(02)08649-X]

5 **Lo CM**, Ngan H, Tso WK, Liu CL, Lam CM, Poon RT, Fan ST, Wong J. Randomized controlled trial of transarterial lipiodol chemoembolization for unresectable hepatocellular carcinoma. *Hepatology* 2002; **35**: 1164-1171 [PMID: 11981766 DOI: 10.1053/jhep.2002.33156]

6 **Llovet JM**, Burroughs A, Bruix J. Hepatocellular carcinoma. *Lancet* 2003; **362**: 1907-1917 [PMID: 14667750 DOI: 10.1016/S0140-6736(03)14964-1]

7 **Poon RT**, Tso WK, Pang RW, Ng KK, Woo R, Tai KS, Fan ST. A phase I/II trial of chemoembolization for hepatocellular carcinoma using a novel intra-arterial drug-eluting bead. *Clin Gastroenterol Hepatol* 2007; **5**: 1100-1108 [PMID: 17627902 DOI: 10.1016/j.cgh.2207.04.021]

8 **Varela M**, Real MI, Burrel M, Forner A, Sala M, Brunet M, Ayuso C, Castells L, Montañá X, Llovet JM, Bruix J. Chemoembolization of hepatocellular carcinoma with drug eluting beads: efficacy and doxorubicin pharmacokinetics. *J Hepatol* 2007; **46**: 474-481 [PMID: 17239480 DOI: 10.1016/j.jhep.2006.10.020]

9 **Brown KT**, Do RK, Gonen M, Covey AM, Getrajdman GI, Sofocleous CT, Jarnagin WR, D'Angelica MI, Allen PJ, Erinjeri JP, Brody LA, O'Neill GP, Johnson KN, Garcia AR, Beattie C, Zhao B, Solomon SB, Schwartz LH, DeMatteo R, Abou-Alfa GK. Randomized Trial of Hepatic Artery Embolization for Hepatocellular Carcinoma Using Doxorubicin-Eluting Microspheres Compared With Embolization With Microspheres Alone. *J Clin Oncol* 2016; **34**: 2046-2053 [PMID: 26834067 DOI: 10.1200/JCO.2015.64.0821]

10 **Sacco R**, Bargellini I, Bertini M, Bozzi E, Romano A, Petruzzi P, Tumino E, Ginanni B, Federici G, Cioni R, Metrangolo S, Bertoni M, Bresci G, Parisi G, Altomare E, Capria A, Bartolozzi C. Conventional versus doxorubicin-eluting bead transarterial chemoembolization for hepatocellular carcinoma. *J Vasc Interv Radiol* 2011; **22**: 1545-1552 [PMID: 21849247 DOI: 10.1016/j.jvir.2011.07.00217]

11 **Lammer J**, Malagari K, Vogl T, Pilleul F, Denys A, Watkinson A, Pitton M, Sergent G, Pfammatter T, Terraz S, Benhamou Y, Avajon Y, Gruenberger T, Pomoni M, Langenberger H, Schuchmann M, Dumortier J, Mueller C, Chevallier P, Lencioni R. Prospective randomized study of doxorubicin-eluting-bead embolization in the treatment of hepatocellular carcinoma: results of the PRECISION V study. *Cardiovasc Intervent Radiol* 2010; **33**: 41-52 [PMID:

19908093 DOI: 10.1007/s00270-099-9711-7]
12 **Song MJ**, Chun HJ, Song DS, Kim HY, Yoo SH, Park CH, Bae SH, Choi JY, Chang UI, Yang JM, Lee HG, Yoon SK. Comparative study between doxorubicin-eluting beads and conventional transarterial chemoembolization for treatment of hepatocellular carcinoma. *J Hepatol* 2012; **57**: 1244-1250 [PMID: 22824821 DOI: 10.1016/j.jhep.2012.07.017]
13 **Facciorusso A**, Di Maso M, Muscatiello N. Drug-eluting beads versus conventional chemoembolization for the treatment of unresectable hepatocellular carcinoma: A meta-analysis. *Dig Liver Dis* 2016; **48**: 571-577 [PMID: 26965785 DOI: 10.1016/j.dld.2016.02.005]
14 **Spreafico C**, Cascella T, Facciorusso A, Sposito C, Rodolfo L, Morosi C, Civelli EM, Vaiani M, Bhoori S, Pellegrinelli A, Marchianò A, Mazzaferro V. Transarterial chemoembolization for hepatocellular carcinoma with a new generation of beads: clinical-radiological outcomes and safety profile. *Cardiovasc Intervent Radiol* 2015; **38**: 129-134 [PMID: 24870698 DOI: 10.1007/s00270-014-0907-0]
15 **Odisio BC**, Ashton A, Yan Y, Wei W, Kaseb A, Wallace MJ, Vauthey JN, Gupta S, Tam AL. Transarterial hepatic chemoembolization with 70-150 μm drug-eluting beads: assessment of clinical safety and liver toxicity profile. *J Vasc Interv Radiol* 2015; **26**: 965-971 [PMID: 25979305 DOI: 10.1016/j.jvir.2015.03.020]
16 **Blümmel J**, Reinhardt S, Schäfer M, Gilbert C, Sun L, Ren J. Drug-eluting Beads in the Treatment of Hepatocellular Carcinoma and Colorectal Cancer Metastases to the Liver. *Eur Oncol Haematol* 2012; **8**: 162-166 [DOI: 10.17925/EOH.2012.08.3.162]
17 **Lencioni R**, de Baere T, Burrel M, Caridi JG, Lammer J, Malagari K, Martin RC, O'Grady E, Real MI, Vogl TJ, Watkinson A, Geschwind JF. Transcatheter treatment of hepatocellular carcinoma with Doxorubicin-loaded DC Bead (DEBDOX): technical recommendations. *Cardiovasc Intervent Radiol* 2012; **35**: 980-985 [PMID: 22009576 DOI: 10.1007/s00270-011-0287-7]
18 **Malagari K**, Pomoni M, Moschouris H, Kelekis A, Charokopakis A, Bouma E, Spyridopoulos T, Chatziioannou A, Sotirchos V, Karampelas T, Tamvakopoulos C, Filippiadis D, Karagiannis E, Marinis A, Koskinas J, Kelekis DA. Chemoembolization of hepatocellular carcinoma with HepaSphere 30-60 μm. Safety and efficacy study. *Cardiovasc Intervent Radiol* 2014; **37**: 165-175 [PMID: 24263774 DOI: 10.1007/s00270-013-0777-x]
19 **National Cancer Institute**. Common terminology criteria for adverse events v4.0. NCI, NIH, DHHS. May 29, 2009. NIH publication 09-7473. Available from: URL: http://www.hrc.govt.nz/sites/default/files/CTCAE manual - DMCC.pdf
20 **Lencioni R**, Llovet JM. Modified RECIST (mRECIST) assessment for hepatocellular carcinoma. *Semin Liver Dis* 2010; **30**: 52-60 [PMID: 20175033 DOI: 10.1055/s-0030-1247132]
21 **Kim BK**, Kim SU, Kim KA, Chung YE, Kim MJ, Park MS, Park JY, Kim do Y, Ahn SH, Kim MD, Park SI, Won JY, Lee DY, Han KH. Complete response at first chemoembolization is still the most robust predictor for favorable outcome in hepatocellular carcinoma. *J Hepatol* 2015; **62**: 1304-1310 [PMID: 25637785 DOI: 10.1016/j.jhep.2015.01.022]
22 **Xia J**, Ren Z, Ye S, Sharma D, Lin Z, Gan Y, Chen Y, Ge N, Ma Z, Wu Z, Fan J, Qin L, Zhou X, Tang Z, Yang B. Study of severe and rare complications of transarterial chemoembolization (TACE) for liver cancer. *Eur J Radiol* 2006; **59**: 407-412 [PMID: 16621394 DOI: 10.1016/j.ejrad.2006.03.002]
23 **Malagari K**, Alexopoulou E, Chatzimichail K, Hall B, Koskinas J, Ryan S, Gallardo E, Kelekis A, Gouliamos A, Kelekis D. Transcatheter chemoembolization in the treatment of HCC in patients not eligible for curative treatments: midterm results of doxorubicin-loaded DC bead. *Abdom Imaging* 2008; **33**: 512-519 [PMID: 17938995 DOI: 10.1007/s00261-007-9334-x]
24 **Golfieri R**, Giampalma E, Renzulli M, Cioni R, Bargellini I, Bartolozzi C, Breatta AD, Gandini G, Nani R, Gasparini D, Cucchetti A, Bolondi L, Trevisani F. Randomised controlled trial of doxorubicin-eluting beads vs conventional chemoembolisation for hepatocellular carcinoma. *Br J Cancer* 2014; **111**: 255-264 [PMID: 24937669 DOI: 10.1038/bjc.2014.199]
25 **Xie ZB**, Wang XB, Peng YC, Zhu SL, Ma L, Xiang BD, Gong WF, Chen J, You XM, Jiang JH, Li LQ, Zhong JH. Systematic review comparing the safety and efficacy of conventional and drug-eluting bead transarterial chemoembolization for inoperable hepatocellular carcinoma. *Hepatol Res* 2015; **45**: 190-200 [PMID: 25388603 DOI: 10.1111/hepr.12450]
26 **Facciorusso A**, Mariani L, Sposito C, Spreafico C, Bongini M, Morosi C, Cascella T, Marchianò A, Camerini T, Bhoori S, Brunero F, Barone M, Mazzaferro V. Drug-eluting beads versus conventional chemoembolization for the treatment of unresectable hepatocellular carcinoma. *J Gastroenterol Hepatol* 2016; **31**: 645-653 [PMID: 26331807 DOI: 10.1111/jgh.13147]
27 **Wang B**, Xu H, Gao ZQ, Ning HF, Sun YQ, Cao GW. Increased expression of vascular endothelial growth factor in hepatocellular carcinoma after transcatheter arterial chemoembolization. *Acta Radiol* 2008; **49**: 523-529 [PMID: 18568538 DOI: 10.1080/02841850801958890]
28 **Kobayashi N**, Ishii M, Ueno Y, Kisara N, Chida N, Iwasaki T, Toyota T. Co-expression of Bcl-2 protein and vascular endothelial growth factor in hepatocellular carcinomas treated by chemoembolization. *Liver* 1999; **19**: 25-31 [PMID: 9928762]
29 **Bonomo G**, Pedicini V, Monfardini L, Della Vigna P, Poretti D, Orgera G, Orsi F. Bland embolization in patients with unresectable hepatocellular carcinoma using precise, tightly size-calibrated, anti-inflammatory microparticles: first clinical experience and one-year follow-up. *Cardiovasc Intervent Radiol* 2010; **33**: 552-559 [PMID: 19957182 DOI: 10.1007/s00270-009-9752-y]
30 **Maluccio MA**, Covey AM, Porat LB, Schubert J, Brody LA, Sofocleous CT, Getrajdman GI, Jarnagin W, Dematteo R, Blumgart LH, Fong Y, Brown KT. Transcatheter arterial embolization with only particles for the treatment of unresectable hepatocellular carcinoma. *J Vasc Interv Radiol* 2008; **19**: 862-869 [PMID: 18503900 DOI: 10.1016/j.jvir.2008.02.013]
31 **López-Benítez R**, Richter GM, Kauczor HU, Stampfl S, Kladeck J, Radeleff BA, Neukamm M, Hallscheidt PJ. Analysis of nontarget embolization mechanisms during embolization and chemoembolization procedures. *Cardiovasc Intervent Radiol* 2009; **32**: 615-622 [PMID: 19387732 DOI: 10.1007/s00270-009-9568-9]
32 **Nicolini A**, Martinetti L, Crespi S, Maggioni M, Sangiovanni A. Transarterial chemoembolization with epirubicin-eluting beads versus transarterial embolization before liver transplantation for hepatocellular carcinoma. *J Vasc Interv Radiol* 2010; **21**: 327-332 [PMID: 20097098 DOI: 10.1016/j.jvir.2009.10.038]
33 **Nicolini D**, Svegliati-Baroni G, Candelari R, Mincarelli C, Mandolesi A, Bearzi I, Mocchegiani F, Vecchi A, Montalti R, Benedetti A, Risaliti A, Vivarelli M. Doxorubicin-eluting bead vs conventional transcatheter arterial chemoembolization for hepatocellular carcinoma before liver transplantation. *World J Gastroenterol* 2013; **19**: 5622-5632 [PMID: 24039354 DOI: 10.3748/wjg.v19.i34.5622]

P- Reviewer: Edeline J, Jin B, Ohira M **S- Editor**: Ji FF
L- Editor: A **E- Editor**: Li D

Published by **Baishideng Publishing Group Inc**
7901 Stoneridge Drive, Suite 501, Pleasanton, CA 94588, USA
Telephone: +1-925-223-8242
Fax: +1-925-223-8243
E-mail: bpgoffice@wjgnet.com
Help Desk: http://www.f6publishing.com/helpdesk
http://www.wjgnet.com